INFORMATION TO USERS

This manuscript has been reproduced from the microfilm master. UMI films the text directly from the original or copy submitted. Thus, some thesis and dissertation copies are in typewriter face, while others may be from any type of computer printer.

The quality of this reproduction is dependent upon the quality of the copy submitted. Broken or indistinct print, colored or poor quality illustrations and photographs, print bleedthrough, substandard margins, and improper alignment can adversely affect reproduction.

In the unlikely event that the author did not send UMI a complete manuscript and there are missing pages, these will be noted. Also, if unauthorized copyright material had to be removed, a note will indicate the deletion.

Oversize materials (e.g., maps, drawings, charts) are reproduced by sectioning the original, beginning at the upper left-hand corner and continuing from left to right in equal sections with small overlaps. Each original is also photographed in one exposure and is included in reduced form at the back of the book.

Photographs included in the original manuscript have been reproduced xerographically in this copy. Higher quality 6" x 9" black and white photographic prints are available for any photographs or illustrations appearing in this copy for an additional charge. Contact UMI directly to order.

UMI

A Bell & Howell Information Company
300 North Zeeb Road, Ann Arbor MI 48106-1346 USA
313/761-4700 800/521-0600

PROTON TRANSFER BETWEEN TWO METHYLAMINES

IN THE GAS PHASE

IN THE PRESENCE OF EXTERNAL ELECTRIC FIELDS

By

Jian Yin

A dissertation submitted to the Graduate Faculty in Chemistry in partial fulfillment of the requirements for the degree of Doctor of Philosophy, The City University of New York

1998

This manuscript has been read and accepted for the Graduate Faculty in Chemistry in satisfaction of the dissertation requirement for the degree of Doctor of Philosophy.

September 9, 1998
Date

Chairman of Examining Committee

Sept. 17, 1998
Date

Executive Officer

Supervisory Committee

THE CITY UNIVERSITY OF NEW YORK

Abstract

PROTON TRANSFER BETWEEN TWO METHYLAMINES IN THE GAS PHASE IN THE PRESENCE OF EXTERNAL ELECTRIC FIELDS

By

Jian Yin

Adviser: Michael E. Green

A model molecular system: methylamine + proton + methylamine (MPM), in which two methylamines are fixed at predetermined positions, and only the proton is allowed to move, in the presence of electric external fields, has been extensively explored in our work. The potential energy surfaces (PES) under different fields in each nuclear configuration are set up by extensive *ab initio* calculation using the Gaussian 94 package. Then taking this surface as background, the properties of the 3D molecular system have been solved by using a 3D Fourier Grid Hamiltonian (FGH) formalism, which is an extension of Marston and Balint-Kurti's 1D FGH method.

This model is motivated by a series of related works on voltage-dependent ion channel gating, by Green and coworkers[1]. The major concern in our work is: what is the molecular basis of the process regulating the opening and closing the channels? But in this thesis we do not intend to give a complete answer to this question. Instead we concentrate on the very beginning

of the gating process and try to give a quantum mechanical picture of a postulated first step in the gating mechanism.

We have used the system, MPM, to help understand this type of proton transfer. It is a fairly realistic model of systems which are of importance (e.g., amino acids), and small enough to calculate in a reasonable time period with our computer. The proton is transferred, with the aid of an external electric field, from a potential well approximately 1 Å from one methylamine nitrogen to a well neighboring the other when the two nitrogens are constrained to remain either 3.2 Å or 3.6 Å apart. The potential energy surface for the system has been determined by *ab initio* calculation, using Gaussian 94, in 3D Cartesian space, and the wave function of the proton then found using the 3D Fourier Grid Hamiltonian method. When the methylamines are allowed to optimize without constraint they form a potential surface for the proton such that the proton is shared between the two methylamines, so that transfer is not a relevant possibility. Under conditions in which the methylamines are constrained to be further apart than optimal, two wells are formed which localize the proton in one or the other. We have found that a field shift of less than 10^5 V m^{-1} causes a shift of the wave function peak from ≈15:1 in one direction to a correspondingly complete shift in the other direction, with the 3.6 Å separation: the separation is also sharp, but less so, at 3.2 Å separation. It disappears at the optimized distance. This field is superimposed on a considerably larger field due to the asymmetry in the wells.

Similar calculations have been carried out on another model system: Water + Proton + Methylamine (WPM). The results have been discussed and compared with those of MPM models'. The problem is of additional interest if one thinks of the methylamines as models for the basic groups on proteins comprising ion channels in biological membranes. If proton transfer is a step in channel gating (as we have elsewhere postulated), it is necessary that a change in field of appreciably less than 10^7 V m^{-1} suffices to effect the shift. The present result supports the hypothesis.

ACKNOWLEDGEMENT

My investigations into the intermolecular proton transfer in the presence of external electric fields with its applications to the gating mechanism of voltage-dependent ion channels would have been impossible without the introduction, the patience, and the encouragement of my mentor, Professor Michael E. Green. His extensive multidisciplinary knowledge and sharp and critical mind have provided me with a comfortable research environment for extensive investigations.

TABLE OF CONTENTS

LIST OF TABLES

LIST OF ILLUSTRATIONS

❑ INTRODUCTION

1. PROTON TRANSFER THEORY

Proton transfer through a hydrogen bond represents a reaction class that plays a fundamental role in chemistry and biochemistry[4-7]. For a typical hydrogen bond, the potential energy function shows a double-well structure. In classical physics, if a proton experiences a double minimum potential surface it would stay in one of the wells unless it has sufficient energy to pass the potential barrier separating the two wells. However, quantum mechanical particles like electrons and protons may penetrate through the potential barrier from one well to the other, and this phenomenon is known as *tunneling*. The tunneling effect has been first discussed independently by Gamow[8] and Gurney and Condon[9] in 1928, in order to explain the radiative decay of unstable nuclei. The tunneling effect was first used to explain the inversion of the pyramidal ammonia molecule by Dennison and Uhlenbeck[10] in 1932. Despite its widespread importance and intensive studies for the last six decades, the quantum character of proton transfer has not been satisfactorily elucidated[7]. This deficiency persisted because of the complexity of treating the thermal and quantum fluctuations of many atoms in conjunction with a highly accurate description of both the strong and weak interactions[11].

One of the important features of proton transfer reactions is the sensitivity to their solvents. This is due to the fact that a polar solvent can shift the equilibrium within a hydrogen-bonded complex

$$A - H \cdots B \Leftrightarrow A^{+} \cdots H - B^{-}$$

The essential driving force under this feature is the electric field. In quantum mechanical language, this feature may be stated in the following way, that the wave function of a double or multiple well potential is very sensitive to an external electric field. That means a solute in a solvent can be

approximately described by that of a molecule in an external field in gas phase. Because the technical difficulty in the latter case, there have been no direct experiments done for a hydrogen bond in an external field in gas phase. Transfer of a proton between two potential wells under the influence of an electric field in the gas phase has been studied to only a very limited extent in literature. Work on proton transfer in a proton wire has drawn extensive interest. Recently Pomes and Roux[12] have carried out a Feynmann path integral formulation of this problem. These workers found a mechanism for long range proton transfer in which cooperative fluctuations play a critical role. Kiefer et al[13] have proposed a model applicable to hydrogen bonds in which a one-dimensional proton coordinate is used. Their model depends on an effective potential at each site, and the coupling between two electronic states. Guo et al[14] carried out a Wentzel-Kramers-Brillouin (WKB, semiclassical) calculation on the intramolecular hydrogen bond in malonaldehyde, considering the vibrational mode effects on the tunneling splitting. Sanchez and Galan[15] studied proton transfer experimentally in the 3,5-dinitro-2-hydroxybenzoic acid/ ammonia system, finding results consistent with proton tunneling dependent on a hydrogen bond. Work by Dakhnovskii and coworkers[16] has described the consequences of a strong added electric field in effecting an electron transfer. This group has solved a master equation for several cases, including transfer of an electron in a polar solvent, and in metal complexes[17], affected by the field from a laser. Theoretical work by Cukier and Morillo, and coworkers[18-22] has generated several methods of computation, including methods applicable to imposed fields. A four level system, in which two pairs of tunneling doublets existed, one pair in each well, was used by Morillo et al[18] to show how the external field controls proton transfer in the presence of vibrations. Morillo and Cukier[19] considered external field control of proton transfer, in the presence and absence of a medium. Random fields were applied, and the influence of solvent considered, in a related model by Cukier and Morillo[20-22]. These models were able to demonstrate that strong external fields are capable of

suppressing tunneling in systems with matched levels. They also showed that added noise could affect, and sometimes effect, tunneling, by partly destroying the ability of the external field to cause the levels to be mismatched. Three important conclusions arise from their work: a) for external electric fields that satisfy a precise connection between frequency and amplitude, tunneling can be suppressed in the absence of medium; b) static fields, if strong enough, can also suppress tunneling; c) the medium-*reorganization* (which is defined by Morillo and Cukier in their paper as the difference of the solvent potential energy after the proton has transferred to the other well on the other side with the medium still in the equilibrium configuration for the original state before the transfer, and the potential energy of the medium with proton in the original state) if sufficiently large can also suppress tunneling; in case this energy is quite small, a relatively modest external fields should produce substantial effects on the tunnel rate. Since from their theory, the external field acts much like another source of reorganization energy that may add to or subtract from the usual reorganization energy. We will apply these important results in analysis of our data later.

Within the adiabatic regime, the proton is in the lowest stretch vibrational state moving on the electronic ground state surface and eventually becomes trapped on either side by molecule-field interaction or molecular polarization and intramolecular vibrational interaction. Just like polar solvents, external electric fields may also have a strong influence on the proton motion in H-bonds because of their high polarizability. The electric field on the protein molecule dipoles, as well as the ionic fields, changes the potentials of the H-bond protons and destroys or increase their symmetry. For a symmetric potential energy structure, a dipole moment different from zero arises when the symmetry of the potential is disturbed, e.g. by outer electric fields with a non-vanishing component in the bond axes. The potential well in the field direction is lowered and the wave function becomes asymmetrical, too. In the ground state, the position probability becomes greater in the lower well than in the higher well; therefore the hydrogen bond is polarized in the direction of

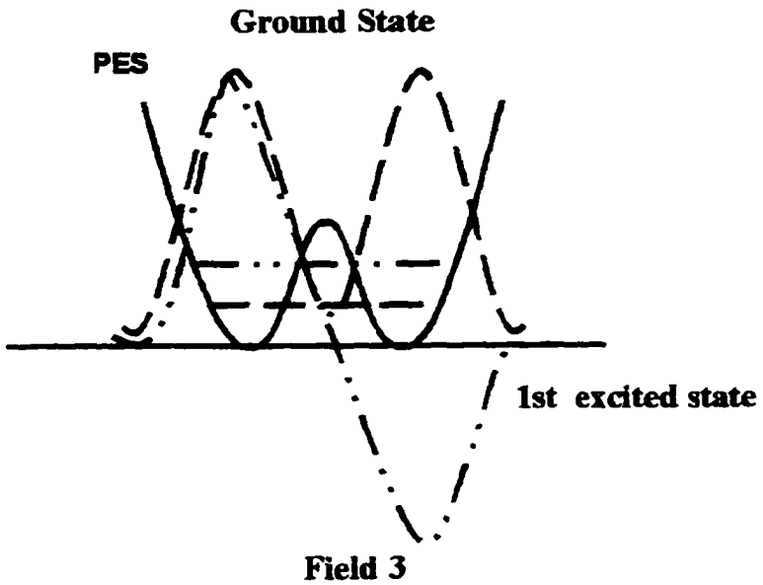

Fig.1 — Tunneling mechanism for symmetric double-well PES. The line ' - - - - - - - ' represents ground state and the line ' — · · — · · — · ' represents the first excited state.

the field. In the first excited state, however, the position probability increases in the higher well; the H-bond is polarized in the opposite direction to the direction of the field. The wave functions are extremely sensitive to disturbances of the symmetry of the potential surface topology. A tiny displacement of the potential wells relative to each other is sufficient to localize the proton in the deeper well in the ground state and the proton is in the higher well in the first excited state, almost completely. The main reason for this sensitivity of the wave functions to the double-well symmetry

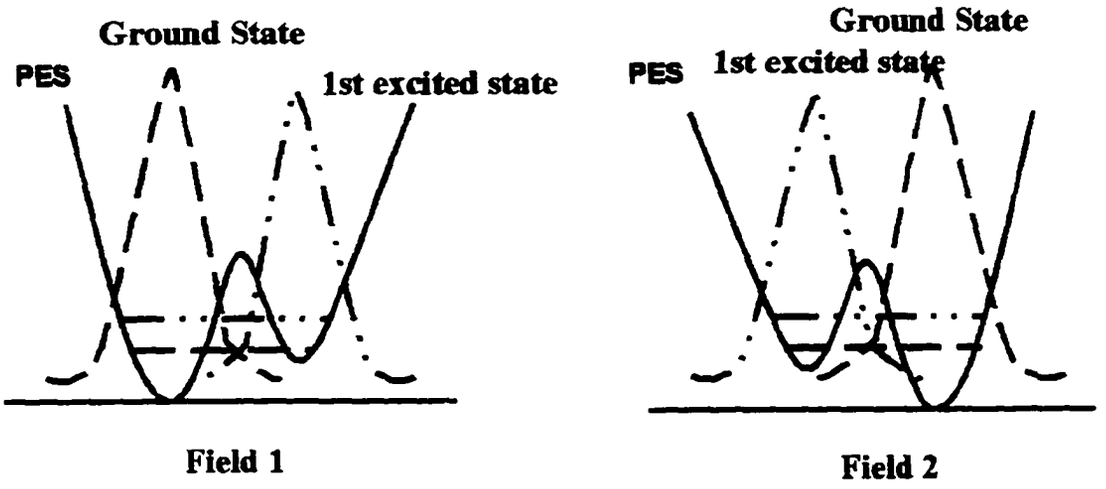

Fig.2 — Tunneling mechanism for asymmetric double-well PES.

is that the lowest levels on both sides of the barrier penetrating the potential barrier lie pair-wise close to each other. To each pair of the levels belongs a state of even and a state of odd parity (*Fig.* 1). The wave functions in an asymmetrical potential can be thought of as a superposition of the states in a symmetrical potential. A small field or a weak asymmetry is sufficient to cause a considerable superposition of the almost degenerate states, i.e. the pair of states the levels of which

lie close to each other, and to give rise to an asymmetrical charge distribution (*Fig.*2).

Our work is motivated by an interest in the behavior of charge in ion channels of biological membranes. The background of voltage gated channels will be given later in more detail. In particular, we have proposed a model for voltage gating of channels in which the initial step is a transition across a critical potential threshold[1]. We propose that this critical initial step is the transfer of a proton from one basic amino acid to another, as the membrane is depolarized. For this to occur, it must be possible to transfer the proton virtually completely with only a relatively small change in local potential, hence in local field. There is some evidence for the importance of proton motion in channel gating, including the effect of D_2O substitution[23,24] . No detailed physical explanation has been proposed for the D_2O results. The existence of a very rapid component of gating current[25] (faster than 2 μs, how much faster not yet determined) may also indicate tunneling. It has been suggested that the fast component is a form of diffusion[26], but independent evidence of this is lacking. The alternate possible interpretation, proton tunneling, seems at least as reasonable.

The calculated *total* fields in the channel can in some locations be very large, up to approximately 10^9 V m^{-1}, which is not out of the range of fields that may be expected in other proteins.[1,27,28]. While a detailed discussion of the steps in channel gating is not the purpose of this work, we can state that the transfer of a proton with a small change in the field is of sufficient possible importance in this field to help make the calculation of this model worthwhile. There are other reasons for interest in the system, but we shall not discuss these here.

We are particularly interested in amides and peptides, and in the transfer of protons along hydrogen bonds in these systems; this has been studied explicitly by Kearley, et al[29]. There are other systems that could be models of biological relevance, including carboxylic dimers[30,31]. While there is a limited literature on transfer by tunneling of protons or electrons in an external field, there appears to be very little if anything on field assisted tunneling by protons in actual molecules

which could be models for proteins. Much of the work on field assisted tunneling consists of calculations on models, and the work on actual molecules does not include external fields. Of course, using actual molecules also means that the calculation must be three-dimensional.

It is well known in condensed-phase theory that proton transfer reactions can be activated at high temperature. The corresponding activation energy of the tunneling does not arise from the barrier along the proton's reaction coordinate, but rather from the reorganization energy of the medium required to approximately equalize the proton's energy in the initial and final states[26]. *A principle role of the medium is to localize the tunneling object to one side of the double-well potential and turn the periodic motion into an irreversible process.* Morillo and Cukier have shown that[22] when the reorganization energy of dicarboxylic acid dimer is small, a relatively modest external field could produce substantial effects on the tunneling rate. Another interesting phenomenon, obtained in the investigation of the tunneling object with respect to the external field[22], is that tunneling systems in the crystal are all oriented in the same direction when no external field applied. Later we will compare our results with the results obtained by Morillo and Cukier and explore what consequences may be inferred.

Simulation of reactive processes in the condensed phase that involve fast motion of light particles (electrons, protons), occurring under the influence of a fluctuating molecular environment, require dynamical simulation methods that combine a quantum mechanical treatment of a few degrees of freedom, while allowing a classical molecular dynamics (MD) simulation of the remainder of the system. The origin of mixed quantum-classical methods dates back to original works of P. Ehrenfest[32], Dirac[33] and Mott[34]. In a QM/MM simulation, electronic degrees of freedom are usually treated as quantum mechanical variables, whereas positions and momenta of heavy nuclei are treated as classical ones. In time-independent schemes, the Born-Oppenheimer approximation is a common route to separate the quantum and classical degrees of freedom. For

time-dependent Schrodinger equations, a very commonly used scheme is the so called quantum-mechanical molecular dynamics (QCMD)[35]. In a QCMD model, the proton dynamics are described by the time-dependent Schrodinger equation, and the dynamics of the remaining atoms is performed using classical molecular dynamics. Coupling between the quantum proton(s) and the classical atoms is accomplished via extended Hellmann-Feynman forces[36] as well as the time dependence of the potential energy function in the Schrodinger equation.

There have been conventionally two types of quantum simulations: one is the *path-integral Monte Carlo simulation*[37]. This methodology has been largely applied to distinguishable particles subject to Boltzmann statistics (i.e. without including exchange interaction). However, most of the path integral applications are based on model potentials to describe the interactions between the quantum nuclei instead of on a direct sampling of the electronic degrees of freedom based on a pure Coulomb Hamiltonian. Furthermore, one cannot expect that path-integral simulation properly represents the dynamics of the quantum particle by using ensemble averages. The other one is *ab initio Molecular Dynamics*[38], which treats the interactions between the nuclei, directly obtained from electronic structure calculations carried out as particles are propagated. In this method, the forces on the particles are obtained for each configuration from electronic structure calculations, thus eliminating the need to obtain an empirical potential at the outset. The drawback is that the nuclei are approximated as classical particles, which might be too crude in many situations.

Recently Car and Parrinello[39] formulated a first principle variational model for molecular dynamics simulation in which a fictitious kinetic energy term is used to obtain a system of coupled equations for wave function and nuclei, which permits an adiabatic propagation of the electronic state in parallel with nuclear motion. Thus, the Car-Parrinello method converts the electronic structure problem to a classical mechanical problem in which the coefficients are regarded as

mechanical variables and the electronic energy functional becomes, in effect, a potential energy for their mechanics. The Car-Parrinello method essentially solves the many-electron Schrodinger equation in Born-Oppenheimer (i.e. adiabatic) approximation for the ground state for every time step, using a density functional Hamiltonian.

There are several other quantum dynamic methods, such as the *time-dependent density functional theory* (TDDFT)[40], the *time-dependent self-consistent field model* (TDSCF)[41], and the *density matrix evolution method* (DME)[42], etc. All of these current theories, developed to treat reaction dynamics of quantum particles in the condensed phase, can be divided into two categories: One describes the quantum degrees of freedom only implicitly but describes the effects of fluctuating terms in the Hamiltonian by expressing the latter in terms of mean field and stochastic properties. Another incorporates the dynamics of the quantum subsystem directly into the MD of the classical environment.

2. Original Problem --- Voltage-Dependent Ion Channels and Their Gating Mechanism

As we mentioned before, our model results from a series of studies in our group. This work concerns the gating mechanisms of the voltage dependent ion channels. The cells of nervous systems are called *neurons* or *nerve cells*. Their primary function is the carriage of information in the form of changes in the electrical potential across the cell membrane. Ion channels constitute a class of transmembrane (TM) proteins that are ultimately responsible for generating and assisting the signals passing through the brain, the heart, and the muscle. Experiments have shown that ion channels function as physiologic proteins, sources of disease, and targets for therapy. Ion channels are macromolecular protein pores that span the lipid bilayer of the cell membrane. Approximately

30% of the energy expended by cells is used to maintain the gradient of sodium and potassium ions across the cell membrane. The manner in which an ion channel uses this stored energy is much like a switch releasing the electrical energy of a battery. During the opening of a single channel, 10^7 ions traverse the membrane in one second. There are basically three types of mechanisms controlling ion channel open-close configurations, and they are named accordingly. There are extracellular *ligand gated* ion channels, transmembrane *voltage gated* ion channels, and intracellular *second messenger gated* ion channels. This thesis is concerned with voltage-dependent ion channels only.

Voltage dependent ion channels control action potential (AP) propagation and initiate neurotransmitter release and therefore are central to information transfer and synaptic function in neurons. Because many voltage-dependent K, Na, and Ca channels share a similar structural organization, it is often presumed that they share a common structure and function relation and activate by a common mechanism[43]. Understanding at molecular level of gating mechanisms of voltage-dependent ion channels remains as a challenge to scientists. A major obstacle is single ion channel crystallization, however this has been accomplished for a bacterial K channel very recently. Although this thesis does not intend to go deeply into the gating mechanism, beyond a molecular model in gas phase, some of the related background knowledge, which inspired us to carry out our studies, will be discussed below.

Voltage dependent channels share three properties[5]. First, they are highly-selective pathways for the transport of ions across cellular membranes. Second, most of them can inactivate, i.e. they can spontaneously close themselves even in the presence of a continuing, activating level of membrane potential. The third, which is the motive of our work, is the ability of these channel proteins to sense tiny changes in transmembrane voltage, physically opening the

channel to allow ion fluxes to pass.

The molecular genetic approach to study voltage gated K channels has revealed multiple subfamilies, such as *Shaker*, *Shal*, *Shab*, and *Shaw*, discovered in Drosophila and largely conserved in man[44]. Most K voltage-dependent ion channels open only after the membrane is depolarized, but some only after it is hyperpolarized. Some open very rapidly but others do not. The K channel of axons was given the name 'delayed rectifier', because it changes the membrane conductance to inward rectify with delay after a voltage step. All members of the broader family of K, Na, and Ca voltage dependent ion channels have steeply voltage dependent gates that open with a delay in response to membrane depolarization. They show some form of inactivation during a maintained depolarization and shut off rapidly again after a repolarization. With a depolarization of adequate rate and threshold magnitude, voltage dependent Na channels will be activated to open with a resulting 4000-5000-fold increase in Na permeability. The first few activated Na channels begin to depolarize the cell producing a positive feedback effect of depolarization --- further channel gating --- further depolarization and so on. This regenerative cycle of gating and depolarization is critical for rapid onset and magnitude of the AP. The enormous transient influx of Na creates the characteristic sharp *upward* deflection or upstroke. Voltage dependent K channels will also be gated with this depolarizing threshold potential resulting in a 50-fold increase in permeability of positive K ions. K channels are gated at a higher threshold and open at a slower rate vs. Na channels; thus the repolarizing effect of K efflux is not noted until a later phase of the AP. Na channels show rapid inactivation (spontaneous closure regardless of threshold potential) resulting in a significant decrease in Na *influx* and a halt to upstroke. Although gated earlier, the slower, higher threshold K channels provide increasing permeability for K *efflux*. With complete inactivation of the Na channels, the large K permeability is free to bring the membrane potential back toward the *resting potential* (RP). This downstroke is associated with the increase in K

permeability. After hyperpolarization, once the membrane potential returns to its resting potential, it may then become transiently more negative than the normal RP. This undershoot is due to the contribution of both voltage dependent and non-gating populations of K channels being open. The RP is regained as the K channels close, the Na/K pump restores resting ion concentrations and only limited K efflux via the non-gating K channel is left.

The first fundamental works done on ion channels are Hodgkin and Huxley's works[45]. In Hodgkin and Huxley (HH, 1952) theory ions are assumed to traverse the membrane independently. This independent principle states that each ion permeates the membrane as if there were no interference from ions of other kinds in the membrane. Gating current was also first proposed by Hodgkin and Huxley[44] to account for the voltage dependence of the Na and K conductances in the squid giant axon. They proposed the existence within the membrane of charged gating particles that move in response to changes in the transmembrane electric potential, turning the conductance of ions on or off. One transmembrane segment (designated S4) of the voltage-dependent channel proteins has been proposed to serve this function, because of the concentration in this region of basic residues in a motif that is conserved among the otherwise divergent families of voltage-dependent Na, K, and Ca channels. Hodgkin and Huxley confirmed that *the relation between ionic current and membrane potential is linear* (as in Ohm's Law). Ionic conductances have proven a useful measure of how many channels are open, although they are only approximations. Both irregularities of channels and asymmetry of ionic concentrations can contribute to non-linearity of the I-E relation in open channels. During a step depolarization, g_{Na}, the conductance of Na, rises rapidly with a short delay, reaches a peak, and falls again to a slow value; there is fast 'activation' and slow 'inactivation'. If the membrane potential is returned to rest during the period of high conductance, g_{Na} falls exponentially fast. Potassium conductance activates and falls back almost 10 fold slower than sodium conductance. The larger the depolarization, the larger and

faster are the changes of the conductances, but there are some limits due to saturation. In the HH model, the conductances depend only on voltage and time, not on the concentrations of ions or on the direction or magnitude of the current flows. Furthermore conductances are independent of each other. In the HH model, activation and inactivation are independent of each other too.

Three ways exist to stop an AP and return the voltage to the resting potential: (1) Once you enter the positive feedback loop with Na channels, the voltage goes quickly to near the Nernst

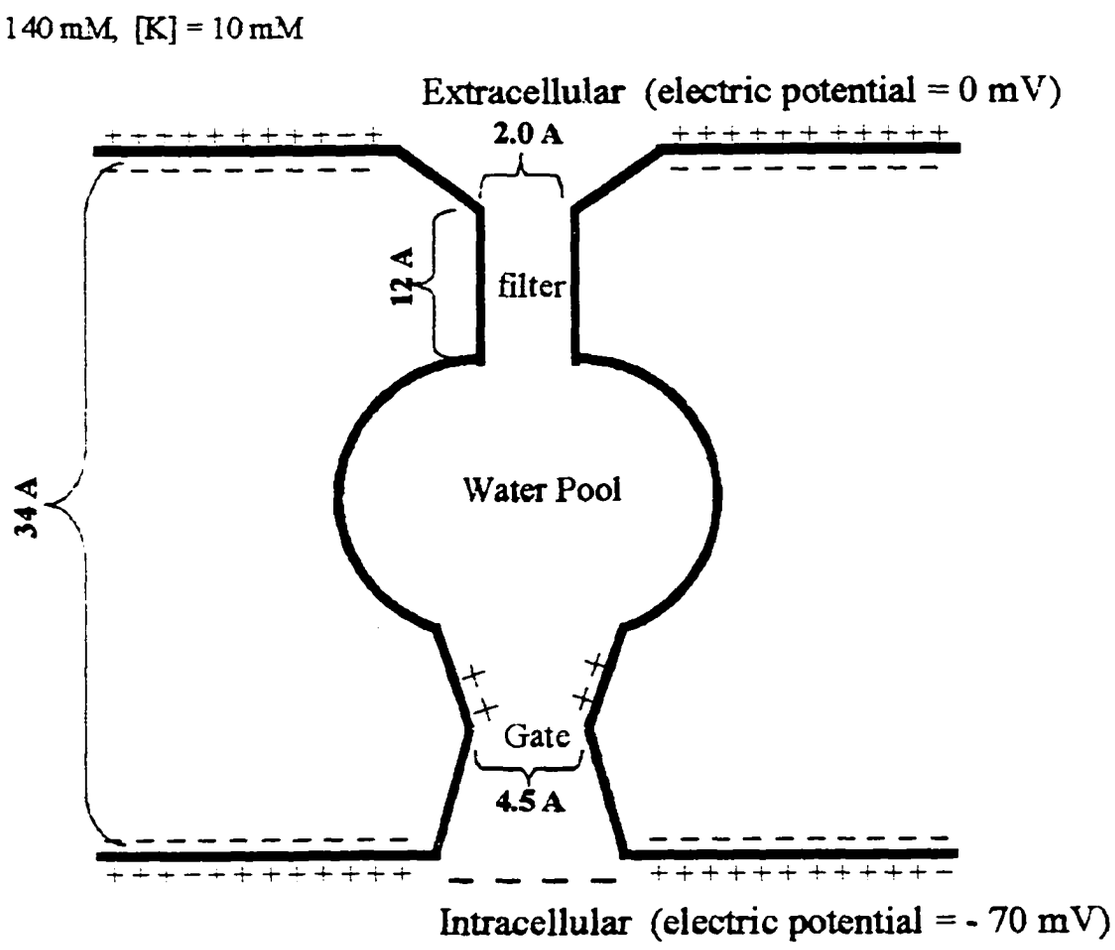

Fig.3 — Voltage-gated ion channel structure profile.

potential for Na; this stops further Na entry, even through open channels. (2) The Na channels spontaneously close after a short time (inactivation). (3) K channels open, which brings the voltage back to near the Nernst potential for K, which is near -70mV.

Voltage-dependent ion channels are formed by integral membrane proteins. Electrophysiologists study their 3D molecular structures by combining mutagenesis and functional analysis. Current common knowledge of the structure and function of many voltage-dependent ion channels suggests that their permeation pores often have narrow regions that can be occupied by only one or few permeant ions at a time. *Fig.*3 shows the K channel profile based on most recent experimental data and analysis[127]. Near the mouth of the channel there is the selectivity filter, which is most narrow part comparing to other portions of the channel. and usually there are two K ions sited in it. After the selectivity filter is there a water pool containing approximately 60 water molecules. The diameter of the pool is large enough (about 6 to 10 Angstrom) in order to minimize the free energy of ion phase transition from filter to aqueous channel. The channel gate is sited just behind the pool having a diameter around 4 to 6 Angstrom. Several discrete-state models have been set up to describe ion permeation.[46,47] They are only accurate under very restricted conditions. Recently some new diffusion models[48] of permeation have begun to appear.

Modern theory on ion channel structure believes that Na channel proteins have fourfold internal repeats or domains, i.e. they are tetramers[49], while K channels sub-units contain four copies of a single internal domain. Within each of the four monomers of Na channels or single domain for K channels there are six transmembrane segments, denoted S1 through S6 (*Fig.*4). It has been generally accepted that voltage dependent ion channels control AP propagation. In the S4 segment there are cationic Arginine(R) or Lysine(K) residues at every third position, with non-polar and hydrophobic residues in between, a pattern that is conserved among the known Na, K, and Ca channels in evolution[2]. These charged residues are now believed to contribute to the gating

charge of the channel[50]. During voltage dependent activation, charged amino acids in the protein sense a change in the transmembrane voltage and initiate charge-conformational changes that can

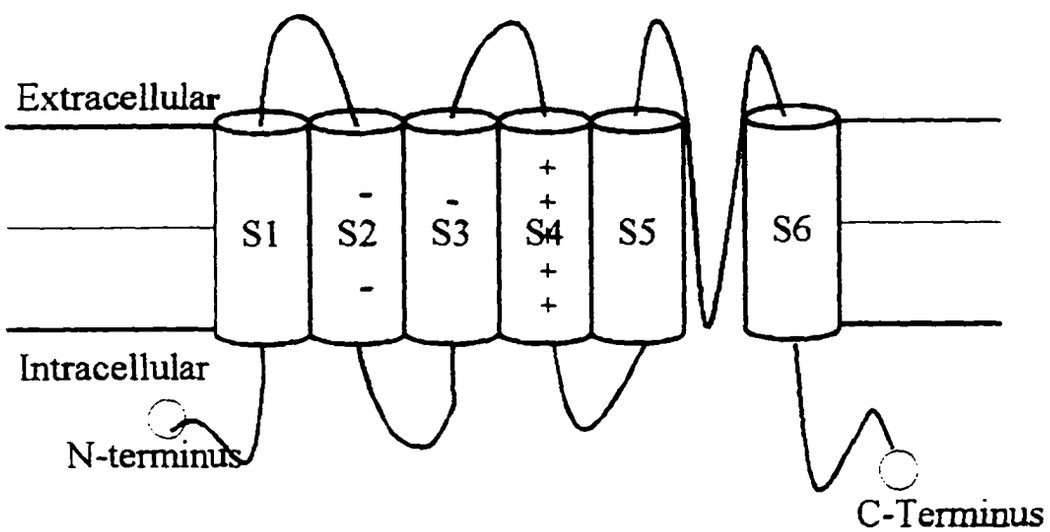

Fig.4 — Single domain structure for Kv ion channel.

open the channel, according to the most commonly accepted model at present. The gating charges can be detected as gating currents[51]. Mutagenesis experiments of the S4 segment showed that this

segment is strongly involved in the gating process[2, 52, 53]. There are also three negatively charged amino acids on segments S2 and S3, which form salt bridges to specific basic amino acids sited on segment S4. Papazian, Bezanilla et al have recently studied five positively charged and three negatively charged residues[54]: R362, R365, R368, R371, and K374 in S4; E283 and E 293 in S2; and D316 in S3. Of these eight residues, four contributed significantly to the gating charge: E293, an acidic residue in S2, and R365, R368, and R371, three basic residues in the S4 segment. Their results also suggest that the electric field is focused in the central part of the S4 segment, which is in agreement with the proposal of Yang et al[55], that conformational changes might be needed to transfer a significant amount of charge across the transmembrane field, leading to channel opening. It is now believed that the voltage gated channel contains buried, positively-charged residues, and it is also believed that these basic residues are stabilized through hydrogen bonding to uncharged residues and through salt bridges to the conserved acidic residues E283 and E 293 in the S2 segment and D316 in the S3 segment. The contribution of the S4 segment to gating charge in the Shaker K channel has also been confirmed by an experiment done by Aggarwal and MacKinnon[56] in 1996.

Gating charge motion can be detected as gating current. Gating currents are roughly two orders of magnitude smaller than corresponding ionic currents[43]. Gating currents have an amplitude of about 1 fA per elementary charge when recorded through a system with an 8 kHz window, which is 1000-fold smaller than ionic currents. However, a typical patch clamp system have noise levels of around 100 to 200 fA RMS. Gating currents generated by a single channel are therefore lost in the noise generated from these patch clamp systems[57]. Gating current fluctuations have been observed in a similar manner[58]. One of most surprising attributes of gating current is that it is not a continuum of microsteps in which an individual gating charge flows virtually continuously for hundreds of microseconds to open a channel; rather, most of the gating charge for one channel moves in a series of two or three brief (< 25 μs) steps carrying an average equivalent

z_g (gating charge) of two or three charges per step[58]. The gating current behaves like a capacitive current and it corresponds to charge reorientation in the membrane field.

What are the gating charges? Looking for these charges has been and is still a great challenge for scientists. In early electrophysiology it was proposed that the gating charge movement might arise from the rotation of dipoles. This was soon discarded because it is difficult to imagine how such dipole moment changes of the required magnitude could come about[43]. Another candidate for the gating charge is the S4 region. Lockhart and Kim[3] have measured the electric field at the amino terminus of an α-helix in water solution, finding 0.43×10^9 Vm^{-1}, by using internal Stark shift. Lu and Green[1] have calculated comparable results near the polarizable waters inside a model taped cylinder channel by Monte-Carlo simulation. There are also some other calculations and references that lead to the same order of magnitude. One of the most popular models has the S4, as an α-helix bearing positive charges, being moved outward in a helix-screw motion in response to membrane depolarization[59]. In order to account for the displacement of $3e_0$ (elementary electric charge unit) per sub-unit, this helix would have to move a distance as large as some 20 Å, in order to move the side-chains with seven charged residues sufficiently so that they encounter an average potential difference of about 3/7 of the full membrane potential. Such a large movement seems unlikely for several reasons including the charge rearrangements they appear to require, and the activation energy that would be needed for so much rearrangement of a protein. Several alternative models have been proposed.[2,43,47] Most of them involve a similar large conformational rotational or translational movement of either one or several segments, or several charged residues in the S4 segment, in order to account for channel opening. Because a direct measurement for voltage dependence is not available, all these conclusions were drawn from indirect measurements of voltage dependent accessibility.

In this thesis we would like to propose a model in which the major movement involved in gating is that of the gating charges themselves and that these charges are protons, in order to make a gating model kinetically and energetically consistent with experiments. We noticed that all current models fail to explain the following experimental facts: 1) There is an initial gating step, i.e. gating charge movement step, faster than 2 μs[55] (this is extremely difficult to accomplish by conformation-change of secondary structure of proteins). 2) An energy difference $\Delta E = qEx$ under a 10^5 Vm^{-1} field across 80 Å distance for a single charge e_0 would be 0.077 kJ/mol (This is too small to account for conformation-change of secondary structure of proteins). The tunneling mechanism is consistent with these two facts.

❑ THEORETICAL BACKGROUND

Molecular quantum mechanical calculations can be divided into two classes: *ab initio* and *Semi-empirical*. Semi-empirical calculations, such as *Hückel theory* (HMO), *Extended Hückel theory* (EHT)[133], *complete neglect of differential overlap* (CNDO)[134], *intermediate neglect of differential overlap* (MNDO)[135], *Austin model 1* (AM1)[136], and *parametric model 3* (PM3)[137], use a simplified Hamiltonian and incorporate into the calculation experimental data or parameters that can be adjusted to fit experimental data. For example, the Hückel molecular orbital (HMO) method, which was developed in 1930s for treatment of conjugated hydrocarbons, neglects σ electrons and σ-π interactions, ignore Coulomb repulsion between π-electrons, and assume fixed empirical values for Hamiltonian elements. The Hückel theory is good in predicting the longest-wavelength bands of aromatic hydrocarbons, but it cannot be used to predict the complete

electronic spectrum of an aromatic hydrocarbon due to, for example, neglecting inter-electronic repulsions. Several semi-empirical π-electron theories have been developed to take electron repulsion into account, such as *Pariser-Parr-Pople* (PPP) *method*. Other popular semi-empirical methods are the *Xα method*, *pseudo-potential method*[94], and *empirical force field* (EFF) *method* (or *molecular mechanics method* (MM)).[138, 139, 140] MM uses empirically-derived potential functions in the Hamiltonian operator. When a true Hamiltonian is used, the calculation method is *ab initio*. The primary idea in *ab initio* calculation is the 'Self-Consistent Field' (SCF). A good *ab initio* method also needs to meet the following three criteria: well-defined, size-consistent, and variational. Using *ab initio* methods today's computers are able to handle 100 atoms at a time, about 10 times less than the number of atoms they are able to handle using semi-empirical quantum mechanical methods.

The central equation of all quantum chemistry is the time-independent, non-relativistic, Schrödinger equation

$$H\Psi = E\Psi \qquad (1)$$

where E is the total energy, Ψ is the molecular wave function from which all chemical properties can be calculated literally, and H is the molecular Hamiltonian (in atomic units). Within the Born-Oppenheimer approximation, the electronic Schrödinger equation can be solved at any fixed nuclear configuration

$$H_{elec}\Psi_{elec} = E_{elec}\Psi_{elec}$$

where $\Psi_{total} = \Psi_{elec}(r;R)\Psi_{nucl}(R)$

In our model system MPM, the proton is treated quantum mechanically while other atoms are fixed at some predetermined positions. The effective Hamiltonian of the proton tunneling system MPM is

$$H_P = T_P + V_P$$

where T_P and V_P are proton kinetic energy and potential energy, respectively. They are functions of other atom's positions, in the coordinate representation. The potential energy function V can be obtained via electronic ground state energy of the total system MPM under the Born-Oppenheimer approximation. The electronic ground state energy as a function of the proton position is then the potential energy surface (PES). To set up the PES of the system MPM we use Gaussian 94[141] to accomplish *ab initio* calculations. Once the PES was set up, quantum mechanical system Eq.(1) was solved by using *Fourier Grid Hamiltonian* method and the corresponding proton eigenvalues and eigenvectors, i.e. proton wave functions, were obtained. In this section we will give some theoretical background of our calculation.

1. HARTREE-FOCK (HF) METHOD

A major goal of quantum chemistry is the prediction of the structures and energies of molecular systems. A characteristic feature of electronic structure calculations is that one needs enormously high relative precision (as a function of configuration) in the energy, typically on the order of one part in 10^7. The Hartree-Fock (HF) level of *ab initio* theory is the method most commonly used in actual applications today. The method is the most straightforward first principle approach and is variational. In Hartree-Fock SCF method the molecular orbitals are found by the *Self-Consistent-Field* (SCF) procedure introduced by Hartree[60]. The simplest independent-electron model results from a complete neglect of electron-electron interactions (Hartree scheme). One step further is the Hartree-Fock model[61]. In this model, the averaged electron-electron interactions are taken into account. Then the eigen-system is an integro-differential equations system, the operator $\hat{H}_{elec}^{HF}$ being the sum of the bare-nucleus operator and certain integral operators which depend on

the functions φ_j. In exact mathematical form, let

$$\hat{H}_{elec}^{HF} = \hat{H}_{elec} \qquad \text{(HF operator)} \tag{2}$$

Hartree-Fock SCF method includes correlation energies statically, i.e. to find a 'suitable' set of single electron spin-orbitals $\{\varphi_i\}$, one uses the variational principle: minimizing the following object function, which gives the total electronic energy of the corresponding system

$$< \Psi_{HF} | \hat{H}_e | \Psi_{HF} >$$

subject to the orthonormal condition $< \varphi_i | \varphi_j >= \delta_{ij}$, $i, j = 1,2,\cdots, N$.

The process leads to the Hartree-Fock equation

$$\hat{F}\psi_j = \sum_{k=1}^{N} \varepsilon_{jk}^{HF} \psi_k \tag{3}$$
$$(\varepsilon_{jk}^{HF})^* = \varepsilon_{kj}^{HF}$$

where

$$\hat{F} \equiv \hat{h}(1) + \sum_{k=1}^{N} [\hat{J}_k(1,2) - \hat{K}_k(1,2)]$$
$$= \hat{h}(1) + \sum_{k=1}^{N} [\hat{J}_k(1,2)(\hat{I} + \hat{P}_{12})]$$

is the *Fock operator*. $\hat{I}$ the unit operator, P_{12} the 1,2-exchange operator, and

$$\hat{h}(i) = -\frac{1}{2m_i}\nabla_i^2 - \sum_{\alpha} \frac{Z_\alpha e^2}{r_{\alpha i}} \quad (i = 1, 2, \ldots, N)$$

$$\hat{J}_k(1) = \int \frac{\psi_k^*(2)\psi_k(2)}{r_{12}} d\tau_2 \qquad \textit{(Coulomb operator)}$$

$$\hat{K}_k(1) = \int \frac{\psi_k^*(2)\hat{P}_{12}\psi_k(2)}{r_{12}} d\tau_2 \qquad \textit{(Exchange operator)}$$

The corresponding Hartree-Fock energy is

$$E_{HF} = \langle \psi_{HF} | \hat{H}_e | \psi_{HF} \rangle = \sum_{j=1}^{N} \varepsilon_j^{HF} - \frac{1}{2} \sum_{j=1}^{N} \sum_{k=1}^{N} (J_{jk} - K_{jk}) \quad (4)$$

These spin-orbitals are allowed complete freedom to spread throughout the entire molecule and their exact forms are determined variationally to minimize the total energy. By employing the basis set expansion technique, quantum mechanical equations (such as Schrödinger equation) and integro-differential equations (such as Hartree-Fock equations) are converted into matrix equations, algebraic equations for the expansion coefficients of the unknown wavefunctions[62]. Once the algebraic approximation has been invoked, the Fock operator F is replaced by its matrix representation and the one-electron function φ_j is approximated by a linear combination of the basis functions. These integro-differential HF equations become a set of simultaneous linear pseudo-eigen equations upon invoking the algebraic approximation.

The success of the HF SCF method, in describing the electronic structure of most closed-shell molecules has made it natural to analyze the wave function in terms of the molecular orbitals. The two fundamental building blocks of the HF SCF are the *molecular orbital* and its *occupation number*. In closed-shell systems each occupied molecular orbital carries two electrons with opposite spin. The orbitals themselves are only defined as an occupied one-electron subspace of the space spanned by the eigenfunctions of the Fock operator. Transformations between different set of pseudo-eigen-systems leave the total HF wave function invariant. Normally the orbitals are obtained in a delocalized form as solutions to the HF equations. The formulation is the most relevant one in studies of spectroscopic properties of the molecule, that is, excitation and ionization. The invariance property, however, makes a transformation to localized orbitals

possible. Such localized orbitals can be of value for an analysis of the chemical bonds in the system. The HF SCF method can be extended to open-shell systems in two ways. In the restricted HF method (RHF)[63], the open-shell orbitals are added to the closed-shell orbitals and the resulting wave function is then projected to have the correct spin and space symmetry. In some cases, this leads to a wave function comprising more than one Slater determinant. An alternative formulation is the unrestricted HF (UHF) method[64], where the spin orbitals for a closed-shell electron pair are no longer assumed to be equal. In the UHF theory, the two sets of spatial orbitals are defined by two sets of coefficients.

$$\phi_i^{\alpha} = \sum_{\mu=1}^{N_\alpha} c_{\mu i}^{\alpha} \phi_\mu, \quad \phi_j^{\beta} = \sum_{\nu=1}^{N_\beta} c_{\nu j}^{\beta} \phi_\nu \qquad (5)$$

Those coefficients are varied independently, leading to the UHF generalizations of the Roothaan-Hall equations[62]. As a result the method is capable of describing the spin polarization of paired electrons in the presence of unpaired spins. For this reason the UHF has been extensively used in studies of spin polarization of radicals. In contrast to the closed shell HF method the UHF also gives a qualitatively correct description of bond dissociation. The major drawback of the UHF and U-post-HF methods is that the wavefunctions are not eigenfunctions of the spin operator S^2.

The accuracy of the electronic structure calculations is limited not only by the form of the wave function but also by the basis set used to expand the wave function. Basis sets optimized to describe correlation effects in atoms also describe molecular correlation effects well. In practical calculations. the molecular orbitals are further restricted to be linear combinations of a set of a number of known one-electron functions (usually known atomic orbitals) ϕ. These functions ϕ are known as *one-electron basis functions*, or simply as *basis functions*. They constitute the *basis set*. If the basis functions are just some atomic orbitals for the atoms making up the molecule, the linear combination is called the *linear combination of atomic orbitals* **(LCAO)** *approximation*. There

are three other types of atomic basis functions, *Slater-type atomic orbitals* (STOs), *Gaussian-type atomic functions* (GTO) and *Contracted Gaussians* (CG). The major strength of the Gaussian-type functions lies in the fact that multi-center integrals can be easily manipulated since the product of two Gaussians centered at A and B is itself a Gaussian with center P on line AB. The major disadvantage of Gaussians is that they have an inappropriate form both in regions near its center nucleus and far away from them. This results in more Gaussians than STOs being required to obtain a certain accuracy in approximation.

There are three levels of basis sets that have been extensively applied to hydrogen bonding: *minimum Slater bases*, *Double Zeta bases*, and Double Zeta plus polarization bases[65]. Kollman[66] indicated that the Double Zeta plus polarization and diffuse function bases do extremely well in prediction of the hydrogen bond energy. The basis set 6-31G** can be considered an extended basis set of the Double Zeta plus polarization type. The 6-31G** basis set[67] is a double *split-valence basis* with polarization functions on all atoms. Within HF level calculation, the 6-31G** basis set only cannot give proper correction of electron-correlation energy. Pople et. al. indicated that unless very extensive basis sets (at least equivalent to 6-311G**(2d)) are used, the inclusion of correlation corrections to computed protonation energies cannot necessarily be expected to improve accuracy[68]. Another basis set used in our work is the Dunning Double-Zeta basis set, D95[65]. This large basis set was used at high level, B3LYP, optimizations in our calculation. In order to correctly describe hydrogen bond properties, polarization and diffuse functions are supplemented into this set for heavy atoms only. Experience shows that this set of basis function, D95, with polarization functions is remarkably accurate in quantitative reproduction of both structural and energetic aspects of systems involving hydrogen bonding at both HF level and MP2 level *ab initio* calculations[69].

All of the above-mentioned basis sets are actually optimized for the purpose of lowering

the total atomic, ionic, or/and molecular energies. They may or may not be suitable for molecular clusters. For describing intermolecular interaction a proper basis set must satisfy the demands of all four fundamental interaction energy components, electrostatic interaction, induction interaction, dispersion interaction, and exchange interaction[70]. A thorough discussion of the basis set dependence of the total interactions in the context of the basis set effects in its components was given by Cybulski et. al.[71]. A general recommendation can be drawn from their discussion that the basis set should be at least of DZ or TZ equivalent quality, plus diffuse functions and polarization functions, in order to carry out an economic and proper *ab initio* calculation of super-molecules. The basis sets D95+* and 6-31+G* which are used in our post-HF calculation are all valid by these criteria.

2. POST-HF METHODS

Within the HF approximation electrons interact with each other only via the average static electron density. In reality, the instantaneous repulsion between the electrons are constantly changing. Usually the *correlation energy* is defined as the difference between the exact eigenvalue of the non-relativistic Hamiltonian for the molecule and the HF energy, i.e.

$$E_{correlation} = E_{exact} - E_{HF}$$

While this definition works well for closed shell systems, it becomes less meaningful when degeneracies or near-degeneracies occur between different nuclear configurations (i.e. non-adiabatic). The reason behind this is, of course, that the HF model breaks down in cases where several configurations become degenerate or near degenerate. This is the case in most bond dissociation processes and also along the reaction path for a symmetry-forbidden chemical reaction. *As a consequence, the HF model is not good in general as a qualitatively correct model*

for a potential energy surface[69]. Thus the HF model is a valid approximation for most molecules around their equilibrium geometry, but it cannot in general be used as a qualitatively correct model for energy surfaces. There have been many methods developed to calculate the electron correlation energy. The most popular ones are:

- Many-body perturbation theories (MBPT)
- Configuration Interaction (CI)
- Coupled Cluster theories (CC)
- Multi-Configuration SCF (including CASSCF and GVB)
- Density Functional Theories (DFT)

2.1) MANY-BODY PERTURBATION THEORY(MBPT)[72]

In the well-known Rayleigh-Schrödinger Perturbation Theory (RSPT), the Hamiltonian is written in two parts:

$$\hat{H}(\lambda) = \hat{H}_0 + \lambda \hat{H}', \quad \hat{H} = \hat{H}(1) \tag{6}$$

such that $\hat{H}_0$ is exactly soluble, i.e.

$$\hat{H}_0 \Phi_k = \varepsilon_k \Phi_k \tag{7}$$

and $\hat{H}'$ is a perturbation applied to $\hat{H}_0$.

If, in particular, we take the reference Hamiltonian $\hat{H}_0$ as the sum of the one-electron Fock operators:

$$\hat{H}_0 = \sum_j \hat{F}_j \tag{8}$$

then the HF determinant and all substituted determinants are eigenfunctions of $\hat{H}_0$. This is the starting point of the so called *Møller-Plesset perturbation theory* (MPPT). Using first quantization operators, one may conveniently write down the expressions for the nth order energy correction as

$$E^{(n)} = \langle \Phi_0 | \hat{H}' | \Psi^{(n-1)} \rangle \tag{9}$$

and n-th order state correction as

$$\Psi^{(n)} = \hat{R}_0 \hat{H}' \Psi^{(n-1)} - \sum_{k=1}^{n-1} E^{(n-1)} \hat{R}_0 \Psi^{(n-k)} \tag{10}$$

where

$$\hat{R}_0 = \frac{\hat{Q}}{E^{(0)} - \hat{H}_0}, \qquad \hat{Q} = \sum_{k(\neq 0)} | \Phi_k \rangle \langle \Phi_k | \tag{11}$$

Although the above perturbation theory is well-defined and size-consistent, it is not variational. The various orders of the MPPT are the most commonly used methods for calculating the correlation energy. Generally the higher the orders collected, the higher the accuracy obtained but the also the higher the computational cost. MP2 scales as nN^4, MP3 as n^2N^4. MP4(SDQ) (which includes all single, double, and quartet substitutions) as n^2N^4 and MP4(SDTQ) (which includes all terms from single to quartet substitutions) as n^3N^4, where n is the number of occupied orbitals and N the basis set size[73]. MP2 recovers a substantial fraction of the correlation energy, often in the range of 80-90% if a large basis set is used. For the first row, errors in vibrational frequencies and equilibrium configurations are reduced by as much as a factor of two or three from corresponding HF values, while HF vibrational prediction has usually been over- estimated and needs correction by a scaling factor 0.9. MP2 is one of the few correlation strategies for which a

serious attempt has been made to reformulate the algorithm for large scale calculations. The most significant barrier to large scale MP2 calculations has been storage of the two electron integrals on disk during the integral's transformation steps.

Another major attribute of MP theory is the intermolecular Møller-Plesset perturbation theory, designated *symmetry-adapted perturbation theory*[74]. It is able to produce directly all four fundamental terms of intermolecular interaction in consecutive order from the HF level to the complete treatment of correlation via the coupled-cluster theory. Therefore MPPT methods are particularly suitable for our calculation on our model system MPM.

2.2) CONFIGURATION INTERACTION (CI)[75]

Conceptually simple, traditional configuration interaction (CI) mixes Φ_0, the Fermi vacuum state, with single, double. . . . excitations, and the unknown coefficients $a_i^a, a_{ij}^{ab}, \cdots$ are determined variationally. If all possible excitations are included, the method gives the exact solution within the basis set, and is referred to as full CI (FCI).

EXPANSION THEOREM Let $\{\varphi_j \mid j = 1,2, \ldots, N\}$ be an finite orthonormal set of spin orbitals and Ψ be any normalizable state in configuration space, then we have the following *Configuration Expansion*

$$\Psi(x) = \sum_K \Psi_K(x) C_K \qquad (12)$$

where $\Psi_K(x)$ is the Slater Determinant, in which $x=(x_1, - - - , x_N)$ is the coordinate vector of the electrons and $K=(k_1 \ldots k_N)$ is the occupied orbital sequence, and it satisfies the orthonormal condition

$$< \Psi_K | \Psi_L >= \delta_{K,L}$$

Or more explicitly,

$$\Psi = \Phi_0 + \sum_{i,a} c_i^a \Psi_i^a + \sum_{i,a} \sum_{j,b} c_{ij}^{ab} \Psi_{ij}^{ab} + \cdots \qquad (13)$$

where the Slater determinant Φ_0, or more generally the *Fermi vacuum* is invariant under unitary transformations. Using the second quantization operator representation, i.e. using the *occupation number representation*, the CI expansion can also be written as

$$\Psi = (1 + C_1 + C_2 + \cdots + C_n + \cdots)\Phi_0 \qquad (14)$$

where C_j is a sum of j-fold excitations with coefficients which must be determined and Φ_0 is the Slater determinant with no excitations.

A FCI yields the exact solution to the electronic Schrödinger equation within a given basis set but is feasible only for small molecular systems using modest basis set. For larger molecular systems and basis set, the CI expansion is truncated to include excitations of only limited number of electrons. The most commonly used CI expansions of this kind is *CI singles* (CIS)

$$\Psi_{CIS} = \Phi_0 + \sum_{i,a} c_i^a \Psi_i^a \qquad (15)$$

Using the cluster operator we may write the FCI projection equations. The *CI singles and doubles* (CISD) is

$$\Psi_{CISD} = \Phi_0 + \sum_{i,a} c_i^a \Psi_i^a + \sum_{i,a} \sum_{j,b} c_{ij}^{ab} \Psi_{ij}^{ab} \qquad (16)$$

The HF and MPPT methods are energetically size consistent, as is FCI; however, any truncated version of CI is not size consistent at all. For CISD the correlation energy per monomer in a system grows only as the square root of the size of the system.

2.3) COUPLED CLUSTER METHODS (CC)

The electron correlation technique that has had the highest amount of formal development is the *coupled cluster* method (CC). The coupled-cluster method was originally invented by Coester and Kummel for studies in nuclear physics in the late 1950s[76], and it was introduced into quantum chemistry by Cizek[77]. The CC methods use a wave function expansion, like CI, in terms of excitations from occupied to virtual HF orbitals. However, instead of expressing its wave function in an algebraic sum, the CC wave function is written in an exponential form:

$$\Psi = \exp(T)\Phi_0 \tag{17}$$

where T is the *cluster operator* operating on the reference function. The cluster operator is usually separated into one-body, two-body, etc. cluster contributions as follows:

$$T = T_1 + T_2 + T_3 + \cdots \tag{18}$$

where $T_n = \frac{1}{n!} \sum_{i_1, i_2, \cdots, i_n} \sum_{a_1, a_2, \cdots, a_n} t_{i_1 i_2 \cdots i_n}^{a_1 a_2 \cdots a_n} a_{i_1 i_2 \cdots i_n}^{a_1 a_2 \cdots a_n}$, and $\{ t_{i_1 i_2 \cdots i_n}^{a_1 a_2 \cdots a_n} \}$ are the expansion coefficients to be determined and $\{ a_{i_1 i_2 \cdots i_n}^{a_1 a_2 \cdots a_n} = a_{a_1}^{+} a_{i_1} \cdots a_{a_n}^{+} a_{i_n} \}$ are products of creation and annihilation operators. The various parts, T_j's, which are operators generating all j-fold particle excitations, of the cluster operators are represented as expansions of second quantized excitation operators and the problem of determining the cluster operator is reduced to the problem of finding the expansion coefficients of the second quantized operators. Various types of anti-symmetric wave functions may be formed by applying various functions, for example g, of the $\hat{T}_j$ operators to Φ_0

$$\Psi = g(T_1, T_2, \cdots)\, \Phi_0 \tag{19}$$

and then determining the unknown coefficients a's by applying projection of the Schrödinger function $(\hat{H}-E)\Psi$, where the $\hat{H}$ is the full Hamiltonian and E the total energy. The simplest choice for the configuration function g is linear, leading to the CID and CISD wave functions.

In coupled cluster doubles (CCD) and coupled cluster singles and doubles (CCSD) approaches, the wave function in Eq.(19) takes the forms

$$\Psi_{CCD} = \exp(\hat{T}_2)\,\Phi_0$$

$$\Psi_{CCSD} = \exp(\hat{T}_1+\hat{T}_2')\,\Phi_0$$

in which $\hat{T}_2' \equiv \hat{T}_2 - \frac{1}{2}\hat{T}_1$, respectively.

The distinction between MBPT and CC theory is that MBPT perturbation theory is usually used to include all terms through some finite order in electron correlation with full fourth order(MP4) being common, while CC theory sums selected categories of MBPT diagrams to all order.

2.4) COMPLETE ACTIVE SPACE SCF (CASSCF)[78]

The *complete active space self-consistent-field* (CASSCF) model, one of the most popular forms of the *Multi-configuration Self-consistent Field* (MCSCF) methods, is an attempt to generalize the HF model to a multi-configuration situation, while trying to keep as much of the conceptual simplicity of the HF approach as possible. The CASSCF method is based on a multi-configuration wave function, and its building blocks are, as in the HF method, the occupied molecular orbitals (i.e. the *active* and *inactive* orbitals). Its total electronic wave function is formed as a linear combination of all the configurations, in the N-electron space, that fulfil the given spin and space symmetry requirements. It is 'complete' in the configuration space spanned by the active orbitals. The inactive orbitals in these configurations are kept doubly occupied; they

represent an SCF sea in which the active electrons move. These inactive orbitals thus have the occupation numbers exactly equal to 2, while the active orbitals have occupation numbers varying between 0 and 2. In CASSCF, the molecular orbitals are obtained as expansions in a set of atom-centered basis functions (the *linear combination of atomic orbitals* (LCAO) method). These molecular orbitals are further divided into three sub-spaces: the *inactive*, the *active*, and the *external orbitals*. The inactive and active orbitals consists of the *internal* (occupied) *orbital subspace*, while the external orbitals are unoccupied. Once the active and inactive orbitals in CASSCF method are chosen the wave function is completely specified. The CASSCF wave function is formed as a linear combination of configuration state functions (CSFs), which usually are HF CI's obtained in a preliminary calculation, generated from these orbitals in the following way:

(1) The inactive orbitals are doubly occupied in all CSFs.

(2) The remaining (active) electrons occupy the active orbitals. Using these electrons and orbitals, a full list of CSFs which have the required spin and molecular symmetry is constructed. The CASSCF wave function is written as a linear combination of all these CSFs, comprising a complete expansion in the active orbital subspace.

The geometry optimization using CASSCF consists of finding expansion coefficients and molecular orbitals that make the energy stationary with respect to all parameters. It has been suggested[78] that the deep-lying inactive orbitals (the core orbitals) should be determined in a preceding SCF calculation and kept frozen during the CASSCF optimization.

3. BECKE'S 3 PARAMETER LYP FUNCTIONAL (B3LYP), A DENSITY FUNCTIONAL APPROACH

3.1) DENSITY FUNCTIONAL THEORY

During the last decade, the density functional theory (DFT) has emerged as an computationally-inexpensive tool for including electron correlation energy. DFT was originally developed for use in solid state physics, and computes the electron correlation energy (and in some cases the exchange energy) as an empirical functional of the electron density. DFT methods have been confined in electronic structure calculations only.

Although the Hohenberg-Kohn (HK) theory[79] showed, as early as the 1960's, that if we have a known electron density, $\rho(r)$, then we have sufficient knowledge to determine the ground state electronic energy and consequent properties of the given system, it is still difficult to construct even a general approximation of this functional with a satisfactory accuracy. Consider a system under no external field; the exact total energy, by HK theorems, can be written as

$$E(\rho) = T(\rho) + V_{ee}(\rho) \qquad (20)$$

where $T(\rho)$ is the kinetic energy of the electrons; $V_{ee}(\rho)$ the electron-electron interaction potential energy (here we omit the external field term for simplicity, so as to make the basic idea of KS scheme more clear; usually in DFT we put the nuclei-electron interaction into the external field term). From a configuration representation point of view, V_{ee} is a local functional. T is not: so do in density representation. The basic difference between DFT and HF theory is the difference in representations, electron density representation and configuration representation. By HK theorems an electron density representation of a many-body quantum mechanical system is possible only for the ground state of the system. The difficulty is that we do not know how to construct a approximate, finite, analytical, and general form of T in density representation.

To circumvent this difficulty, the most popularly adopted formalism is the Kohn-Sham

(KS) theorems[80], the basic ideas in this formalism are: (1) introducing the concepts of (spin-) orbitals, ψ_j's, called *Kohn-Sham orbitals*; (2) introducing a *non-interacting electron system* following the real one, meaning it has the *same electron density* as the real, interacting system. (note: the interacting part is introduced by taking the difference between the kinetic functional and an artificial configuration kinetic functional); (3) separate the total energy into two parts: classical and non-classical. The procedure is as follows: we may rearrange the terms in the expansion (1) as

$$E(\rho) = \underbrace{T_s(\rho) + J(\rho)}_{\text{classical}} + \underbrace{E_{xc}(\rho)}_{\text{nonclassical}} \qquad (21)$$

where $J(\rho)$ is the classical, i.e. Hartree-Fock, Coulomb electron-electron interaction:

$T_s(\rho)$ is the kinetic energy of the child non-interacting system, which can be given explicitly by

$$T_s(\rho) = \sum_{j=1}^{N} \left\langle \psi_j \left| -\frac{1}{2}\nabla^2 \right| \psi_j \right\rangle \qquad (22)$$

(note: ψ_j's are orbitals of the interacting system as well as the non-interacting system, following assumption (2), because they have the same electron density and the obitals are universal functionals of the density) and

$$E_{xc}(\rho) = (T(\rho) - T_s(\rho)) + (V_{ee}(\rho) - J(\rho)) \qquad (23)$$

is the non-classical part, i.e. the so called *exchange-correlation functional* of the system in density functional theory. E_{xc} is the only term in Eq.(21) we do not know. Once we know the exact, finite, analytical form of this quantity in terms of only the electron density, as the HK theorem indicates, then we would have the exact solution to the many-body quantum mechanical problem (of course here we suppose we are able to solve the partial differential equations for this particular system). One thing that needs to be emphasized here is that local or non-local, and interacting or non-interacting, in DFT both are representation-dependent concepts.

The orbitals, ψ's, are obtained by a scheme similar to the SCF scheme for the N-electron Kohn-Sham equation:

$$[-\frac{1}{2}\nabla^2 + v_{eff}(r)]\psi_j = \varepsilon_j\psi_j \qquad j = 1,2,\ldots,N \tag{24}$$

in which the effective potential

$$v_{eff}(r) = \frac{\delta(J(\rho) + E_{xc}(\rho))}{\delta\rho} = \int\frac{\rho(r')}{|r-r'|}dr' + v_{xc}(r) \tag{25}$$

which, not like in HF SCF the Fock operator results directly from Slater-Condon rule, is a direct result of the *Euler equation* in the variational principle; the first term is a Laplacian corresponding to the kinetic energy.

3.2) LOCAL DENSITY APPROXIMATION (LDA)

Many of the current forms for E_{xc} are constructed to give accurate results for selected properties; but there still exists no clear connection between the form of the functional and its ability to accurately predict the properties of interest. Exchange energy is by far the dominant component of the exchange-correlation energy (usually exchange-to-correlation ratio is approximately 10 to 1).

It is a general practice to construct an approximate E_{xc} by commencing with the *local density approximation* (LDA) scheme

$$E_{xc}(\rho) = \int\varepsilon_{xc}(\rho)d\rho \tag{26}$$

In this approximation, one assumes that E_{xc} can be split into exchange and correlation parts

$$E_{xc}(\rho) = E_x(\rho) + E_c(\rho) \tag{27.a}$$

or

$$\varepsilon_{xc}(\rho) = \varepsilon_x(\rho) + \varepsilon_c(\rho) \qquad (27.b)$$

Although in the DFT system energy is a functional of the system electronic density, current DFT calculations usually include both the density and the gradient of the density to enhance the accuracy and convergence. Gradient correction improves the evaluation of energy by extending LDA with non-local terms. Recently hybrid schemes[81], which combine elements of HF method and of the KS procedure of the DFT, have become a very popular approach to calculate the electronic structure of molecules. The basic reason is that these hybrid methods, while requiring the moderate computational effort of HF procedures, deliver energetic and structural results of an accuracy which is comparable to that of results obtained by computationally much more

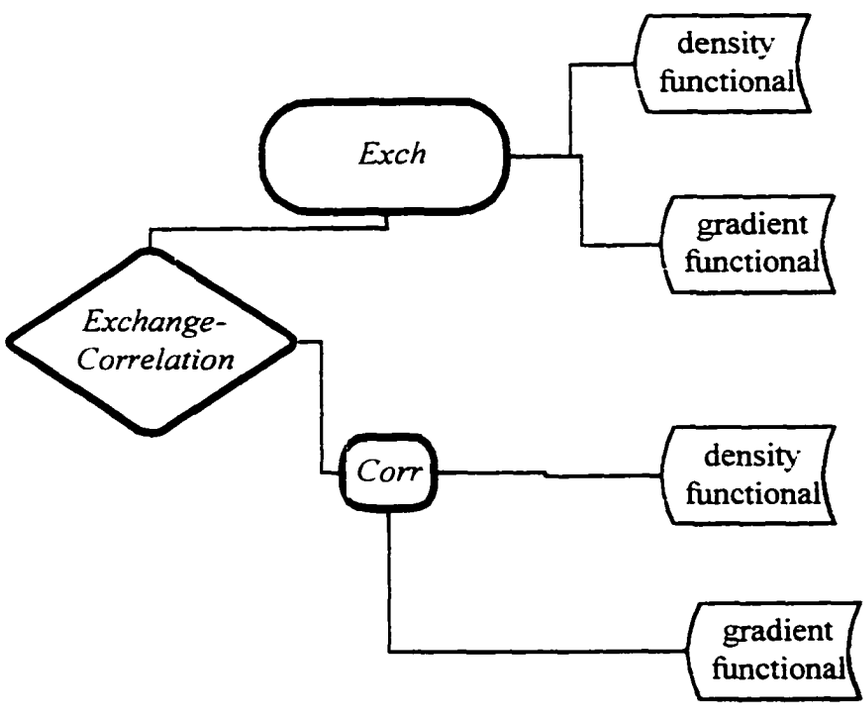

Fig.5 — Density functional decomposition scheme

demanding methods. The rigorous DFT formal basis of the Hybrid schemes has been given by Gorling and Levy[82] (1996) recently. The following flow chart (*Fig.5*) shows the essential idea in current schemes for calculation of the exchange-correlation energy: first the Exchange-correlation is split into two parts, the exchange part and the correlation part; then each part is further split into two parts, the density functional part (which is the major contribution) and the gradient correction functional part. Specifically, the *Becke's 3 parameter LYP functional* (B3LYP)[83, 142] has the form:

$$A * E_X^{Slate} + (1-A) * E_X^{HF} + B * \Delta E_X^{Becke} + E_C^{VWN} + C * \Delta E_C^{LYP,Non-local} \qquad (28)$$

where E_X^{Slater} is the *Slater exchange energy*, $\rho^{\frac{4}{3}}$ with coefficient 2/3, or the *Local Spin Density Exchange functional*[79,80,84]; E_X^{HF} is the HF exchange energy; ΔE_X^{Becke} the gradient correction of *Becke 88 exchange functional*[85]; E_C^{VWN} the Vosko-Wilk-Nusair (VWN) *correlation functional* or *Local Spin Density(LSD) correlation*[86]; and finally $\Delta E_X^{LYP,Non-local}$ is the non-local correlation provided by LYP correlation functional[87]. The three constant parameters A,B, and C[85], which are called the *Becke's three parameters*, are those determined by Becke by fitting to the G1[88] molecule set (A = 0.80, B = 0.72, and C = 0.81).

Although the DFT is a powerful method, it has many potential shortcomings: 1) Systematic corrections are not possible; 2) Poor treatment of transition states; 3) Excited states inherently not treatable; 4) Requires both a basis and an integration grid.

As a final remark in this part, it is worth emphasizing that *ab initio* methods use the first principles of quantum mechanics and may be able to get very good or excellent accuracy. Due to

the amount of computation load (physical memory and CPU time), *ab initio* methods are only common nowadays in gas phase quantum mechanical calculation. In condensed phase, such as in solutions, a pure quantum mechanical calculation is not plausible yet. Some semi-empirical and hybrid schemes have been developed (for examples, AM1, PM3, and MM/QC). As a compensation of lower demand of computing, semi-empirical methods and hybrid MM/QC methods generally have poorer results than those of *ab initio* methods.

4. Fourier Grid Hamiltonian method

4.0 Introduction

The Fourier Grid Hamiltonian (FGH) method used in our calculations was first explicitly formulated in 1D cases in Marston and Balint-Kurti's fundamental work[89]. This method can be taken as a special case of the *discrete variable representation methods* (DVR)[90-93] and is based on the *Fourier method* of Kosloff[94]. The most important attribute of this method is its extreme simplicity while being no less accurate than any other numerical calculation method. A version of multidimensional system FGH for bound states, called FGH-Hartree, has been given by Dutta et. al[95]. The basic strategy going from 1D to 3D in their work is formally factoring the 3D Hamiltonian into three 1D Hamiltonians in Cartesian coordinates, and then in each dimension applying 1D FGH, while in our 3D FGH the factorization is carried out in *Kronecker direct product* and *Kronecker direct sum* formulation. The effective Hamiltonian in each dimension in Dutta's version contains an averaged potential contribution from other dimensions. Therefore their formalism, like Hartree-Fock SCF, is SCF in character, and their equations are mean-field equations. However, the correlation between different dimensions has to be taken into account.

The FGH equations have to be solved sequentially until the ground state energy E_0 converges to the desired accuracy. In contrast to Dutta's 3D FGH, our 3D FGH is a straightforward tensor factorization and avoids the drawback of losing correlation between different dimensions. Details of their multidimensional HF FGH method and ours will be given later.

Generally, there are two basic strategies in numerical calculation in solving the system Schrödinger equation. Methods in the first category rely on matrix diagonalization and represent the wave function in terms of a finite set of basis functions. The basis set is a subset selected from a complete orthogonal basis set of the system. In the second category the iterative methods require repeated numerical integrations of the Schrödinger equation, accompanied by adjustments of the eigenvalues to converge to some finite limits. The multidimensional FGH scheme of Dutta et. al.'s belongs to the second category, while that of ours the first category. There are also several different numerical methods which are popular in modern numerical calculation, such as *finite-difference methods*[96], *finite element methods*[97], *spectral methods*[98] and *complex-scaling methods*[99]. Instead of using a finite basis representation as an approximation of the infinite Hilbert space, the finite difference methods invoke numerical representation of the Hamiltonian operator itself. All finite-difference based methods give rise to a matrix-eigenvalue problem $(T + V)\psi = E\psi$, where the potential energy matrix is independent of the method, while the kinetic energy is best represented in the plane-wave limit. It can be shown that finite-difference methods are equivalent to finite-element methods at various levels of approximation[100]. Unlike the spectral methods and various DVR (to be discussed later in section 4.1) methods, finite element methods have been developed in describing non-perturbative time dependent phenomena such as laser multiphoton excitations, by including simultaneously bound and continuum electronic states [97e]. The spectral method was first introduced by Feit and co-workers in 1982. The spectral

method utilizes numerical solutions to the time-dependent Schrodinger equation to generate the energy eigenvalues and eigenfunctions of the corresponding time-independent Schrodinger equation. In this method one needs to compute the correlation function of a numerical solution ψ to the time-dependent Schrodinger equation with the same wave function at the starting time point t = 0. The solution ψ can be accurately generated with the help of the split operator Fast-Fourier-Transform method[101]. The eigenvalues can be found as a set of sharp local maxima of the numerical Fourier transform of the correlation function. Once the eigenvalues are known, the corresponding eigenfunctions can be computed by numerically evaluating some integrals of known functions. This idea is the origin of the Fourier method later formulated by Kosloff[94]. Another important method which has close connection with FGH method is the complex scaling method. It is well known that the energies and lifetimes of resonance states characterized by complex energies correspond to poles of the resolvent operator

$$(E - \hat{H})^{-1}$$

in the complex-energy plane of the complex scaled Hamiltonian. When one solves the time-independent Schrodinger equation $H\Psi = E\Psi$ for a self-adjoint Hamiltonian H subject to the standard boundary conditions, one obtains a spectrum $\sigma = \{E\}$ of real eigenvalues E which are either discrete (corresponding to closed states) or continuous (corresponding to scattering states). As a result of the complex scaling transformation

$$r \rightarrow r e^{i\alpha}$$

the eigenvalues corresponding to the bound states of H stay invariant, while the branch cuts associated about their respective thresholds by an angle -2α (assume $0 < \alpha < \pi/2$), exposing the complex resonance states in appropriate strips of the complex energy plane. A crucial point from the computational point of view is that the eigenfunctions associated with the complex-scaling

resonance wave functions are localized, i.e. square integrable. The complex-scaling method was first established by the fundamental work of Balslev and Combes[99a], and Simon[99b,c]. Comprehensive theoretical investigations of the complex-scaling method can be found in Lowdin's work[99d] and Moiseyev and Hirschfelder's work[99e]. All of the complex-scaling schemes developed were basis set dependent before the work of Shih-I Chu[99f]. Chu developed a complex-scaling FGH method without the use of basis set expansion. Consider a Hamiltonian system

$$\hat{H}(x) = \hat{T} + V(x)$$

where $\hat{T}$ is the kinetic energy operator. Under the complex scaling transformation

$$\hat{H}(x) \rightarrow \hat{H}(xe^{i\theta}) = e^{-2i\theta}\hat{T} + V(xe^{i\theta})$$

Then the FGH method is applied. One problem is obviously crucial to implement the FGH method, that is how to calculate the second term in Eq.(1) by use of an *ab initio* potential energy surface V(x). This problem was first attacked by Mandelshtam and Moiseyev[95g] in 1995.

4.1 Discrete Variable Representation (DVR) [90-93]

Grid methods and *basis methods* are two broad categories of methods in quantum mechanical calculation. Hartree-Fock SCF and Kohn-Sham SCF methods are in the second category, while FGH is in the first. The basis methods usually represent a system (operators, eigenfunctions) in an orthonormal basis set of functions; these functions are usually selected from the eigen-system of a suitable sub-Hamiltonian $\hat{h}$, and in this case we say it is a *pseudospectral method*. In particular, when the sub-Hamiltonian is exactly the original Hamiltonian $\hat{H}$ of the system, we say it is a *spectral method* with complete basis set.

The DVR is the representation in the finite basis in which the coordinate operator is diagonal. There exists an isomorphism between the *finite basis representation* (FBR) and a discrete representation of coordinate eigenfunctions based on the *quadrature* points (see the appendix at the end of this section). This isomorphism is the result of the existence of a unitary transformation between the two representations; the quadrature points are the eigenvalues of the FBR of the coordinate operator, so that the corresponding eigenvector matrix specifies the transformation between the coordinate eigenfunctions and the original finite basis functions. In the configuration representation, the basis functions of the DVR are related to the basis functions $\{\phi_j\}$ of the FBR as follows:

$$\langle x|\alpha\rangle = \langle x|\phi\rangle\langle\phi|\alpha\rangle = \sum_{j=1}^{N} \phi_j(x)T_{j\alpha} \tag{1}$$

where

$$T_{j\alpha} = \langle \phi_j|\alpha\rangle \tag{2}$$

The basis functions of the DVR are eigenfunctions of the appropriate configuration operator in FBR, with eigenvalues equal to the DVR grid points $\{x_\alpha\}$:

$$x_{jj'} = \langle j|x|j'\rangle \tag{3}$$

and

$$X_{Diag} \equiv \mathrm{diag}(x_\alpha) = T^H X T \tag{4}$$

where $T^H \equiv (T^T)^*$, is the *Hermite transpose* of T.

Generally, the above DVR approach starts by diagonalizing a function of the coordinate operator in a set of N delocalized spectral basis functions chosen to simplify the formal kinetic

energy matrix h (i.e. $H = h + V$). The eigenvalues define a set of grid points in the coordinate representation, and the matrix of N eigenvectors defines a unitary transformation between the discrete variables and spectral bases. There is another DVR scheme that identifies the unitary transformation by introducing a quadrature approximation for the evaluation of the spectral overlap and potential matrix elements. The grid is defined by the quadrature points. The basic idea of the standard Gaussian quadrature DVR is (1) there is a finite basis set $\{\phi_j : j = 1, \cdots, N\}$ in which to expand the wavefunction for a system; (2) a (Gaussian) quadrature rule consisting of a set of quadrature points $\{x_\alpha : j = 1, \cdots, N\}$ and weights $\{w_j : j = 1, \cdots, N\}$ is used to compute matrix elements in this basis. In the standard Gaussian quadrature DVR, functions (e.g. V(x)) are approximated by their values at the DVR points. This is equivalent to evaluating the matrix elements in the FBR by an N-point Gaussian quadrature, provided the basis functions are orthogonal polynomials. $\{f_j\}_{j=1,2,\cdots,N}$ in the configuration representation multiplied by a square root of their common weight function $w(x)$. Namely,we have

$$\langle\phi|\phi\rangle_\alpha = I_{DVR} \quad \text{or} \quad \sum_\alpha \phi_j^*(x_\alpha)\phi_{j'}(x_\alpha) = \delta_{jj'} \tag{5}$$

$$\sum_j \phi_j^*(x_\alpha)\phi_j(x_{\alpha'}) = \delta_{\alpha\alpha'} \tag{6}$$

and

$$T_{j\alpha} = \sqrt{w(x_\alpha)}\phi_j(x_\alpha) \tag{7}$$

where $|\phi_j\rangle \equiv f_j w^{\frac{1}{2}}$, and the x_α's (the eigenvalues of the coordinate operator) are the Gaussian quadrature points. Furthermore we assume that a function that is diagonal in the DVR is equivalent to the Gaussian quadrature evaluation of the FBR matrix elements, i.e.

$$V_{jj'}^{FBR} \approx \sum_{\alpha} w_{\alpha} \phi_j^*(x_\alpha) V(x_\alpha) \phi_{j'}(x_\alpha)$$

$$= \sum_{\alpha} T_{j\alpha}^* V(x_\alpha) T_{j'\alpha} = \left(T^H V^{DVR} T\right)_{jj'} \qquad (8)$$

For an N-function basis, these integrals are evaluated exactly to order (2N-1) in the polynomial power series of the product, i.e. $\phi_j^* V \phi_j$.

The particular importance of the DVR methods is that Gaussian quadrature is defined only for polynomial bases and in multidimension only for direct products of polynomial bases. For more general situations when one may wish to employ nonpolynomial bases or non-direct product bases which cannot be transformed into a polynomial or to a direct product of polynomial bases, a more general DVR theory is needed. The *general discrete variable representation* [93](GDVR) approach was developed by Light and coworkers and used to solve the above DVR problem.

The GDVR, like the standard DVR, is a point-wise representation that is isomorphic with the set of n basis functions of the FBR. The 1D DVR is defined as follows: let $\left\{\left|f_j\right\rangle\right\}$ be an orthonormal set of unit vectors in a Hilbert space and $\left\{x_\alpha\right\}$ be some grid points in coordinate space. Completeness is defined by

$$\delta(x - x') = \langle x|f\rangle\langle f|f\rangle^{-1}\langle f|x'\rangle \qquad (9)$$

In FBR, the number of basis functions is limited by some integer N, so the above definition still works. A Hamiltonian, at this approximation level, can be written as

$$H_{FBR} = \langle f|H|f\rangle \qquad (10)$$

Suppose we formally have the closure relation in a N grid point space representation

$$I_x = |x\rangle\langle x| = \sum |x_\alpha\rangle\langle x_\alpha| \qquad (11)$$

Insert Eq.(12) into Eq.(11) to get formal DVR of the Hamiltonian

$$H_{FBR} = \langle f|x\rangle\langle x|H|x\rangle\langle x|f\rangle = \langle f|x\rangle H_{DVR}\langle x|f\rangle \tag{12}$$

So, to make sense of this formal definition, the following two conditions must satisfied:

a) The inverse matrix $\langle f|x\rangle^{-1}$ must exist;

b) The matrix $\langle f|x\rangle$ must be unitary;

Although the first condition is easily satisfied, the second is not true in general. In GDVR one overcomes this problem by the following strategy. Assume that the first condition is satisfied, then we notice that the matrix

$$\Delta = \langle x|f\rangle\langle f|x\rangle \tag{13}$$

is positive-definite. If $\{|f_j\rangle\}$ is orthonormal on $\{x_\alpha\}$, then $\Delta = I$. It is well-known in linear algebra that there exists an unique square-root matrix of Δ, which is positive-definite itself, and denoted by $\Delta^{-\frac{1}{2}}$. Define

$$\Xi = \Delta^{-\frac{1}{2}}\langle f|x\rangle \tag{14}$$

then we have

$$\Xi^H\Xi = \langle x|f\rangle\Delta^{-1/2}\Delta^{-1/2}\langle f|x\rangle = I \tag{15}$$

where Ξ^H = Hermitian conjugate of Ξ.

Now Ξ is a unitary matrix. We again define a new finite basis set of vectors

$$|\varphi\rangle = |f\rangle\Delta^{-\frac{1}{2}} \tag{16}$$

Then Eq.(13) becomes

$$H_{FBR} = \langle\varphi|x\rangle\langle x|H|x\rangle\langle x|\varphi\rangle = \langle\varphi|x\rangle H_{DVR}\langle x|\varphi\rangle \tag{17}$$

or if

$$H_{FBR}|\Psi\rangle = E|\Psi\rangle$$

then

$$\langle\varphi|x\rangle\langle x|H|x\rangle\langle x|\varphi\rangle|\Psi\rangle = \langle\varphi|x\rangle H_{DVR}\langle x|\varphi\rangle|\Psi\rangle = E|\Psi\rangle \qquad (18)$$

or equivalently

$$H_{DVR}\Xi|\Psi\rangle = E\Xi|\Psi\rangle \qquad (19)$$

i.e.

$$H_{DVR}|\Psi_{DVR}\rangle = E|\Psi_{DVR}\rangle \qquad (20)$$

where $|\Psi_{DVR}\rangle = \Xi|\Psi\rangle$. Furthermore, since Δ is positive-definite one can get the following equation

$$\Delta U = U\Lambda \qquad (21)$$

where U is the matrix consisting of N linearly independent eigenvectors of Δ and Λ is the corresponding diagonal matrix consisting of eigenvalues

$$\Lambda = \mathrm{diag}(\lambda_1, \cdots, \lambda_N), \quad \lambda_j > 0 \ (j = 1, 2, \ldots, N)$$

Then

$$\Delta^{-\frac{1}{2}} U = U\Lambda^{-\frac{1}{2}}$$

Then the above unitary transformation method can be replaced by the simple transformation

$$|\Phi\rangle = \Lambda^{-\frac{1}{2}} U^H |\Psi\rangle$$

making Eq.(20)

$$H_U|\Phi\rangle = E|\Phi\rangle, \ H_U = U^H H_{FBR} U$$

The above equation sets up another DVR scheme.

Both DVR and GDVR are based on an isomorphism which transforms one representation to another. Transform methods not only provide a convenient way to evaluate operator matrix elements, they can lead to a scaling reduction of computation time from N^2 down to $N \log N$, where N is the total number of coupled states. The application of transform methods in a pseudospectral way in conjunction with fast transform algorithms, such as fast Fourier transform (FFT), may readily provide the $N \log N$ scaling in low dimensionality. For instance, in the *Hamiltonian fast Fourier transform* methods of Kosloff, the pseudo-spectral method essentially consists in realizing the Hamiltonian through a transformation between FBR in momentum space where the kinetic energy operator is local, and a DVR in coordinate space where potential energy operator is local. This is a split operator pseudo-spectral approach.

In general, it is much more convenient to factor a quantum mechanical system into several identical 1D system Hamiltonians and then treat each systematically with a common 1D numerical method. Furthermore, it is well-known that a quantum mechanical multidimensional system Hamiltonian like ours can be factorized into a Kronecker direct product in such a manner in Cartesian space. Based on this idea, for any Hamiltonian operator we have

$$H^{DVR} = T^{H} H^{FBR} T \tag{22}$$

and in case of a three-dimensional Hamiltonian (N_x, N_y, N_z), we have

$$T_{N_x,N_y,N_z} = T_{N_x} \otimes T_{N_y} \otimes T_{N_z} \tag{23}$$

The same idea has been applied in our 3D FGH extension formalism which will be discussed next. While both DVR and GDVR approaches can be generalized easily to a multidimensional direct product representation, only the latter can be generalized to a nondirect product representation[90,102].

The development of time-dependent DVR (TDDVR) could be traced back to Kosloff's breakthrough work[94.a)]. The discretization in his paper is based on the *collocation method.*

Discrete variable representation and Fourier method are two special cases of the collocation method. The Fourier method is particularly suitable in describing a common dynamical quantum mechanical evolution pattern: it begins with an initial state which, under the influence of the potentials, evolves through time to produce a final asymptotic state. The central idea behind the numerical approximation is to discretize the quantum Hilbert space of the system and to construct a new corresponding discrete Hilbert space in which Hermitian operators are mapped into Hermitian operators. Recently TDDVR has been extensively developed in various aspects[103 a)-d)]. However, those TDDVR methods are not our current concern and we do not intend to consider them further. In the following section we give the FGH method in detail, which is a special case of the DVR theory.

Appendix *(on Gaussian Quadrature)*

All integration formulae in 1D are of the following form:

$$\int_a^b f(x)dx \approx \sum_{j=0}^{n} w_j f(x_j) \qquad (24)$$

where the n+1 values w_j's are *weights* to be given to the n+1 functional values $f(x_j)$'s, the right-hand side formula is called the *quadrature* approximation of the left-hand side integration.

Theorem (Gauss) There exists a set of pairs, i.e. $\{(w_j, x_j) | j = 0,1,\cdots,n\}$, which give the maximum precision attainable by a mechanical quadrature for a polynomial with degree 2n-1. Such a quadrature is called *Gaussian quadrature*.

4.2 Time-Independent Fourier Grid Hamiltonian Formulation (TI-FGH)

4.2.1 Theory

Since a local representation is the most efficient way to implement a numerical calculation, the FGH method is based on the following consideration: the Hamiltonian operator in the Schrödinger equation can be split into the sum of a kinetic energy operator and a potential energy operator; the kinetic operator is intrinsically local in momentum space, and the potential operator is intrinsically local in configuration space. Fourier transform emerges as a bridge between these two representations. We find that the 3D FGH theory may be expressed most comfortably in Kronecker tensor product and Kronecker tensor sum formalisms. Therefore we will use these formalisms in our discussion.

Let H be a non-relativistic Hamiltonian operator, written as

$$H(q) = T(q) + V(q) \tag{25}$$

in configuration space (q). Since the abstract Hilbert space **B** of the state vectors of a quantum system can be represented either in configuration space (q), as **B**(q), or in momentum space (p), as **B**(p), these two Hilbert spaces are isomorphic to each other by way of the original Hilbert space **B**. It is well-known that the Fourier transform $F[P,Q]$

$$\psi(P) = F[P,Q]\psi(Q) \tag{26}$$

is such an isomorphism between Hilbert spaces **B**(q) and **B**(p). For any linear operator $\hat{A}(q)$ on Hilbert space **B**(q), the corresponding linear operator $\hat{A}(p)$ on Hilbert space **B**(p), under the Fourier transform F[p,q], is

$$A(p) = F[P,Q]A(q)F^{-1}[P,Q] \tag{27a}$$

or

$$A(q) = F^{-1}[P,Q]A(p)F[P,Q] \tag{27b}$$

In case q and p are replaced by the explicit basis set, say Q and P respectively, Eqs.27 are still valid. Accordingly, in the configuration representation, the Hamiltonian operator may be given formally as

$$H(Q) = < Q | H | Q > = < Q | T | Q > + V(Q) \tag{28}$$

The kinetic operator in Eq.25 can then be factored as

$$\begin{aligned} T(Q) &= < Q | T | Q > = < Q | P >< P | T | P >< P | Q > \\ &= F^{-1}[P,Q]T(P)F[P,Q] \end{aligned} \tag{29}$$

by using the unit operator $I = |P >< P| = |Q >< Q|$ (this closure relation is universal on every representation of Hilbert space **B**), where $T(P) = < P | T | P >$, and $F[P,Q] = < P | Q >$, $F^{-1}[P,Q] = F[Q,P]$ are the Fourier transform and its inverse in (Q,P)-representation. The general form of the elements in the formal matrix <P|Q> is

$$\langle p | q \rangle = \frac{1}{\sqrt{2\pi}} e^{i p \cdot q} \tag{30}$$

Inserting Eq.29 into Eq.28 one gets,

$$H(Q) = F^{-1}[P,Q]T(P)F[P,Q] + V(Q) \tag{31}$$

The matrix element in H(Q) is

$$H_{q'q} = < q' | H | q > = \int < q' | p > T_p < p | q > dp + V(q)\delta(q' - q) \tag{32}$$

Eq.31 and Eq.32 are the theoretical basis of the FGH method.

4.2.2 Discretization and Algorithm

To this point the FGH theory follows exactly from the Schrödinger equation and no approximation has been introduced. In this section the discussion will concentrate on the 1D FGH method only. To achieve a numerical calculation based on the method, Marston and Balint-Kurti

introduced a discretization scheme. First they replaced the continuous range (-∞, +∞) of the configuration space q by a series of discrete values:

$$q_{j_q} = j_q \Delta q, \quad j_q = 1, 2, \ldots, N \tag{33}$$

where Δq is the uniform spacing between the grid points. The total length of the range in configuration space is $N\Delta q$. This length determines the longest wavelength λ, thus the lowest frequency, in momentum space, following the fundamental relations (atomic units will be used unless otherwise stated):

$$p = k \tag{34}$$

and

$$k = \frac{2\pi}{\lambda} \tag{35}$$

therefore

$$\Delta p = \Delta k = \frac{2\pi}{\lambda} = \frac{2\pi}{N\Delta q} \tag{36}$$

This is the corresponding spacing in discrete momentum space. Therefore the grid points in momentum space are

$$p_{j_p} = \begin{cases} j_p \Delta p, & j_p = 0, \pm 1, \pm 2, \ldots, \pm[(N-1)/2]; & \text{if } N = \text{odd} \\ j_p \Delta p, & j_p = 0, \pm 1, \pm 2, \ldots, \pm[(N-1)/2], N/2; & \text{if } N = \text{even} \end{cases}$$

where [x] represents the largest integer which is smaller than or equal to x. Then the eigenvalues of the kinetic energy operator T(p) are

$$\begin{aligned} T_{j_p} &= \frac{p^2}{2m} = \frac{(j_p \Delta p)^2}{2m} \\ &= \frac{2}{m}\left(\frac{\pi j_p}{N\Delta q}\right)^2 \end{aligned} \tag{37}$$

From this point, one can obtain the standard secular system, Eq.38a,

$$H(Q)\Psi(Q) = E\Psi(Q) \tag{38a}$$

i.e.

$$\sum_{j}(H_{j'j} - E\delta_{j'j})\Psi_j = 0, \quad j' = 1, 2, \ldots, N. \tag{38b}$$

where $\delta_{j'j}$ are Kronecker delta functions with j, j' the lattice point indices . To implement the above FGH calculation, first set up the proper Hamiltonian matrix $H(Q)$, then solve the homogeneous simultaneous equations. We adapt Marston and Balint-Kurti's algorithm to set up $H(Q)$ by calculating each j-th column of H(q) using the equation in the following steps

1) $T^{(j)}(Q) = \{F^{-1}[P,Q]T(P)F[P,Q]\}e_j$ (39a)

2) Phase-shift $T^{(j)}(Q)$ (39b)

3) $H^{(j)}(Q) = T^{(j)}(Q) + V^{(j)}(Q)$ (39c)

where $A^{(j)}$ represents the j-th column of matrix A, e_j is the j-th standard unit column vector in q-space, j=1,2, ... , N. Step 2), phase-shift in this discrete momentum space, is vital. Since the discretization range in momentum space is determined both by Eqn.36 and by the form of the kinetic energy operator in momentum space, discretization projects the momentum space, under the standard discrete Fourier transform, from $(-\infty, +\infty)$ to $\{p_{-[(N-1)/2]}, p_{-[(N-1)/2]-1}, \ldots, p_{-1}, p_0, p_1, \ldots, p_{[(N-1)/2]}\}$ when N is an odd integer or $\{p_{-[(N-1)/2]}, p_{-[(N-1)/2]-1}, \ldots, p_{-1}, p_0, p_1, \ldots, p_{[(N-1)/2]}, p_{N/2}\}$ when N is an even integer, *not to* $\{p_1, p_2, \ldots, p_N\}$. This phase shift scheme allows us to select even as well as odd integers N as the total number of grid points. A simplified algorithm for the phase-shift is given as follows: a phase-shift of $T(Q)$ in matrix form is a similarity transformation, i.e., because even number grid point schemes leave one finite p-value, $N/(2N\Delta q)(N = \text{even})$, non-degenerate, which conflicts with the symmetry requirement for the kinetic operator in momentum

space, use of an even number of grid points in 1D requires caution. Generally, when using the FGH method, which projects infinitely many periods of momentum space into one period, topologically the grid point $N/(2N\Delta q)\,(N = \text{even})$ in momentum space corresponds to $\pm\infty$. For a continuous Fourier transform these two infinite points set up the integration limits. FGH truncation makes them indistinguishable.

$$T(Q) \overset{\text{phase-shift}}{\rightarrow} XT(Q)X^{-1} = (XF^{-1}[P,Q]X^{-1})(XT(P)X^{-1})(XF[P,Q]X^{-1}) \qquad (40)$$

where X is an N-by-N first kind elementary similarity transformation. That is, the Hamiltonian matrix becomes

$$H(Q) = XT(Q)X^{-1} + V(Q) \qquad (41)$$

The key point implied in phase shift is that the grid points of the discrete range in configuration space should be matching with their corresponding points of discrete range in momentum space, in phase. For technical reasons, it is practical to use first a backward phase shift on the potential energy matrix, then a forward phase shift on the wave function to compensate.

To solve the Eqs.38 we use the FORTRAN 77 subroutine ch.f with double precision in the EISPACK subroutine package.

In our *ab initio* FGH calculation, the dimensions of H(Q) range from 4000 to 6000, the upper limit determined by the capability of our computer, a DEC ALPHA Server 2100A 5/300. To use the Fourier transform in the FGH method most efficiently, we also adopt the fast Fourier transform technique (FFT) introduced by Cooley and Tukey[104]. To be suitable for our calculation our FFT program is insensitive to the radix in the factorization of dimension N. Straightforward computation of an N-point FT requires a number of arithmetic operations proportional to N^2. The Cooley-Tukey FFT algorithm significantly reduces the computational cost, being proportional to

NlogN at radix-2 FFT. If the dimension of the Fourier transform N is a composite integer number, i.e. N=RS, where R and S are integers greater than 1, the mixed-radix Cooley-Tukey tensor factorization formula is[105]

$$F(N) = P(N,S)[I_R \otimes F(S)]P(N,R)Q_R(N)[I_S \otimes F(R)]P(N,S) \qquad (42)$$

where $\otimes$ is the matrix *Kronecker tensor product* (or *direct-product*), P(N,S) is the (N,S)-*stride-permutation matrix*, which can be defined as the unique matrix such that for $\forall a \in C^R$ and $\forall b \in C^S$, where C^R is the R-dimensional column linear space on complex scalar field C, we have one equation

$$P(N,S)(a \otimes b) = b \otimes a \qquad (43)$$

$Q_R(N)$ is the *twiddle-factor matrix*, which is defined as a matrix direct sum

$$Q_R(N) = \sum_{j=0}^{S-1} {}^{\oplus} D_R^j(N) \qquad (44)$$

where $\sum^{\oplus}$ means the matrix direct sum. matrix D's are block-diagonal matrices defined as

$$D_R(N) = \mathrm{Diag}(1, z_N, z_N^2, \cdots, z_N^{R-1}), z_N = \exp\frac{2\pi i}{N} \qquad (45)$$

where $\mathrm{Diag}(1, z_N, z_N^2, \cdots z_N^{R-1})$ represents the diagonal matrix with diagonal elements $(1, z_N, z_N^2, \cdots z_N^{R-1})$. The basic scheme of the implementation is: keep the right (or left)-most factor in Eq.42 as prime factor, i.e. R = prime, then apply Eq.42 to the left (or right) factor S, until it is a prime.

4.2.3 MULTIDIMENSIONAL FGH-HARTREE METHOD[95]

The basic idea of the multidimensional FGH-Hartree method is: concentrate on one particle at a time and average over the remaining particles, thereby generating an effective one-particle Hamiltonian for each particle. The statement given here is only about the two-particle system FGH-Hartree, from which one may derive the higher dimensional FGH-Hartree scheme without much difficulty.

Let the system Hamiltonian be

$$\begin{aligned} H &= H(x) + H(y) + V(x,y) \\ &= T(x) + V(x) + T(y) + V(y) + V(x,y) \end{aligned} \tag{46}$$

where V(x,y) is the non-separable inter-dimensional potential, and x and y are Cartesian coordinates in which the kinetic energies T's are separable.

As a first assumption, we suppose that the system FGH solutions for the following two uncoupled systems are known:

$$h_x|\phi_i^0(x)> = \varepsilon_i^0(x)|\phi_i^0(x)> \quad (i = 1, 2, \cdots) \tag{47}$$

$$h_y|\phi_j^0(y)> = \varepsilon_j^0(y)|\phi_j^0(y)> \quad (j = 1, 2, \cdots) \tag{48}$$

where

$$h_x = T(x) + V(x)$$
$$h_y = T(y) + V(y)$$

and $\phi_i^0(x)$'s ($\phi_j^0(y)$'s), which correspond to the value of the coordinate representation of the state function or the wave function at the grid points, are now the unknown coefficients to be evaluated by the following variational procedure (Note: the x and y in the argument position are not arguments, but only indicative of space representations).

The expectation value of the energy corresponding to the state function

$$|\psi_0\rangle \approx |\phi_0^0(x)\rangle|\phi_0^0(y)\rangle$$

is

$$E = \frac{<\psi_0|H|\psi_0>}{<\psi|_0\,\psi_0>} = \frac{<\phi_0^0(x)\phi_0^0(y)|H|\phi_0^0(x)\phi_{j0}^0(y)>}{<\phi_0^0(x)\phi_0^0(y)|\phi_0^0(x)\phi_0^0(y)>} \qquad (49)$$

where the approximate eigenstates of H have been constructed by superposing the products of the eigenstates of h^0_x and h^0_y.

The unknown coefficients $\phi^0_{0,p}(x)$'s and $\phi^0_{0,q}(y)$'s are to be treated as parameters and determined variationally by requiring

$$\delta E\big|_{E=E_0} = 0 \qquad (50)$$

by taking these coefficients as arguments, subject to the constraint

$$1 = \langle\phi_0^0(x)\phi_0^0(y)|\phi_0^0(x)\phi_0^0(y)\rangle \qquad (51)$$

Then under this constraint, the *Lagrange-multiplier* variational procedure is applied to the numerator of the above ratio of Eq.(49)

$$\langle\psi_0|H|\psi_0\rangle = \langle\phi_0^0(x)\phi_0^0(y)|h_x + h_y + V(x,y)|\phi_0^0(x)\phi_0^0(y)\rangle$$

i.e.

$$\delta_{\phi(x)}[\langle\phi_0^0(x)\phi_0^0(y)|H|\phi_0^0(x)\phi_0^0(y)\rangle + E(1 - \langle\phi_0^0(x)\phi_0^0(y)|\phi_0^0(x)\phi_0^0(y)\rangle)] = 0$$

then

$$h_0^{eff.0}|\phi_0^{eff.0}(x)\rangle = E^{(0)}|\phi_0^{eff.0}(x)\rangle \qquad (52)$$

where $h_x^{eff.0} = \langle\phi_0^0(y)|h_x + h_y + V(x,y)|\phi_0^0(y)\rangle / \langle\phi_0^0(y)|\phi_0^0(y)\rangle$. After solving Eq.52, put the solution into the corresponding simultaneous linear equations in the y-direction

$$h_y^{eff.0}|\phi_0^{eff.0}(y)\rangle = E^{(1)}|\phi_0^{eff.0}(y)\rangle \qquad (53)$$

where $h_y^{eff.0} = \langle \phi_0^{eff.0}(x) | h_x + h_y + V(x,y) | \phi_0^{eff.0}(x) \rangle / \langle \phi_0^{eff.0}(x) | \phi_0^{eff.0}(x) \rangle$. Eqs 52 and 53 are mean-field equations and must be solved in turn iteratively until $E^{(n)} \longrightarrow E_0$ as $n \rightarrow \infty$.

This method, although very simple to implement compared with other methods mentioned in this thesis, needs a large enough number of grid points on each Cartesian axis (more than 100) so as to obtain a set of sufficiently accurate values of the wave function. It is apparently unrealistic for current computing ability to fulfil the speed and memory requirement for a system as large as two methylamines plus a proton.

The converged FGH-Hartree eigenvectors can be used as a basis for expanding ψ_0 and the linear expansion coefficients then determined variationally. The corresponding method may be called the *FGH-CI method*. Alternatively one could bypass the SCF steps in Eqs.52 and 53, and expand ψ_0 in terms of the products of the eigenvectors of h_x and h_y, which leads to a *FGH-valence bond scheme* (FGH-VB). Various derivatives of FGH-Hartree may be found in Dutta, Adhikari and Bhattacharyya's work[95].

4.2.4 Our FGH treatment of multidimensional systems

Our FGH extension of the 1D FGH method to 3D requires only careful manipulation, but is not difficult in principle. To simplify our discussion, the following concepts are useful: let $a \in C$ be a complex number and $B = (b_j) \in C^S$ be an S-dimensional complex column matrix; then we define

$$a \oplus B = \begin{pmatrix} a + b_1 \\ a + b_2 \\ \vdots \\ a + b_S \end{pmatrix} \in C^S \qquad (54)$$

and call it the *Kronecker tensor sum* of a and B, whose jth column element is $a + b_j$, in which b_j is the jth element of B. More generally, for the R-dimensional column matrix $A = (a_j) \in C^R$ we define the kronecker tensor sum $C = A \oplus B \in C^{RS}$ of column vector A and column vector B as

$$C = \begin{pmatrix} a_1 \oplus B \\ a_2 \oplus B \\ \vdots \\ a_R \oplus B \end{pmatrix} \in C^{RS} \tag{55}$$

There is an isomorphism V_c between the R-dimensional diagonal matrix space and the R-dimensional column vector space, i.e. for any R-dimensional diagonal matrix $\mathrm{Diag}(a_1, a_2, \cdots, a_R)$ we define operator V_C as

$$V_C \mathrm{Diag}(a_1, a_2, \cdots, a_R) = \begin{pmatrix} a_1 \\ a_2 \\ \vdots \\ a_R \end{pmatrix} \tag{56}$$

and obviously

$$V_C^{-1} \begin{pmatrix} a_1 \\ a_2 \\ \vdots \\ a_R \end{pmatrix} = \mathrm{Diag}(a_1, a_2, \cdots, a_R)$$

Using this relation we extend the definition of Kronecker direct sum for column vectors to diagonal matrices: for any diagonal matrices $A = \mathrm{Diag}(a_1, a_2, \cdots, a_R)$ and $B = \mathrm{Diag}(b_1, b_2, \cdots, b_S)$

$$A \oplus B \equiv V_C^{-1}[(V_C A) \oplus (V_C B)] \tag{57}$$

More generally, let $a \in C$ be a complex number and $B = (b_{ij}) \in C^{R \times S}$ be an R×S-matrix, then we define

$$a \oplus B = \left(a + b_{ij}\right) \in C^{R \times S} \tag{58}$$

and call it the *kronecker tensor sum* of a and B. whose jth column element is $a + b_{ij}$, in which b_{ij} is the (i,j)-th element of B. For a non-diagonal matrix $A = (a_{ij}) \in C^{R' \times S'}$ we define the kronecker tensor sum $C = A \oplus B \in C^{R'R \times S'S}$ of A and B as

$$C = \begin{pmatrix} a_{11} \oplus B & a_{12} \oplus B & \cdots & a_{1S'} \oplus B \\ a_{21} \oplus B & a_{22} \oplus B & \cdots & a_{2S'} \oplus B \\ \vdots & \vdots & \ddots & \vdots \\ a_{R'1} \oplus B & a_{R'2} \oplus B & \cdots & a_{R'S'} \oplus B \end{pmatrix} \tag{59}$$

Further we define the *formal logarithm* of a matrix A as

$$LnA = (\ln a_{ij})$$

By using this formal logarithm of a matrix, as for real positive numbers x and y, we have ln(xy)= lnx+lny, so one can easily prove the following formula

$$Ln(A \otimes B) = LnA \oplus LnB \tag{60}$$

Similarly, one also may define the *formal exponential* of a matrix as

$$ExpA = Ln^{-1}A = (\exp a_{ij})$$

Let $F_{N_x}[P_x, Q_x]$, $F_{N_y}[P_y, Q_y]$, and $F_{N_z}[P_z, Q_z]$ be three 1D Fourier transform matrices, respectively. It is known that direct factorization of the multidimensional Fourier Transform is possible[105]

$$F_{N_x,N_y,N_z}[P,Q] = F_{N_x}[P_x, Q_x] \otimes F_{N_y}[P_y, Q_y] \otimes F_{N_z}[P_z, Q_z] \tag{61}$$

where $P = (P_x, P_y, P_z)$, $\quad Q = (Q_x, Q_y, Q_z)$

and

$$\prod\nolimits_{j=1,\cdots,n}^{\otimes} A_{N_j} = \prod_{j=1}^{n} P(N, N_j)(I_{M_j} \otimes A_{N_j})P(N, M_j) \tag{62}$$

where $\prod^{\otimes}$ represents the multi-tensor-product, $N = \prod_{j=1}^{n} N_j$, $M_j = N / N_j$,

$A_{N_j} \in C^{N_j \times N_j}$, $j = 1, 2, \cdots, n$; $C^{N_j \times N_j}$ represents the $N_j \times N_j$ matrix linear space in the complex scalar field. Furthermore, we need some well-known results.

Some properties of the Kronecker direct product:

$$(A \otimes B)(C \otimes D) = (AC) \otimes (BD) \tag{63}$$

$$A^{-1} \otimes B^{-1} = (A \otimes B)^{-1} \tag{64}$$

$$A \otimes B = (A \otimes I_{dim(B)})(I_{dim(A)} \otimes B) \tag{65}$$

where I_n is an n-by-n unit matrix and dim(A) is the dimension of matrix A, etc. Using these definitions, we get the following 3D FGH formalism, since the 3D kinetic energy operator $T_{N_x,N_y,N_z}(P)$ can be represented as an algebraic sum of three 1D kinetic energy operators, $T_{N_x}(P)$, $T_{N_y}(P_y)$, and $T_{N_z}(P_z)$. i.e.

$$T_{N_x,N_y,N_z}(P) = T_{N_x}(P_x) + T_{N_y}(P_y) + T_{N_z}(P_z) \tag{66}$$

where $P = (P_x, P_y, P_z)$. After FGH discretization we have

Theorem 1(Multidimensional Kinetic Energy FGH Representation) In the matrix form of the FGH discrete momentum representation before 'phase shift', the sum in Eq.66 becomes a Kronecker tensor sum as

$$T_{N_x,N_y,N_z}(P) = T_{N_x}(P_x) \oplus T_{N_y}(P_y) \oplus T_{N_z}(P_z) \tag{67.a}$$

And the corresponding matrix form after 'phase shift' is

$$T^{FGH}_{N_x,N_y,N_z}(P) = T^{FGH}_{N_x}(P_x) \oplus T^{FGH}_{N_y}(P_y) \oplus T^{FGH}_{N_z}(P_z) \tag{67.b}$$

where $T_{N_\alpha}^{FGH}(P_\alpha) = X_{N_\alpha} T_{N_\alpha}(P_\alpha) X_{N_\alpha}^{-1}$ $(\alpha = x, y, z)$, and X_{N_x}, X_{N_y} and X_{N_z} are the corresponding 1D 'phase-shift' transformations, respectively.

proof: The (k,j)-element in $F_{N_x}[P_x, Q_x]$ is

$$f_{kj}^{x} = \frac{1}{\sqrt{2\pi}} e^{\frac{2\pi i}{N} kj} = \frac{1}{\sqrt{2\pi}} e^{i p_{x,k} \cdot q_{x,j}} \tag{68}$$

That means in FGH space we have an one-one correspondence between $F_{N_x}[P_x, Q_x]$ and P_x, and a similar relation exists between P_x and $T_{N_x}(P_x)$. This is the basic idea of the proof. Let C_h be such a mapping: $C_h : ipq \rightarrow \frac{1}{2m} p^2$. Thus we define

$$G_{N_x}[P_x, Q_x] = \sqrt{2\pi} F_{N_x}[P_x, Q_x] \tag{69}$$

and then we have

$$V_C^{-1} C_h (\mathrm{Ln} G_{N_x}[P_x, Q_x])_j = T_{N_x}(P_x) \tag{70}$$

It is easy to see that the above relation is valid for multidimensional FGH too, i.e.

$$G_{N_x, N_y, N_z}[P, Q] = \sqrt{(2\pi)^3} F_{N_x, N_y, N_z}[P, Q] \tag{71}$$

and then

$$\begin{aligned}
&T_{N_x, N_y, N_z}(P) = V_C^{-1} C_h (\mathrm{Ln} G_{N_x, N_y, N_z}[P, Q])_1 \\
&= V_C^{-1} C_h \{\mathrm{Ln}(G_{N_x}[P_x, Q_x] \otimes G_{N_y}[P_y, Q_y] \otimes G_{N_z}[P_z, Q_z])\}_1 \\
&= V_C^{-1} C_h \{\mathrm{Ln} G_{N_x}[P_x, Q_x] \oplus \mathrm{Ln} G_{N_y}[P_y, Q_y] \oplus \mathrm{Ln} G_{N_z}[P_z, Q_z])\}_1 \\
&= V_C^{-1} C_h \{\mathrm{Ln}(G_{N_x}[P_x, Q_x])_1\} \oplus V_C^{-1} C_h \{\mathrm{Ln}(G_{N_y}[P_y, Q_y])_1\} \oplus V_C^{-1} C_h \{\mathrm{Ln}(G_{N_z}[P_z, Q_z])_1\} \\
&= T_{N_x}(P_x) \oplus T_{N_y}(P_y) \oplus T_{N_z}(P_z)
\end{aligned}$$

That proves Eq.67a). For Eq.67b), we notice that the following relations are valid

$$X_{N_x} \mathrm{Ln} G_{N_x}[P_x, Q_x]) X_{N_x}^{-1} = \mathrm{Ln}\{X_{N_x} G_{N_x}[P_x, Q_x] X_{N_x}^{-1}\}$$

$$C_h X_{N_z} = X_{N_z} C_h$$

then the relation (70) is still true, i.e.

$$V_C^{-1} C_h (\mathrm{Ln}\{X_{N_z} G_{N_z}[P_x, Q_x] X_{N_z}^{-1}\})_j = X_{N_z} T_{N_z}(P_x) X_{N_z}^{-1} = T_{N_z}^{FGH}(P)$$

The remainder of the proof is similar to the above proof for Eq.67a)

--- QED

Let $H_{N_x,N_y,N_z}(Q)$ be a 3D Hamiltonian representation in configuration space and $V_{N_x,N_y,N_z}(Q)$ be its potential energy matrix. then

$$H_{N_x,N_y,N_z}(Q) = T_{N_x,N_y,N_z}(Q) + V_{N_x,N_y,N_z}(Q)$$

$$= F_{N_x,N_y,N_z}^{FGH\ -1} T_{N_x,N_y,N_z}^{FGH}(P) F_{N_x,N_y,N_z}^{FGH} + V_{N_x,N_y,N_z}(Q) \qquad (72)$$

where $F_{N_x,N_y,N_z}^{FGH} = (X_{N_x} F_{N_x} X_{N_x}^{-1}) \otimes (X_{N_y} F_{N_y} X_{N_y}^{-1}) \otimes (X_{N_z} F_{N_z} X_{N_z}^{-1})$, is the 3D FGH Fourier transform matrix; it is related to F_{N_x,N_y,N_z} (Eq.61) through the 'phase shift'. The factorization in Eq.42 is mathematically rigorous, with no approximation involved. This enables us to avoid the dimension correlation loss in Cartesian factorization, as in Dutta et. al.[91]. However, it does entail more extensive computation cost. For example, a (15,15,21) 3D grid in our *ab initio* potential energy scanning will produce a 4725 x 4725 FGH Hamiltonian matrix, and to diagonalize such a large matrix a 200 Mbyte physical memory is necessary. A complete run of such a FGH job on our DEC computer needs about 17 CPU hours.

To set up the 3D Hamiltonian matrix $H_{N_x,N_y,N_z}(Q)$ we use again the following three-step scheme corresponding to the 1D case in eqn. 16

1) $T^{(j)}(Q) = \{F^{-1}[P,Q] T(P) F[P,Q]\} e_j$ (73a)

2) Phase-shift of $T^{(j)}(Q)$ (73b)

$$3)\ H^{(j)}(Q) = T^{(j)}(Q) + V^{(j)}(Q) \tag{73c}$$

where $T^{(j)}$ represents the j-th column of matrix T, e_j is the j-th standard unit column vector in q-space, j=1,2, ... , N. The term 'phase shift' is a translation of the momentum grid points such that the midpoint is sited at the origin. Actually the scheme of the 'phase-shift' of the 3D system is similar to that of the 1D system. The following theorem is the key to our factorization scheme of the 3D FGH algorithm:

Theorem 2 (Factorization of Three-Dimensional FGH Kinetic Energy)

$$T_{N_x,N_y,N_z}(Q) = F^{FGH}_{N_x,N_y,N_z}{}^{-1} T^{FGH}_{N_x,N_y,N_z}(P) F^{FGH}_{N_x,N_y,N_z} = X_{N_x,N_y,N_z} F_{N_x,N_y,N_z}{}^{-1} T_{N_x,N_y,N_z}(P) F_{N_x,N_y,N_z} X^{-1}_{N_x,N_y,N_z} \tag{74}$$

where $X_{N_x,N_y,N_z} = X_{N_x} \otimes X_{N_y} \otimes X_{N_z}$.

Proof: To prove this theorem one more lemma is needed.

Lemma Let X, Y, A, B be matrices which make the matrix multiplication valid in the following equations, and $I_{\dim A}$ and $I_{\dim B}$ are unit matrices with dimension dim(A) and dim(B), respectively, then

$$(XA) \oplus B = (X \otimes I_{\dim B})(A \oplus B) \tag{75}$$

$$A \oplus (YB) = (I_{\dim A} \otimes Y)(A \oplus B) \tag{76}$$

(Notice that if one replaces all the direct sum sign with direct product sign the above two equations are still valid). We only give a demonstration of the first equation. Let

$$X = \begin{pmatrix} 1 & & \\ & & 1 \\ & 1 & \end{pmatrix}, \quad A = \begin{pmatrix} a_{11} & a_{12} & a_{13} \\ a_{21} & a_{22} & a_{23} \\ a_{31} & a_{32} & a_{33} \end{pmatrix}, \quad B = \begin{pmatrix} b_{11} & b_{12} & b_{13} \\ b_{21} & b_{22} & b_{23} \\ ba_{31} & b_{32} & b_{33} \end{pmatrix}$$

A direct calculation shows

$$\text{left hand side} = \left\{\begin{pmatrix} 1 & & \\ & & 1 \\ & 1 & \end{pmatrix}\begin{pmatrix} a_{11} & a_{12} & a_{13} \\ a_{21} & a_{22} & a_{23} \\ a_{31} & a_{32} & a_{33} \end{pmatrix}\right\} \oplus B$$

$$= \begin{pmatrix} a_{11}+B & a_{12}+B & a_{13}+B \\ a_{31}+B & a_{32}+B & a_{33}+B \\ a_{21}+B & a_{22}+B & a_{23}+B \end{pmatrix}$$

$$\text{right hand side} = \left\{\begin{pmatrix} 1 & & \\ & & 1 \\ & 1 & \end{pmatrix} \otimes I_3\right\}\left\{\begin{pmatrix} a_{11} & a_{12} & a_{13} \\ a_{21} & a_{22} & a_{23} \\ a_{31} & a_{32} & a_{33} \end{pmatrix} \oplus B\right\}$$

$$= \begin{pmatrix} I_3 & & \\ & & I_3 \\ & I_3 & \end{pmatrix}\begin{pmatrix} a_{11}+B & a_{12}+B & a_{13}+B \\ a_{21}+B & a_{22}+B & a_{23}+B \\ a_{31}+B & a_{32}+B & a_{33}+B \end{pmatrix}$$

$$= \begin{pmatrix} a_{11}+B & a_{12}+B & a_{13}+B \\ a_{31}+B & a_{32}+B & a_{33}+B \\ a_{21}+B & a_{22}+B & a_{23}+B \end{pmatrix}$$

Now we are going to use these formulae and equation to prove our theorem for the two dimensional case only:

$$\begin{aligned}
&(X_{N_x} T_{N_x}(P_x) X_{N_x}^{-1}) \oplus (X_{N_y} T_{N_y}(P_y) X_{N_y}^{-1}) \\
&= (X_{N_x} \otimes I_{N_y})\left\{(T_{N_x}(P_x) X_{N_x}^{-1}) \oplus (X_{N_y} T_{N_y}(P_y) X_{N_y}^{-1})\right\} \\
&= (X_{N_x} \otimes I_{N_y})(I_{N_x} \otimes X_{N_y})\left\{(T_{N_x}(P_x) X_{N_x}^{-1}) \oplus (T_{N_y}(P_y) X_{N_y}^{-1})\right\} \\
&= (X_{N_x} \otimes X_{N_y})\left\{(T_{N_x}(P_x) X_{N_x}^{-1}) \oplus (T_{N_y}(P_y) X_{N_y}^{-1})\right\} \\
&\Rightarrow \cdots\cdots \\
&= (X_{N_x} \otimes X_{N_y})\left\{T_{N_x}(P_x) \oplus T_{N_y}(P_y)\right\}(X_{N_x}^{-1} \oplus X_{N_y}^{-1})
\end{aligned}$$

— QED

A 'phase-shift' scheme for the 3D system, like that for the 1D system, becomes

$$H_1(Q)\Psi_1(Q) = E\Psi_1(Q) \tag{77}$$

where

$$H_1(Q) = T_{N_x,N_y,N_z}(Q) + X^{-1}_{N_x,N_y,N_z} V_{N_x,N_y,N_z}(Q) X_{N_x,N_y,N_z} \tag{78}$$

$$\Psi_1(Q) = X^{-1}_{N_x,N_y,N_z} \Psi(Q) \tag{79}$$

where $\Psi(Q)$ is the eigenfunction of the original Hamiltonian linear system, i.e.

$$H(Q)\Psi(Q) = E\Psi(Q) \tag{80}$$

4.2.5 ACCURACY

As shown by Marston and Balint-Kurti, 1D FGH calculations yield highly accurate eigenvalues and eigenfunctions. The FGH accuracy is determined by the shape of the potential energy surface (PES) V(x), and the location, the range and the density of the grid point region in configuration space, i.e. by the three parameters: (q_1, N, Δq), or (q_1, q_N, Δq), or (q_1, q_N, N) (all of these are equivalent). The PES limits the accuracy of the FGH method and it is an intrinsic error source in the calculation. As a direct input to the FGH, the PES cannot be improved by the FGH itself. The three parameters are assigned by the FGH program and they are the major concern in an FGH calculation. In fact, for a one-particle FGH system like ours, these three parameters uniquely determine the FGH system itself. By using two grid point range schemes, one with 65 and the other 129 points, MBK applied their 1D FGH on a well-known Morse potential Hamiltonian system, H_2. The lowest eigenvalue differs by only 10^{-8} a.u. from that of the analytical eigenvalue in both schemes. The corresponding FGH eigenfunctions also show very good accuracy in both magnitude and curvature. We repeated their calculation using our own 1D FGH program and got similar results.

The major error produced in a FGH calculation comes with the truncation and

discretization (Trunc-Disc) of configuration space from continuous infinite range ($-\infty$, $+\infty$) to discrete finite range $\{p_{-[(N-1)/2]}, p_{-[(N-1)/2]+1}, \ldots, p_{-1}, p_0, p_1, \ldots, p_{[(N-1)/2]}\}$. After this operation, the FGH is exact without losing any further accuracy. Unfortunately, like semiclassical methods, which have become powerful tools in quantum mechanical calculation in recent decades, there is no pure mathematical formalism which can be used in error analysis of FGH methods. Generally, a function that is bounded in momentum space is equivalent to the Fourier transform of the function being band limited. The accuracy of a discrete grid point representation of the function is assured by the well-known Shannon sampling theorem[106], which states that the functional values should be given by a sufficiently dense set of equally spaced sampling points.

For the 3D FGH method, our FGH program has been tested by using the 3D symmetric harmonic Hamiltonian system.

It is well-known that the 3D symmetric harmonic potential Hamiltonian in atomic units is

$$H = \frac{p_x^2 + p_y^2 + p_z^2}{2} + \frac{1}{2}(x^2 + y^2 + z^2) \tag{81}$$

Its analytical eigensystems are:

$$E_{n_x,n_y,n_z} = n_x + n_y + n_z + 3/2$$

$$\Psi_{n_x,n_y,n_z}(x,y,z) = N e^{-\frac{1}{4\pi}(x^2+y^2+z^2)} H_{n_x}\left(\frac{x}{\sqrt{2\pi}}\right) H_{n_y}\left(\frac{y}{\sqrt{2\pi}}\right) H_{n_z}\left(\frac{z}{\sqrt{2\pi}}\right)$$

where $n_x, n_y, n_z = 0, 1, 2, \cdots$: $N = \left[\frac{1}{2^{n_x+n_y+n_z+3/2}\pi^3 n_x! n_y! n_z!}\right]^{1/2}$

A (9,9,9) grid point scheme, with lattice spacing 0.835 a.u., and a (15,15,15) grid point scheme, with lattice spacing 0.653 a.u., have been calculated. The FGH zero-point energy in the (9,9,9)-scheme is less than 10^{-4} a.u. different from the analytical result, while that in the (15,15,15)-scheme is less than 10^{-8} a.u. different from the analytical result in the lowest state, 10^{-7}

a.u. in the highest tested. Additional levels were calculated, with comparable accuracy. *Table* 1 shows the calculated eigenvalues and the analytical eigenvalues.

The 3D particle in a box is not a suitable potential for this approximation, as moving the position of the wall between grid point positions produced discrepancies large compared to those shown above. Solving for a molecular wave function uses a smooth PES, much more like that of the harmonic oscillator; therefore, the particle in a box problem was not be considered further.

TABLE I

Eigenvalues (a.u.) for 3D Harmonic Oscillator, with FGH approximation

Quantum numbers	(9,9,9) grid	(15,15,15) grid	analytical values	degeneracy
(0,0,0)	1.499979569192	1.499999998013	1.500000000000	1
(1,0,0)	2.500152638083	2.500000020381	2.500000000000	3
(1,1,0)	3.497712218151	3.499999285770	3.500000000000	3
(2,0,0)	3.500325706975	3.500000052601	3.500000000000	3
(2,1,0)	4.497885287043	4.499999308139	4.500000000000	6
(1,1,1)	4.500498775867	4.500000084821	4.500000000000	1

- Results and Discussion

In summary, all the work we have done is on the following two models:

1) Model (a): Methylamine + Proton + Methylamine (MPM)

2) Model (b): Water + Proton + Methylamine (WPM)

For model (a) we calculated the PES of the following three molecular configurations at two different *ab initio* levels:

1.1) Low Level Calculation (i.e. HF level)

Full opt (NN ≈ 2.8 A) (MPM28hf)
Partial opt at NN = 3.2 A (MPM32hf) } HF/6-31G** // HF/6-31G** with fields // FGH
Partial opt at NN = 3.6 A (MPM36hf)

where the first method and basis set combination 'HF/6-31G**' represents the optimization and the basis set used in G94, the second method and basis set combination 'HF/31G**', which is separated by double forward slashes, represents the PES scan method and the basis set used in G94, and FGH is the method in the third step for calculating the proton wave function under the corresponding PES background. The following uses the same notations.

1.2) High Level Calculation (i.e. Post-HF level)

Full opt (NN ≈ 2.7 A) (MPM27dft)
Partial opt at NN = 3.2 A (MPM32dft) } B3LYP/D95+* // MP2/6-31+G* with fields //
Partial opt at NN = 3.6 A (MPM36dft)

FGH

For model (b) we calculated the PES of the following three different molecular configurations at HF levels only:

2) HF Level Calculation

Full opt (ON ≈ 2.8 A) (WPWM28hf)
Partial opt at ON = 3.0 A (WPM32hf)
Partial opt at ON = 3.35 A (WPM33hf) } HF/6-31G** // HF/6-31G** with fields // FGH
Partial opt at ON = 3.6 A (WPM36hf)

The general form of the notations of models in our calculation is as follows:

$$\underbrace{A\ A\ A}_{\text{molecular system}}\ \underbrace{B\ B}_{\substack{\text{NN / NO}\\ \text{distance}}}\ \underbrace{C}_{\substack{\text{ab initio calculation}\\ \text{level}}}\ -\ \underbrace{D}_{\text{external field}}$$

For example, MPM36hf-0f means model system is MPM, the NN distance is fixed at 3.6 Å, the *ab initio* calculations were carried out on the HF level (i.e., optimized with HF/6-31G** and scanned with HF/6-31G**); MPM27MP2-f1 means that model is MPM, the NN distance is the distance at the full optimized configuration (since in the full optimized configuration the NN distance is about 2.7 Å), the *ab initio* calculation were carried out on the post-HF level (i.e., optimized with B3LYP/D95+* and scanned with MP2/6-31+G*).

For each configuration of these models, we used different fields in the background when we scanned its PES before carrying out the FGH calculation. One of our major purposes is to locate the *critical field* or *resonance field* that makes the final FGH ground state wave function symmetric. The other purpose is to investigate the field range that makes the asymmetry of the ground state wave functions large enough from both sides, so that we may compare this range with the action potential in ion channel gating. This section we first discuss the results of model MPM, and then that of WPM.

For a satisfactory description of proton transfer, one must consider the displacement of the electrons connected with the displacement of the proton in the H-bond. Hartree-Fock calculations have shown that usually less than one electron charge is dragged by the movement of the proton. The most important contribution to the dipole moment is caused by the electron shifts in the proton acceptor and donor. The electrons are shifted in a direction opposite to that of the proton and thus enhance the dipole moment caused by the proton displacement. Hence, the derivative of the dipole moment with respect to the proton displacement is usually greater than one proton charge. The

accuracy requirements for the calculation are fairly stringent; one must be able to see the shift in the proton with a small field change superimposed on a much larger value. On the other hand, the fact that the difference in field, not only the absolute value, is critical, makes the task in certain respects easier; the difference calculation can be considered to be superimposed on an almost constant background, if the background field is not too high to be plausible. (Recalling that the motivation of our work is to study a possible gating model for ion channels, it is worth pointing out that any gating model would be similar in that it must operate with a small change in field, almost certainly superimposed on a much larger local field; see Discussion.) It is possible, if one has the complete potential energy surface (PES), with a range of fields, including zero field, to find the proton wave function from the PES at each field. We have done this, finding the PES by *ab initio* calculation, for a specific pair of molecules, two methylamines (*Fig.* 6); thus we can directly calculate the effect of field on the transfer of a proton between the two wells accompanying a real pair of molecules. To obtain the wave function, we used the Fourier Grid Hamiltonian (FGH) technique, which we have extended to a full three dimensional calculation.

There are basically two factors that have non-negligible influence on proton transfer: vibrations of the skeleton nuclei and polarization of the surrounding medium. The rearrangement between the two possible 'protomeric' structures of a double well system is closely connected not only with a pure proton displacement but with a change of the configurations of other nuclei in the system[107] also. Usually the thermal motions of the molecules can modulate the potential energy surface of the proton over a period of 10^{-11} to 10^{-13} s[29]. That means if the proton residence time is $\sim 10^{-8}$ or longer, the vibration assisted proton tunneling will take only an averaged form, and consequently a minor correction on the rate of the proton transfer. At one-dimensional approximation level of proton transfer, the reaction path is characterized by the distance between the two minima locations($\Delta\xi$), the well difference (ΔV) between the two minima, and the barrier height

(V_a). Quantum tunneling is most dramatic when the PES has symmetric double minimum-wells, short $\Delta\xi$, and low V_a. Usually with $\Delta\xi \approx 0.5$ Å and $V_a \approx 12$ kJ mol^{-1}, the proton residence time is 10^{-12} s; but it is about 100 times longer for a 0.2 Å increase in $\Delta\xi$ or for a three-fold increase in E_a. However this method only gives a rather approximate quantitative estimation of proton tunneling rate in one-dimension. For three-dimensional PES, a different profile will have different minima distance $\Delta\xi$, and barrier height V_a. Also, residence time may be completely different in mechanism from transition rate. What we are particularly concerned about is the tunneling rate. The two parameters, $\Delta\xi$ and V_a, are not reliable in our study. The energy difference ΔE, in modern terminology, *energy splitting*, which takes minima distance and energy barrier into account in itself, is a far more accurate parameter in proton tunneling rate estimation. The potential energy V(x) of our model system MPM is determined using the Born-Oppenheimer approximation. Orientational degrees of freedom of an interacting pair of non-linear polyatomic molecules generally fluctuate slowly compared to the intramolecular vibrations. One model which may describe a general proton transition process properly has the molecules rotationally and translationally frozen, while their relative hydrogen bond distance varies. The extent to which proton tunneling plays a role depends on the extent of the vibrational overlap between the initial and final states. In our model a homogeneous external electric field is applied to the model system consisting of two weakly interacting molecules, and the adiabatic approximation is assumed to be valid for all electrons, thus defining the potential energy surface. However, proton transitions between two potential wells, one associated with each of the two molecules, may be considered as quantum transitions among vibrational-like levels of the proton in a potential surface dictated by the configuration of all other atoms. The only vibrations that are resonantly enhanced or suppressed are those for which there is a change in equilibrium displacement, i.e., those that are

coupled to the proton transfer. The proton tunneling rate in our model is linearly governed by the energy splitting ΔE, i.e.

$$\Delta E = \frac{\hbar\omega}{\pi} \exp\left(-\frac{1}{\hbar} \int_{-a}^{a} |p(x)| dx \right)$$

where (-a, a) is the tunneling region, p is the momentum and ω the frequency of a single well at the energy of the eigenvalue[108]. That means from the energy splitting, which is linearly proportional to the transition frequency, we may estimate the tunneling rate ω using the above equation, and from the tunneling rate ω we may make further judgement on the extent that the tunneling is assisted by the vibration of other nuclei. Furthermore, recent theoretical studies by Cukier and Morillo[21] show that the proton transition rate, when the reaction happens in an polar solvent, is proportional to the square of the energy splitting. This conclusion is more favorable in supporting application of our results, in the condensed phase. As we already indicated, the tunneling frequency, ω, cannot be too high or too low compared with the vibrational frequencies of other skeleton nuclei, in order to have coherent coupling between tunneling and vibration. This is the characteristic distinction between electron tunneling and proton tunneling. For electron tunneling, the tunneling rate ω is usually too high to cooperate with the vibrations of the surrounding nuclei. When electrons make a transition the nuclei are too slow to follow its step. This is exactly the Franck-Condon rule extensively used in spectroscopy analysis. However, for protons the situation is completely different. In general the proton transition rate ranges from 10^{-3}s to 10^{-15}s, overlapping the range of thermal fluctuation of the potential energy surface, 10^{-11}s to 10^{-13} s. If the transition time is around 10^{-15}s, the Franck-Condon principle is still applicable and vibration-assistance can be neglected. On the other hand, if the transition time is around 10^{-6}s, although the Franck-Condon rule is no longer valid, vibration-assistance may also be overlooked since the faster vibration effect will be coupled into the

transition only in an averaged form. From TABLE II, we see that, at Hartree-Fock level calculation, vibration-assistance can not be overlooked. But as the calculation goes up to post-HF level, the situation becomes completely different. If we also take the medium effect into account, the transition rate will be further slowed down (see next section). Based on this analysis and the nature of our major concern, the vibration-assistance effect will not be considered further in detail in our current work.

The environment of a model system has a strong influence on the proton motion in H-bonds because of the high polarizibility of the H-bond as well as the large magnitude of the field.

TABLE II

Results of energy splitting and transition time estimation

Property / Model	Splitting (a.u.)	Splitting (cm^{-1})	Zero-point freq. (cm^{-1})	Transition time[a] (10^{-12}s)
MPM28-HF-0f	0.00214	74	1.3583	0.011
MPM32-HF-0f	0.00353	124	15.8994	0.0069
MPM36-HF-0f			16.3901	
MPM27-B3LYP-0f	0.00216	76	31.2938	0.011
MPM32-B3LYP-0f	0.00312	109		0.0078
MPM36-B3LYP-0f	0.00391	137		0.0062
MPM32-HF-f1	0.0000467	1.6		0.52
MPM32-HF-f2	0.000113	4.0		0.21
MPM36-HF-f1	0.000146	5.1		0.17
MPM36-HF-f2	0.0000295	1.0		0.82
MPM32-MP2-f1	0.000000121	0.0042		200
MPM32-MP2-f2	0.000000130	0.0046		186
MPM36-MP2-f1	0.000000143	0.0050		169
MPM36-MP2-f2	0.000000116	0.0040		210
MPW36-HF-f1	0.0000126	0.44		1.9
MPW36-HF-f2	0.0000105	0.37		2.3

Note: Energy conversion 1 a.u. ≅ 35,000 cm^{-1} (1 kJ/mole ≅ 3.35 cm^{-1})

[a] Calculation based on Helley's formula

The local electric field changes the potentials of the H-bond protons and changes their symmetry. A dipole moment different from zero arises when the symmetry of the potential is disturbed, e.g., by an external electric field with a non-vanishing component in the bond axes. As discussed before in the case a direct electric field applied, when the external factor becomes a dipole a similar situation appears. The potential well in the field direction is lowered, causing the wave function to become asymmetrical, too. In the ground state, the position probability becomes greater in the lower well than in the higher well; therefore the hydrogen bond is polarized in the direction of the field. In the first excited state, however, the position probability increases in the higher well: the H-bond is polarized against the field. Our *ab initio* plus FGH results are consistent with the expectation that the wave functions are extremely sensitive to disturbances of the symmetry of the potential surface topology. A tiny displacement of the potential wells relative to each other is sufficient to localize the proton almost completely in the deeper well in the ground state, and in the higher well in the first excited state, if the wells are even moderately separated. The high polarizability of hydrogen bonds with a symmetrical double-well potential is decisive for the influence of the molecular environment on the proton transfer and on the coupling of protons in adjacent hydrogen bonds. It is well-known that this proton transfer polarizability is approximately 2-orders of magnitude greater than the usual electron transfer polarizability which is not associated with considerable nuclear displacements[109]. Although proton transfer in condensed phase under the influence of an electric field has been studied to only a very limited extent, proton transfer in solutions has been studied extensively[88]. Since the electronic field is the common essential driving force shared by both of these environments, results in the study of proton transfer in solutions can be used for comparison in study of proton transfer in condensed phase under controllable electric fields.

The fields required for a switch, and the extent of the switch in proton wave function, must be determined: the ratio of the wave function peak in the dominant well to that in the other well may exceed 10^2, or be only, say, 3, a physically considerably different case. We find a field of the order of 10^5 V m^{-1} sufficient to effect a virtually complete switch (ratio of wave function peaks in the two wells > 10, for probability ratios > 10^2:1) in the case of N-N separation of 3.6 Å, while the wave function peak ratio can be as low as ≈3:1 (probability ratio ≈10:1) with the same field difference for 3.2 Å. We are concerned with a transfer which takes place in a time short compared with the time for the field to change, leaving the proton in one of the two wells, and with almost no possibility of transferring back until the field again crosses the value which allows the wells to match. From our previous discussion in 'Introduction', Morillo and Cukier have shown[22] that a constant field may suppress the tunneling of a proton in a symmetric double well system. Once the proton is locked on one well of the double well system, it starts immediately polarizing its environment (on the electronic motion time scale). This is equivalent to re-optimization of the whole system with the proton initially in the other well under a constant external electric field. Usually this medium re-organization would take a much longer time than a proton transfer to get itself into a new equilibrium state, but it is still much shorter than a time period for the field to get into the correct range in magnitude. Until all that happens, the proton resides in one well, with overwhelming probability. The final new equilibrium state will last even after the external field goes back to the original level. We have tested this idea by optimizing our model system with a different initial proton location. We found that with a proton initially localized in a potential well the corresponding optimized system will adjust the system configuration so that the corresponding well becomes a global well of the system. This *initial- privilege* in optimization is not only a general result of theoretical calculation, but a general phenomenon in chemical and biological

systems. Because the proton will almost always be welcomed by its new 'neighbors', its transition rate will be slowed down relative to that of the gas phase medium. The tendency of the medium to slow down proton transitions is ubiquitous. For example, in a typical symmetric tautomerization reaction such as intramolecular proton transition in the α-hydroxy phenoxyl radical, the gas phase rate is estimated around 30 ps[111] while in solution it falls by many orders on magnitude (to about 1 ms at 170 K[112]); another example is that it has been found repeatedly that intramolecular proton transfer reactions in hydrocarbons are very fast (ps)[113] while for the same compound the rate is greatly reduced in polar solvents such as alcohols and ethers[114]. We therefore do not consider the dynamics of the system, merely requiring that transfer leads to wave functions that can be considered separately for each field and are treated as time-independent. The transfer itself should be fast compared to field changes. While we do obtain the pair of levels showing splitting, the implications for a transfer time, and the importance, if any, of the transfer time for the biological system, will not be discussed.

Our calculations were carried out in a 3D grid region. One-dimensional tunneling has been much more clearly understood than two-dimensional and higher dimensional tunneling[115]. Theoretical study on high-dimensional tunneling in reaction dynamics is still a very difficult problem. This is another reason we used the 3D FGH scheme but omitted dynamic studies.

1. Optimization of MPM

The MPM model has been fully optimized first at Hartree-Fock Self Consistent Field (HF) level with 6-31G** basis set and no external electric field applied (see *Fig.*6(a)), and the same procedure were repeated at B3LYP/D95+* level (*Fig.*6(b)). It is well known that the HF method is good for calculation of molecular geometry and vibrational modes, because the HF method with basis set 6-31G* gives accurate bond lengths and bond angles (<1%)[116]. However, we need more

accurate energy values than HF-SCF provides for estimation of the tunneling splitting, so this technique, although fast, was used primarily for comparisons and tests only. For more accurate calculation, post-HF is necessary. In the past decade Hartree-Fock Kohn-Sham (HF-KS) theory

(a) (b)

Fig.6 — Fully optimized MPM model. (a) at HF/6-31G** level; (b) at B3LYP/D95+* level

or hybrid theory has become more popular in calculations of electronic structure of molecules[117-119]. Barone and Adamo[120] have used the B3LYP method to study proton transfer in the ground and lowest excited states of malonaldehyde, with excellent results. The accuracy of Becke-Perdew (BP) and Becke-Lee-Yang-Parr(BLYP) is comparable to that of MP2 and above, second order Mφller-Plesset perturbation theory, in descriptions of hydrogen bonding. So in the second stage of our calculation a post-HF scheme B3LYP/D95+*//MP2/6-31+G* has been adopted, i.e. first (full or partial) configuration optimizatien at B3LYP/D95+* level and then PES scanning with external

fields at MP2/6-31+G* level.

After full optimization and corresponding PES scanning on a proper rectangular 3D lattice grid (*Fig.*7), with no field, the output of the PES was saved. It became an input to a complete FGH calculation using our 3D FGH code. and then the proton wave function is obtained. This is a complete run for a single model in our work.

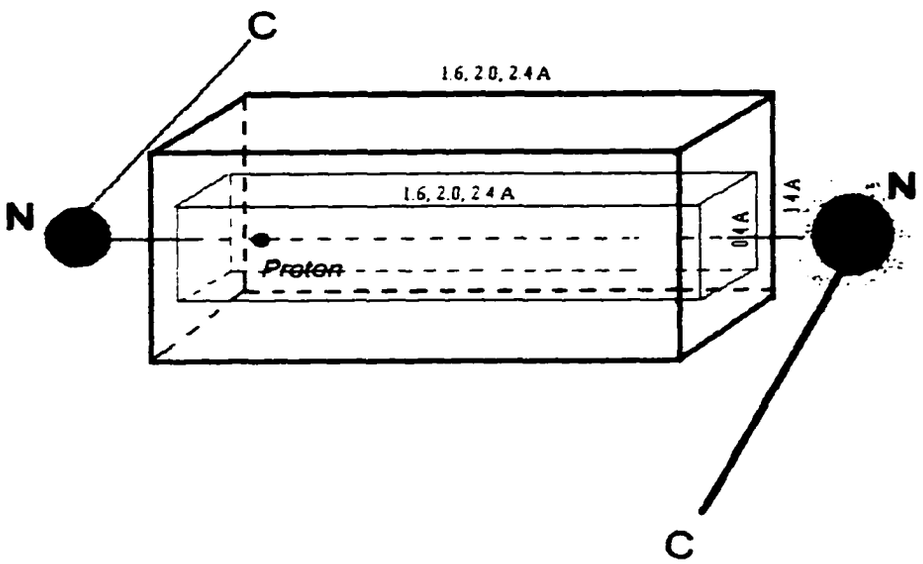

Fig.7 — Grid lattice for establishing PES in scanning. The inside grid lattice is used in the 'sandwich' scanning scheme for post-HF calculation.

Once the first run has been completed, the nitrogen-nitrogen (N-N) distance of MPM was extended to 3.2 Å and 3.6 Å and partially optimized at these fixed N-N distances (i.e., optimized save for the constraint on the N-N distance) and the resulting configurations have almost the same

configuration as the one fully optimized, both for HF level and B3LYP level respectively. Selecting these two extended distances resulted from the simulation of two separated amino acid side chains inside ion channels. In the S4 segment of the transmenbrane ion channel protein, two neighboring basic residues are approximately about 3.6 Å ~ 4.5 Å apart. To study how the proton tunnels under the influence of an external electric field between the two fixed methylamines, we start with the Born-Oppenheimer approximation and calculate *ab initio* energies for each of the levels of approximation for the fixed methylamine configurations (3.2 Å, 3.6 Å) in the presence of external electric fields. The proton in each case is placed on each lattice point of the grid, between the N atoms of the two methylamines. The PES consists of the proton energy, in the presence of the external fields, at all grid points. We will go back and talk about further FGH calculation results in detail later. Now we are going to discuss the three optimized structures first.

Table III and Table IV show the optimization results in three NN distance structures at HF level and B3LYP level, respectively. In Table IIIa) and IVa), the second columns give the total electronic energy of the systems in atomic unit; the third columns give the calculated lowest real vibrational frequencies. For both 3.2 Å and 3.6 Å cases, there are 1 imaginary frequency in each case, which is not shown in the tables. The imaginary frequencies result from the constraints on the NN distances. From the tables we see that in all optimized configurations, including full optimization and partial optimizations, and HF level and post-HF level, the proton is always perfectly sited at approximate 1Å away from one of the two N's, which make angle N-P-N nearly 180°. Although the tables show that in both HF and post-HF calculations, the optimized energies rises consistently when the NN distance increases, but the differences are very small. In contrast, the dipole moments increase from one third to one half for each 0.4 Å increment in NN distance, in both HF and post-HF cases. From the results one can find that the dipole moments of the

optimized systems are 3 to 6 Debye. Usually one proton transfer between two methylamines will produce up to 5 Debye change in dipole moment. Because of the *initial- privilege* property, once the proton is stabilized in the new well by its surroundings, the change in dipole moment of the whole system should be larger still. Another attribute shown in the tables is that all the dipoles are only approximately parallel to the NN orientation. For different proton positions, the dipole will be different, but this attribute is consistent for all the grid points on our PES. That means an external field along the NN direction will produce close to the largest change on PES on average. For an ion channel, the orientation of the membrane field produced by the membrane potential may vary relative to the N-N axis. When we selected the field orientation in our calculation, we first tried three fields with only one non-zero component in the Cartesian coordinates, respectively, then try tc adjust the field only in the direction which is most effective in changing the PES. Finally, at HF level the whole system skeleton C1-N1-N2-C2 is approximately planar and the angle between the NN orientation and dipole moment is small, while for high level optimized structures, the dihedral angle C1-N1-N2-C2 is smaller than that at HF level, and the angle between NN orientation and the corresponding dipole moment is larger than that of the HF level. Since there have been no experimental data we can use to compare with, we do not know which one is more accurate.

TABLE IIIa
Optimized HF energies and corresponding dipole moments

Opt[a] methods (HF/6-31G**)	Energy (a.u.)	Zero-point freq. (cm^{-1})	Dipole moment (Debye)	N-N Direction:
Fopt	-190.8478	1.3583	(3.1838, -0.9793, -0.0376) Tot= 3.3312	(-2.5196, 1.2671, -0.0008)
3.2 Popt	-190.8435	15.8994	(4.6918, -1.2418, -0.0579) Total: 4.4211	(-2.9321, 1.2818, -0.0020)
3.6 Popt	-190.8362	16.3901	(6.0529, -1.4059, -0.0615) Total: 6.2144	(-3.3595, 1.2937, -0.0021)

[a]Fopt, fully optimized: Popt, partially optimized, N - N distance constrained

TABLE IIIb

Optimized HF configurations

Level Opt[a]	N-N Distance (Å)	N1-P Distance (Å)	P-N2 Distance (Å)	N1-P-N2 angle (deg)	C1-N1-N2 angle (deg)	N1-N2-C2 angle (deg)	C1-N1-N2-C2 Dihedral angle (deg)
Fopt	2.820	1.055	1.766	179.5	110.9	112.7	-178.0
3.2 Popt	3.200	1.035	2.165	179.5	111.2	113.8	-177.0
3.6 Popt	3.600	1.024	2.576	179.8	111.6	114.1	-176.8

TABLE IVa

Optimized B3LYP energies and corresponding dipole moments

Opt[a] methods (B3LYP/D95+*)	Energy (a.u.)	Zero-point freq. (cm^{-1})	Dipole moment (Debye)	N-N Direction:
Fopt	-192.1438	31.2938	(1.9089, -0.6435, -0.2115) Total: 2.0255	(-2.3937, 1.2607, -0.0022)
3.2 Popt	-192.1403	39.3649	(4.2518, -1.1820, -0.2661) Total: 4.4211	(-3.9598, 1.2848, -0.0065)
3.6 Popt	-192.1321	40.4800	(5.5577, -1.3739, -0.2652) Total: 5.7311	(-3.3578, 1.2982, -0.0086)

[a]Fopt, fully optimized: Popt, partially optimized, N - N distance constrained

TABLE IVb

Optimized B3LYP configurations

Level Opt[a]	N-N Dist. (Å)	N1-P Dist. (Å)	P-N2 Dist. (Å)	N1-P-N2 angle (deg)	C1-N1-N2 angle (deg)	N1-N2-C2 angle (deg)	C1-N1-N2-C2 Dihedral angle (deg)
Fopt	2.705	1.140	1.565	179.9	111.5	112.4	-169.0
3.2 Popt	3.200	1.070	2.130	179.8	111.4	113.6	-165.9
3.6 Popt	3.600	1.051	2.549	179.8	111.4	114.1	-165.1

2. POTENTIAL ENERGY SURFACE (PES) AND FOURIER GRID HAMILTONIAN (FGH) CALCULATION

The calculated potential energies are at the lattice points in a grid region shown by *Fig.*7. It is a three-dimensional Cartesian rectangular lattice. A lattice spacing of 0.1Å was estimated to provide adequate energy accuracy, with attainable computation times. For HF level this scheme

needs about two to three weeks to complete a single run, a tolerable time and of good accuracy. For high level *ab initio* calculations, it became impractical, because of the time required, to do a 0.1 Å scan of the energy surface, where "scan" means that the proton was placed on each point of the grid, and the energy computed by *ab initio* calculation. However, it was more accurate to do the FGH on a 0.1 Å lattice, so an interpolation procedure was developed for post-HF calculation. Except in the critical regions of the PES (5x5x25 points, for 3.6 Å, and 5x5x21 points, for 3.2 Å N- N separation, with the region defined around the N - N axis), where the complete 0.1 Å lattice was always computed, the energy was evaluated on a 0.2 Å lattice and a three dimensional cubic spline interpolation technique (3D-CSI) was used to complete the lattice for the FGH determination of the wave function. We call this a 'sandwich' scheme. The code for the 3D-CSI was developed by Adams[123]. The complete lattice was 15 x 15 x 21 for the 3.2 Å case (1.4 x 1.4 x 2.0 Å), and 15 x 15 x 25 points for the 3.6 Å case.

While one dimensional cubic spline interpolation has been extensively used in potential energy surface calculations, very few examples of 3D-CSI of PES have been published due to its lower accuracy. The first serious tests of 3D-CSI have been given by Sathyamurthy and Raff [124]. They found a (15×15×15) grid point cubic spline interpolation did not possess sufficient accuracy to give a point-to-point match of a quasiclassical trajectory to that obtained on the analytical surface, although the total reaction cross sections, energy partitioning distributions, and spatial scattering distributions computed by quasiclassical trajectories on the spline surface, were in good accord with those obtained from the analytic surface. However, we choose three-dimensional cubic spline interpolation based on the quality of the interpolation of the PES's of our models. Since all of the PES's used in our work are basically of quadratic form, and their curvature changes smoothly and linearly, our cubic spline interpolation PES is much more accurate than that in

Sathyamurthy and Raff's work. We tested our interpolation scheme for one case, a Hartree-Fock PES, as this could be determined at all grid points for comparison with the interpolated value; however, the quality of the interpolation will be the same for the post HF wave functions, as the curvature is not significantly different, and the FGH procedure identical. The results for the error (interpolated less directly computed values) in the wave function are (averaged over all grid points):

$$E(|\Delta\psi|) = 0.00765$$
$$\sigma = \sqrt{E(\Delta\psi - E(\Delta\psi))^2} = 0.0314$$

where $\Delta\psi = \psi' - \psi$, and ψ, ψ' are wave function values based on the spline values and the complete grid at corresponding grid points, $E(*)$ is the average value of random variable $(*)$, and $\sigma(*)$ is the standard deviation. The interpolation is excellent near the peaks of the wave function. This is also true near the barrier maximum. What error exists in interpolation comes in the region of high slope of the PES. In other words, the error, to the extent that it exists, has no practical effect at all on any feature of the wave function involved in the conclusions. The corresponding average errors for the PES are:

$$E(|\Delta V|) = 0.000836$$
$$\sigma = \sqrt{E(\Delta V - E(\Delta V))^2} = 0.00192$$

2.1) *Zero field*: *Ab* initio calculations of PES on two methylamine molecules with one excess proton were carried out using Gaussian 94 at both Hartree-Fock Self Consistent Field (HF-SCF) level, and MP2 level which includes electron correlation. The post-HF optimization for the system was done using the density functional theory B3LYP approximation, which allowed for correlation energy as well as polarization of the orbitals. This produces a N-N distance of 2.82 Å at HF level

and 2.71 Å at B3LYP level, respectively, with a very low barrier, 0.0147 a.u. (≈ 77 kJ/mole) for MPM28HF (i.e. model MPM at fully optimized separation at HF level, 2.82 Å) and 0.00327 a.u. (≈ 17 kJ/mole) for MPM27B3LYP (i.e. model MPM at fully optimized separation at B3LYP level, 2.71Å), respectively, in the potential well for the proton. It is worth emphasizing that with high level *ab initio*, the barrier is 5 times smaller than that obtained at HF level. As a consequence of the low barrier, the proton is effectively delocalized within the potential well, allowing no possibility of transferring the proton from one location to another. It was not possible to do multiple cases using the B3LYP method, as each point in a scan required 9 minutes; a 5000 point scan would then need 4.5×10^4 minutes, or 750 hours; since each field requires a complete scan, this is out of the question for the field studies. Even with the interpolation method for finding the potential, cutting the number of points to 1325, there was no way to complete an adequate number of scans in a reasonable time. Therefore we moved to a second order perturbation method, MP2. *Fig.* 8a) and 8b) show the PES's for fully optimized configuration at HF/6-31G** level of the entire scan grid region and the middle slice of it, and *Fig.* 10a) and 10b) show the PES for the fully optimized configuration, using the MP2/6-31+G* method and basis set. The corresponding wave function is shown in *Fig.* 9 and 11, respectively; there is almost no separation into separate wells near the two nitrogens.

The second column of TABLE V shows the PES, along the center axis or more clearly the NN axis of the grid region, of model MPM28HF-0f, which is the PES of the model MPM, fully optimized at 2.8 Å NN distance with HF/6-31G** method, scanned with HF/6-31G** too. The third column of TABLE V shows the PES, along the NN axis of the grid region, of model MPM27B3LYP-0f, which is the PES of the model MPM which is fully optimized at 2.7 angstrom NN distance with B3LYP/D95+* method, scanned with MP2/6-31+G* method. From the tables

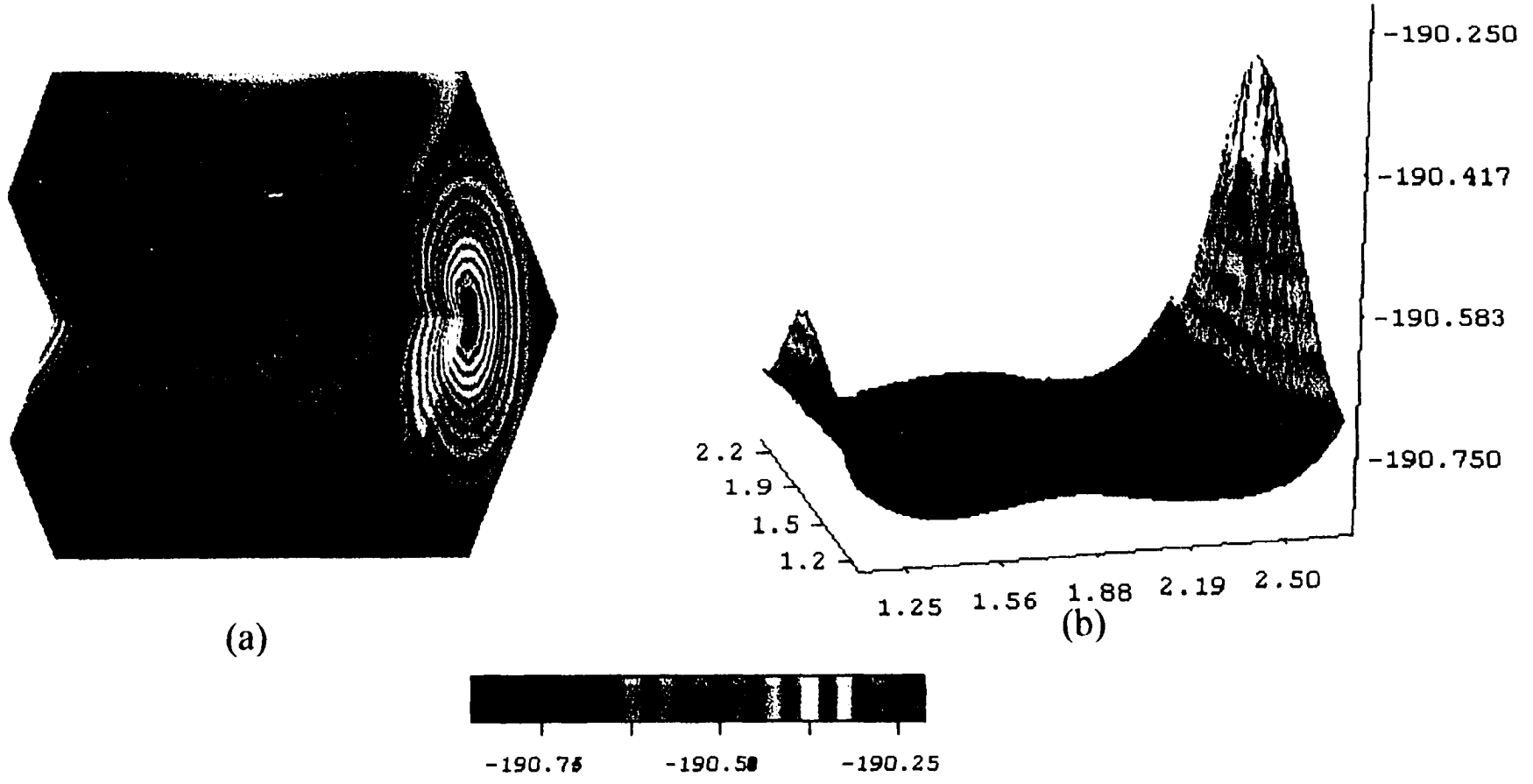

Fig.8 --- (a) PES of MPM28HF-0f; (b) Middle cross-section of (a)

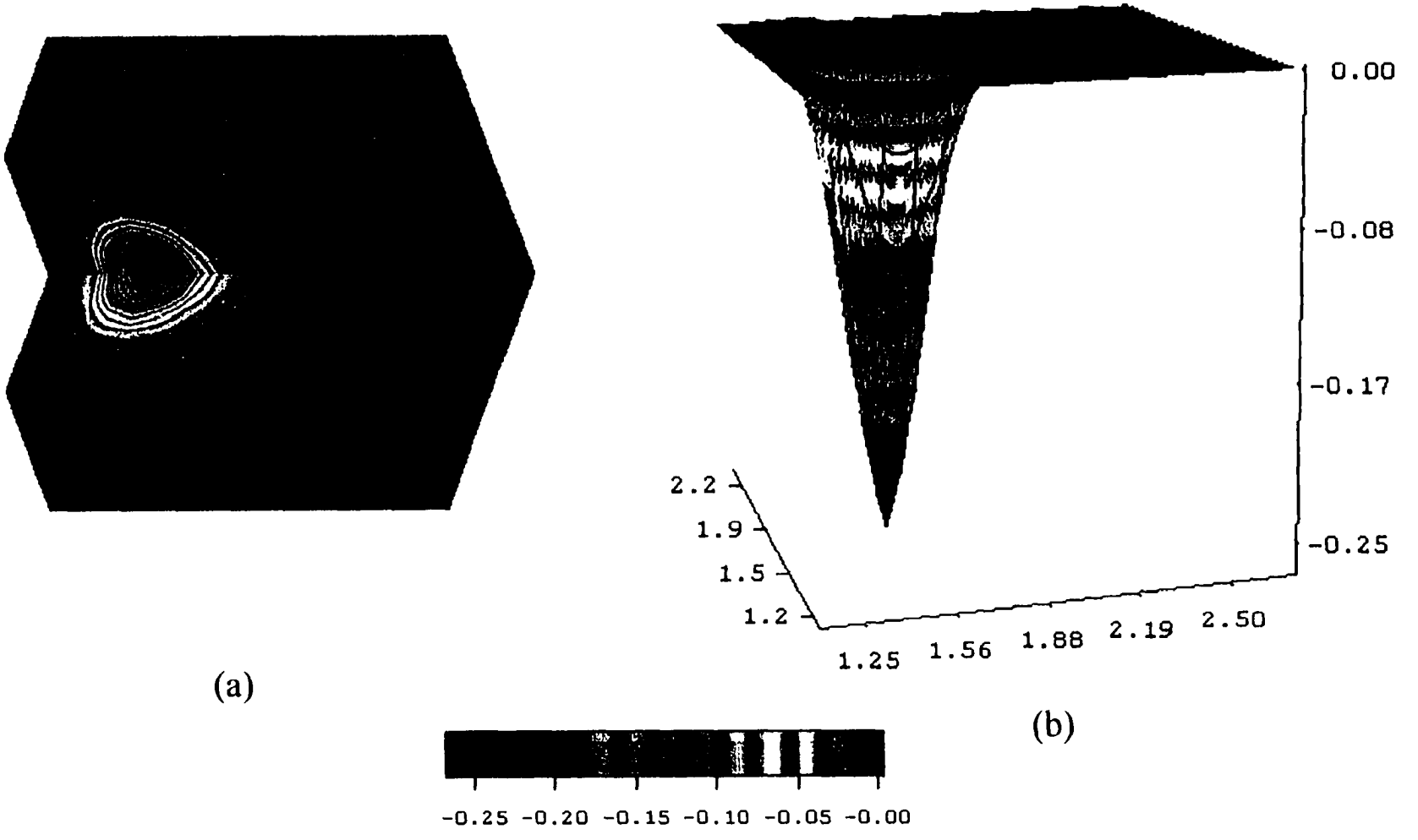

Fig.9 --- (a) Ground State Wave Function(GSWF) of MPM28HF-0f;
(b) Middle cross-section of (a)

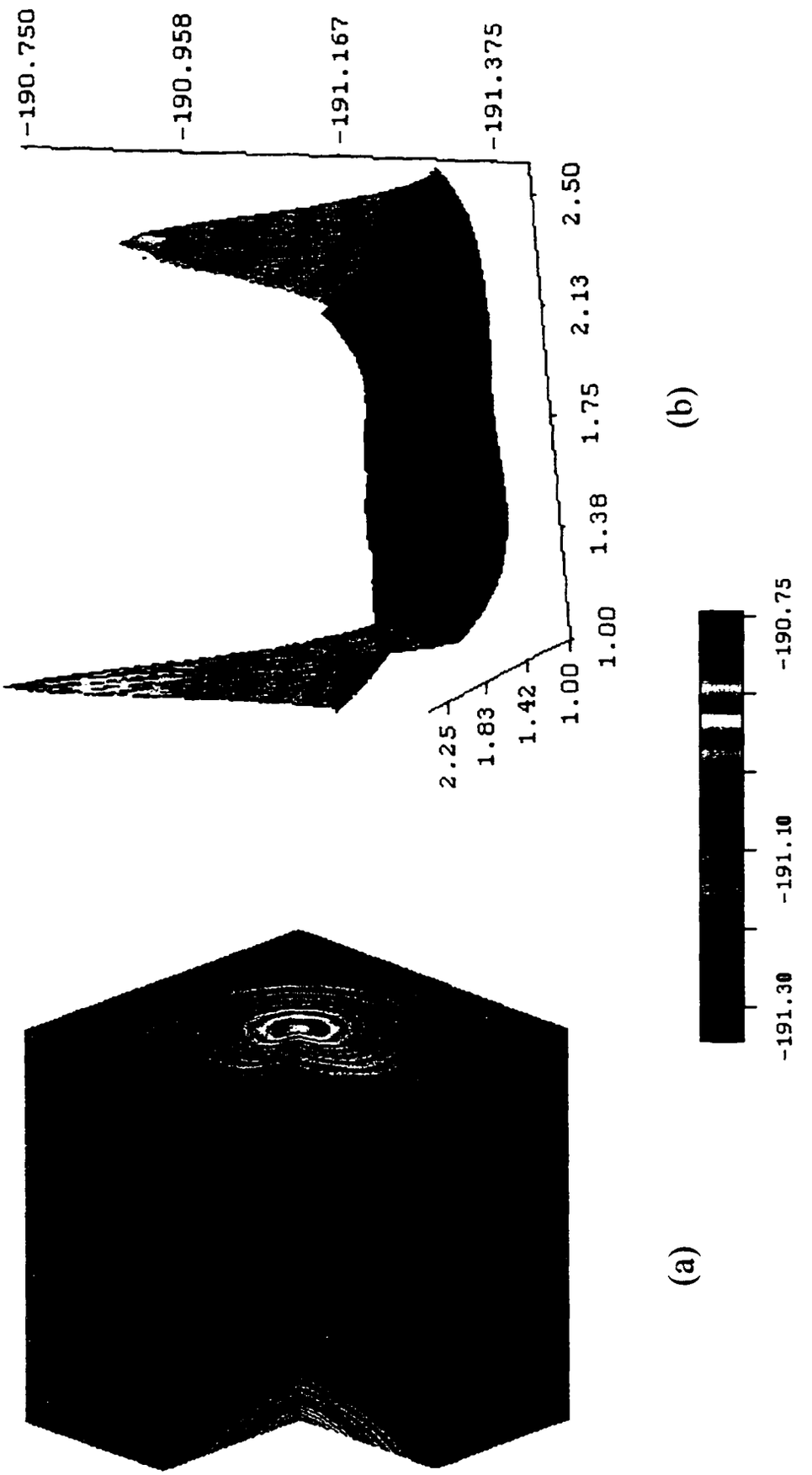

Fig.10 --- (a) PES of MPM27MP2-0f; (b) Middle cross-section of (a)

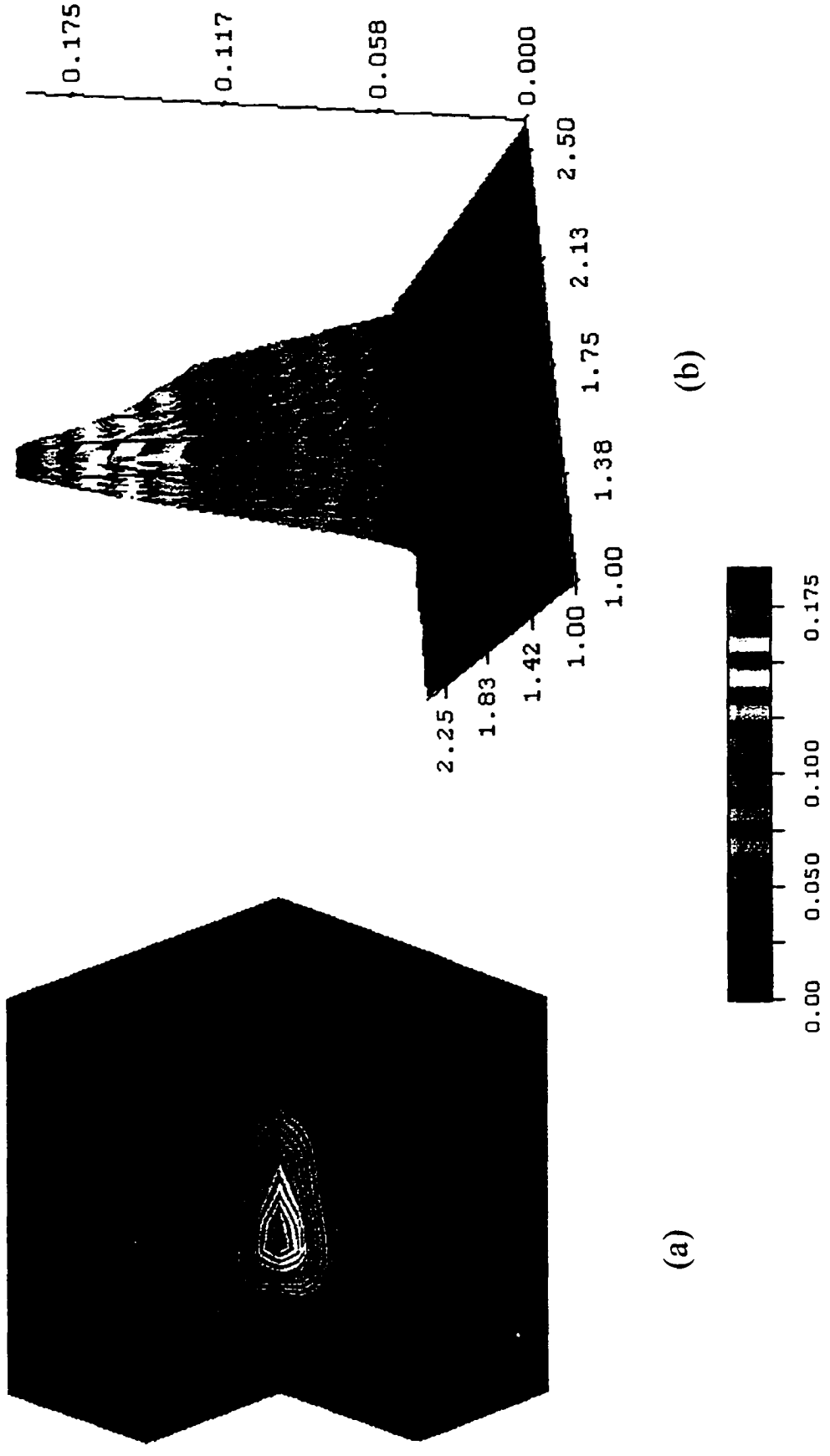

Fig.11 --- (a) GSWF of MPM27MP2-0f; (b) Middle cross-section of (a).

and the figures one sees that there is in fact only one peak in the ground state wave functions in each case, although there are two wells in the PES in case. The distance between the two wells at HF level is 0.7 Å, while the distance between the two wells at B3LYP level is only 0.4 Å, which is much shorter than 0.7 Å. Anyway, even 0.7 Å distance cannot separate the two wells sufficiently. The splittings are actually not the splitting in the usual sense. In MPM28HF-0f, the energy barrier is 0.0147 (a.u.) but the first excited state energy of FGH is 0.0150. Since the FGH calculation takes the lower well in PES as the base line, that means these two number are correct in relative magnitude. Even worse than that, the ground state energy of FGH in MPM27B3LYP-0f is 0.01 while the energy barrier is 0.003. These results are consistent with the results for a proton in between hydroxide ions[121]. For system [HO . . . H . . . OH]$^-$ the PES for the proton transfer between the two oxygen atoms corresponds to a double well potential charaterized by a low barrier at HF/4-31G level, while electron correlation resulted in a flattening of the PES such that the barrier to proton transfer is considerably below the lowest vibrational level for protonic motion at MP2/6-311G** level. Recent theoretical study on the hydrated hydronium ion $H_5O_2^+$ by Schaefer and coworkers[122] also confirmed the *ab initio* dilemma: its potential energy surface is a structure with C_2 (single minimum) symmetry at high level (post-HF) calculations while it becomes C_s (double-well) symmetry at HF level. Therefore from our calculation of MPM we should say there is no splitting at all in the optimized configuration, no matter at what level of the calculation. That seems explain the apparent contradiction that there are two wells in PES's but one peak in each wave function in our results.

When the N - N distance is constrained to be either 3.2 Å or 3.6 Å, there appear two distinct wells in the PES, separated by a higher barrier, 0.0462 (≈ 121 kJ/mol) for MPM32hf-0f (i.e. MPM model with NN separation 3.2 Å) and 0.085 a.u. (≈ 223 kJ/mol) for MPM36hf-0f (i.e.

MPM model with NN separation equals 3.6 Å), respectively, compared with the PES of the fully optimized structures. The first excited state energy of FGH for MPM32hf-0f is 0.0171 a.u. and that for MPM36hf-0f is 0.0166 a.u., which are much lower than the corresponding barriers. These changes are sufficient to prevent easy transfer of the proton between them. The barrier is three to six times higher than the fully optimized barrier. That is, the proton spends the vast majority of its time, or probability, in one or the other well, with little sharing. At these two N-N separations, there is still only one visible peak, although the data tabulated in these tables suggests an extremely small peak on the other side of the barrier in each case. But this one peak-two well situation has completely different quantum mechanical meaning from the one peak-double well situation in the fully optimized configuration systems we discussed before. In the fully optimized systems, the one peak is actually a mixture of two peaks as they are not sufficiently separated from each other. In the partially optimized systems, the one peak is just the peak of the corresponding well when the other well is infinitely separated from it. In the first case there is no tunneling because it does not need tunneling in order to switch between the wells, while in the second case there is no tunneling because it is unable to switch back and forth between the two wells. The second column of TABLE VI shows the PES of model MPM32HF-0f, which is the PES of the model MPM which is partially optimized at 3.2 Å NN distance, with HF method, scanned at HF/6-31G** too. The third column of TABLE VI shows the PES of model MPM36HF-0f, which is the PES of the model MPM, partially optimized at 3.6 Å NN distance, scanned at HF/6-31G** too.

The high level PES calculation was calculated with MP2/6-31+G* instead of B3LYP/D95+* method, which was used in optimization calculation, because of the time considerations cited earlier. The MP2 second order perturbation method with 6-31˚G* basis set of wave functions still allowed for some electron correlation energy; it was compared with the

TABLE V

Fully Optimized PES and FGH Results Without Field

Model Property	MPM28HF		MPM27B3LYP	
PES	-190.6079322360000		-190.7443739208700	
	-190.7515888200000		-191.1038868408300	
	-190.8178887050000		-191.2859585909700	
	-190.8431540440000		-191.3742680015100	
(a.u.)	-190.8476793510000	Well 1	-191.4127949044200	
	-190.8432757480000		-191.4258448315900	
	-190.8369982490000		-191.4273154317500	Well 1
	-190.8329377900000	Barrier	-191.4251664585600	
	-190.8329558030000		-191.4235930245700	Barrier
	-190.8369020090000		-191.4240845081600	
	-190.8425743400000		-191.4258178495600	Well 2
	-190.8454045360000	Well 2	-191.4254045457000	
	-190.8375652880000		-191.4159974401400	
	-190.8058970460000		-191.3854787833200	
	-190.7276465200000		-191.3127508209300	
	-190.5617398890000		-191.1600683909400	
	-190.2299295270000		-190.8566383226300	
Well difference	0.00227 (5.96 kJ/mol)		0.00150 (3.94 kJ/mol)	
Barrier height	0.0147 (38.6 kJ/mol)		0.00327 (8.59 kJ/mol)	
Well-Well distance	0.7 A		0.4 A	
FGH	0.0128957069983		0.0103310363796	
	0.0150396860896		0.0124882379565	
energy	0.0199916581314		0.0174397172708	
	0.0201252290803		0.0175570903481	
	0.0220523492929		0.0177761064454	
	0.0221285769106		0.0194302738842	
	0.0222882132150		0.0195532851902	
	0.0246536453641		0.0237118065675	
	0.0270638271592		0.0244418586619	
	0.0271873789389		0.0245612498696	
	0.0273309371837		0.0246106529597	
	0.0291484660088		0.0246795722181	
	0.0292136124706		0.0246926284028	
	0.0293406231256		0.0262947736326	
	0.0293618886660		0.0264628708947	
	0.0294626617593		0.0265501807536	
	0.0303448714101		0.0302104155982	
	0.0315959149173		0.0302417675909	
	0.0317585527839		0.0306216290058	
	0.0341089824469		0.0313543684348	

Splitting	0.00214 (5.62 kJ/mol)		0.00216 (5.67 kJ/mol)	
Ground	0.0000057586327		0.0000005972716	
	-0.0000388995760		-0.0000001525211	
state WF	-0.0020907951144		0.0001552111374	
	-0.0336205649967		0.0053716852529	
	-0.1395525306192		0.0447442779671	
	-0.2107778753981	Peak (single)	0.1324515004471	
	-0.1524181938826		0.1915208763316	Peak (single)
	-0.0672157845682		0.1823509862053	
	-0.0230708962437		0.1509082833288	
	-0.0080382721288		0.1309448971418	
	-0.0041519308442		0.1139978453528	
	-0.0035178197256		0.0770240334046	
	-0.0029761142364		0.0291595752670	
	-0.0013602266735		0.0044239481514	
	-0.0002496650531		0.0001792437077	
	-0.0000012395269		0.0000029947105	
	-0.0000067199562		-0.0000007384153	

* Note: Energy: 1 a.u. = 627.5 kcal/mole = 2625 kJ/mole : 1 kcal/mole = 4.184 kJ/mole

TABLE VI

HF-PES and FGH Results Without Field

Model Property	MPM32HF-0f		MPM36HF-0f	
PES	-190.3496458640000		-190.419589178000	
	-190.6084745480000		-190.655329890000	
	-190.7433542460000		-190.770304712000	
	-190.8080773940000		-190.820486136000	
(a.u.)	-190.8334182580000		-190.835722028000	Well 1
	-190.8372794730000	Well 1	-190.832496822000	
	-190.8302502370000		-190.820123567000	
	-190.8187591280000		-190.804016789000	
	-190.8068788390000		-190.787478169000	
	-190.7972899920000		-190.772647793000	
	-190.7917203110000		-190.760978114000	
	-190.7910785480000	Barrier	-190.753437609000	
	-190.7954530480000		-190.750591483000	Barrier
	-190.8040928900000		-190.752646131000	
	-190.8153832800000		-190.759463224000	
	-190.8267117120000		-190.770529618000	
	-190.8340520080000	Well 2	-190.784901514000	
	-190.8310344150000		-190.801122636000	
	-190.8071767040000		-190.817029590000	
	-190.7447754780000		-190.829289606000	
	-190.6134268490000		-190.832457616000	Well 2

	-190.3600069320000		-190.817195548000 -190.767003073000 -190.652026603000 -190.416293339000	
Well difference	0.00322 (8.45 kJ/mol)		0.00327 (8.59 kJ/mol)	
Barrier height	0.0462 (121. kJ/mol)		0.0852 (224 kJ/mol)	
Well-Well distance	1.1 A		1.6 A	
FGH energy	0.0136140991767 0.0171484523874 0.0202635959299 0.0203725397803 0.0237533282644 0.0239053228824 0.0262159649722 0.0269995584456 0.0270110486517 0.0275178342875 0.0296072419524 0.0304742346579 0.0304983880494 0.0309703368519 0.0325030017355 0.0326531829143 0.0336843756224 0.0336865641755 0.0342718234487 0.0344580648711		0.0134752669375 0.0166445144011 0.0198483724618 0.0199561628041 0.0229666164021 0.0231010993095 0.0260382099526 0.0263294916194 0.0263631433966 0.0280362339779 0.0291139597986 0.0294231997042 0.0294742689378 0.0311693154928 0.0321630835949 0.0323529208871 0.0327663732186 0.0327711672801 0.0344178260304 0.0345577257418	
Splitting	0.00353 (9.27 kJ/mol)		0.00317 (8.32 kJ/mol)	
Ground state WF	-0.0000031866367 0.0000206356676 0.0010177916119 0.0181800658245 0.0793893406348 0.1165382231419 0.0722084759234 0.0227562317829 0.0043590356621 0.0005661016771 0.0000726190055 -0.0000006965769 0.0000064091873 -0.0000046769636 0.0000044336711 -0.0000033195382 0.0000043973556 -0.0000000763821 -0.0000012745799	Peak 1 Peak 2	0.0000073771750 -0.0002323507808 -0.0115535967148 -0.1058753441270 -0.2593968954396 -0.2200715118605 -0.0808489956795 -0.0151861660331 -0.0016670186607 -0.0001357574063 0.0000030594809 -0.0000078763214 0.0000055963931 -0.0000039098169 0.0000023259966 -0.0000006652595 -0.0000013903839 0.0000038661321 -0.0000105379372	Peak 1

	0.0000019710024 -0.0000020288139 0.0000018913814	0.0000102109105 -0.0000387338622 0.0000294658622 -0.0000220870327 0.0000141311883 -0.0000082422129	Peak 2

HF-SCF method. Both methods produced PES's with almost the same topology and curvature. The HF PES's stay just a little above the corresponding MP2 PES's, particularly in the critical part of the potential diagram near the minima. The overlap of the methylamine wave functions, especially when separated to at least 3.2 Å, was small enough that the potential for the proton was little affected by the inclusion or omission of the correlation energy. Thus, the MP2 minima were about 1% lower than the HF-SCF minima, but the *difference* in the minima, which is the crucial parameter, was appreciably less, approximately 0.3%. All the results are given for the MP2/6-31˜G* calculations. A calculation with the 3-21G basis set showed it to be seriously inadequate, with a difference of about 15% in energy from the other methods; no further work was done with this basis set. The second column of TABLE VII shows the PES of model MPM32MP2-0f, which is the PES of the model MPM, partially optimized at 3.2 Å NN distance with HF method, scanned at MP2/6-31+G*. The third column of TABLE VII shows the PES of model MPM36MP2-0f, which is the PES of the model MPM which is partially optimized at 3.6 Å NN distance with HF method, scanned at MP2/6-31+G*.

The situation in these B3LYP optimizations is similar to that we met before in the HF optimization. We do not repeat it.

2.2) *Finite electric field*: With a field added, the energy minima shift in magnitude but not in the position of the grid region. There are still two potential wells but the responses for the same

TABLE VII

MP2-PES and FGH Results Without Field

Model Property	MPM32MP2-0f		MPM36MP2-0f	
PES	-190.8739204846100		-190.9768454519500	
	-191.1693131509200		-191.2168757642100	
	-191.3177885706800		-191.3356653062700	
	-191.3878639204200		-191.3892790297400	
(a.u.)	-191.4158360801400		-191.4077538522900	Well 1
	-191.4217338754100	Well 1	-191.4077417767300	
	-191.4169648699700		-191.3987283794600	
	-191.4082208145800		-191.3862895922400	
	-191.3994669510900		-191.3737866330200	
	-191.3929153008800		-191.3631961104800	
	-191.3896005894100	Barrier	-191.3555249605000	
	-191.3898664643100		-191.3511121970100	
	-191.3936755896400		-191.3499566724900	Barrier
	-191.4005337589800		-191.3520117501500	
	-191.4090671890300		-191.3572940512100	
	-191.4164782187800		-191.3657492606400	
	-191.4178637576600	Well 2	-191.3769724193700	
	-191.4049497769300		-191.3899184072000	
	-191.3635100415500		-191.4026178283600	
	-191.2683245920300		-191.4117505087500	
	-191.0730744659600		-191.4117947500500	Well 2
	-190.6886674822800		-191.3933164074400	
			-191.3397018738100	
			-191.2209340742000	
			-190.9809470088100	
Well difference	0.00387 (10.2 kJ/mol)		0.00404 (10.6 kJ/mol)	
Barrier height	0.0421 (111. kJ/mol)		0.0618 (162. kJ/mol)	
Well-Well distance	1.1 A		1.6 A	
FGH	0.0127594875841		0.0115413941700	
	0.0158786703373		0.0154554050068	
energy	0.0191972910478		0.0176399413516	
	0.0192894697721		0.0177233464621	
	0.0222401701617		0.0214404703930	
	0.0223710696186		0.0215766063632	
	0.0240313436260		0.0234355656717	
	0.0256690730623		0.0237743802468	
	0.0257139346994		0.0238418935548	
	0.0258921248080		0.0249086082622	
	0.0268976405546		0.0271499780862	
	0.0286424454899		0.0275035829968	
	0.0287194340747		0.0276009676049	

	0.0289184279132		0.0287418936528	
	0.0302016966121		0.0292416352705	
	0.0303037224236		0.0293789531673	
	0.0321338976103		0.0299279579036	
	0.0321509901729		0.0299412104824	
	0.0323395483042		0.0310619383593	
	0.0324918614411		0.0311789771314	
	0.0330089040808			
	0.0331539043734			
Splitting	0.00312 (8.19 kJ/mol)		0.00391 (10.3 kJ/mol)	
Ground	-0.0000044854308		0.0000080780803	
	0.0000312806969		-0.0000121939300	
state WF	0.0017504122392		0.0000175425870	
	0.0340355927169		-0.0000228686430	
	0.1607481979517		0.0000281675194	Peak 1
	0.2610607793684	Peak 1	-0.0000120005243	
	0.1866311764543		0.0000101822796	
	0.0719513731515		-0.0000055014155	
	0.0179477123180		0.0000037531416	
	0.0033219707948		-0.0000024524647	
	0.0005614029019		0.0000016466675	
	0.0000699547882		-0.0000011509047	
	0.0000286128233		0.0000012202953	
	-0.0000078643322		0.0000015938365	
	0.0000125272876		0.0000437563527	
	-0.0000085260588		0.0004796619121	
	0.0000101230176	Peak 2	0.0044881948740	
	-0.0000028852843		0.0287296635406	
	0.0000005784107		0.1138879146651	
	0.0000009906578		0.2392141830779	Peak 2
	-0.0000015980920		0.2247866092014	
	0.0000017562487		0.0754839260633	
	-0.0000040586852		0.0068806784222	
			0.0001373944684	
			0.0000437563527	

homogeneous external field are different. We are most interested in the magnitude of the change in field which is required to shift the proton from one well to another. Qualitatively this is similar to a shift in which the higher well falls below the original lower well after the shift, but not exactly similar. We will see the difference later. A large field is needed to bring the two wells to

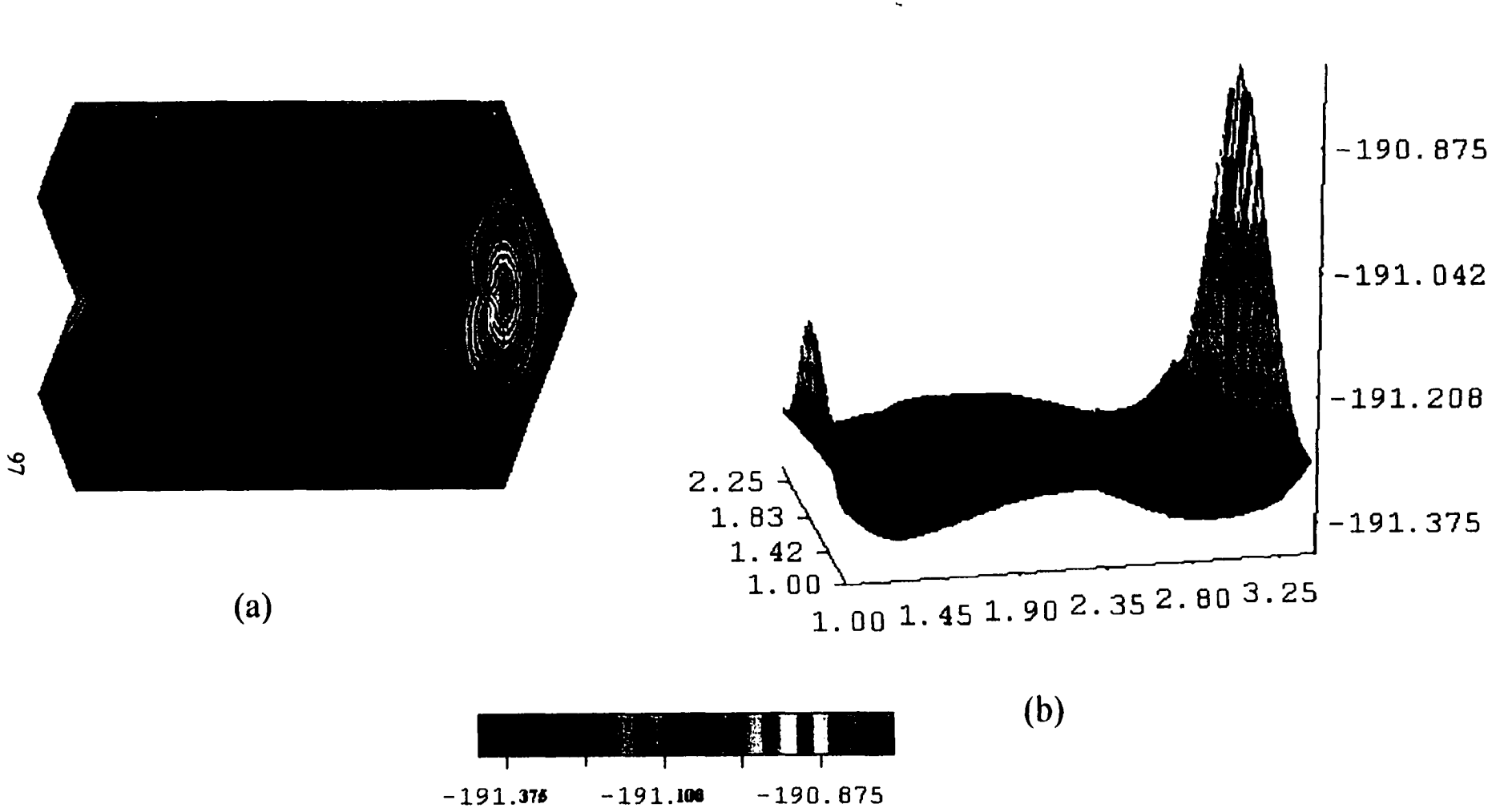

Fig.12 --- (a) PES of MPM36MP2-f1; (b) Middle cross-section of (a)

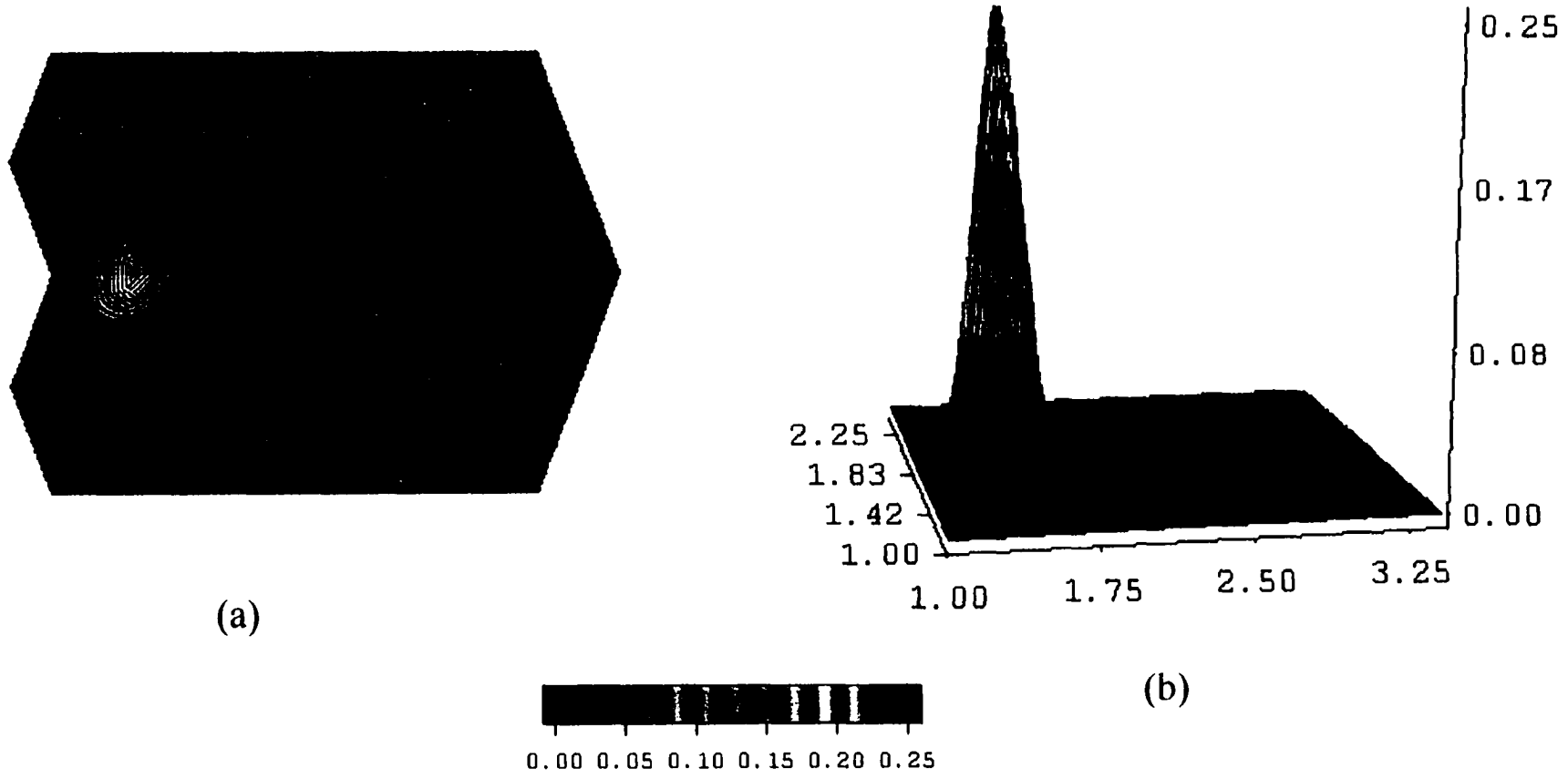

Fig.13 --- (a) GSWF of MPM36MP2-f1; (b) Middle cross-section of (a)

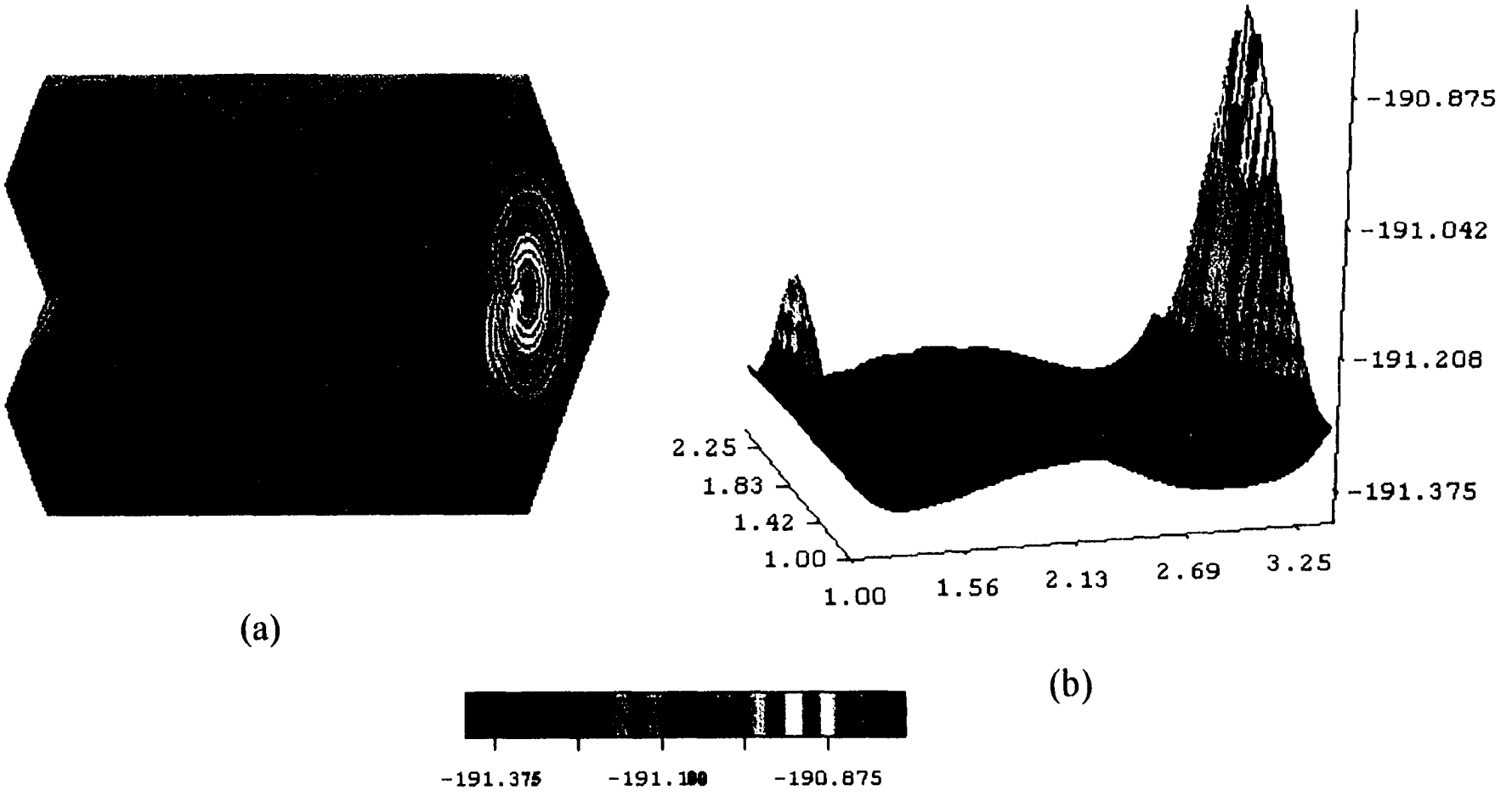

Fig.14 --- (a) PES of MPM36MP2-f2; (b) Middle cross-section of (a)

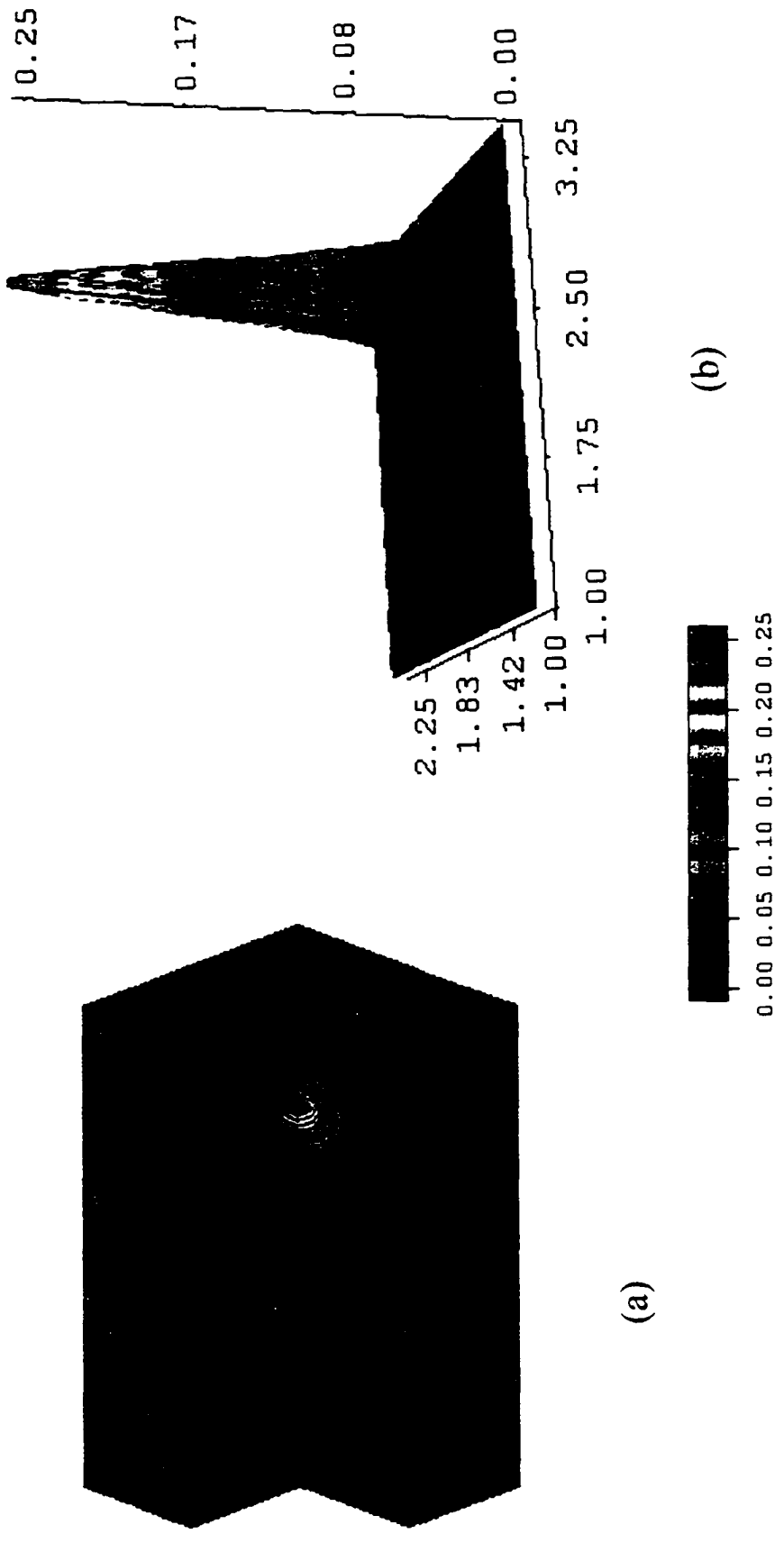

Fig.15 --- (a) GSWF of MPM36MP2-f2; (b) Middle cross-section of (a)

approximate equality from the optimized unequal configuration, which is about the order of the energy equivalent to the resting potential imposed on an voltage-gated ion channel; even after this is accomplished, the wave function is almost entirely in one well or the other. The *change* in field required to transfer the proton is relatively small, and it is this which is the major result of the calculation. *Fig.*12 shows the potential energy surface of model MPM36MP2 with field components (0.19541, 0, 0.73139) x 10^9 V m^{-1}, with the N - N vector at an angle of 61.753° from the electric field vector when the critical field is reached. *Fig.*13 shows the corresponding ground state wave function. There is only one peak at one side of the grid region. As we mentioned earlier this angle is the result of an empirical search to find the value at which the field is most effective, and we believe it is fairly close to optimum. However, there is no way which we are aware to prove this; it is too time consuming to carry out an exhaustive search. Whether or not this is the most effective angle, it is adequate to prove that a very small change in field will effect a large change in the wave function. The corresponding values for model MPM32MP2 are: field, (0.75170, 0, 0.20569) x 10^9 V m^{-1} ; angle to the N - N vector, 55.0577°. *Fig.*14 shows the PES for the same separation of the two nitrogens, with field components as for Fig.12a); one cannot find any difference between these two cases by only looking at Fig.12a) and Fig14.a). The z component of the field in the Fig.14 case has increased by only 0.00005 x 10^9 V m^{-1}, while the other components are unchanged. The wave function peak has shifted from the potential well at one nitrogen to that at the other (*Fig.*15). Even with the shift of only 0.00005 x 10^9 V m^{-1}, the peak of the wave function in the dominant well is about 10-15 times that in the other well (that is, a shift of this amount in field produces a change from A:1 to 1:A', with $10<A,A'<15$. Perfect symmetry was not found, although in principle it could have been. No conclusions would be altered if it had been found.). The square of the wave function gives the probability of finding the proton, and therefore the ratio is >100:1 for the shift in the proton itself (i.e., for the square of the

wave function). For the 3.2 Å case, the shift at the critical field is only somewhat over 3:1, or about 10:1 for the square of the wave function. It is more appropriate actually to give the integral of the peak, and we have integrated over a cube 0.6 Å on a side (0.3 Å, or 3 points of the lattice, from the maximum, in each direction). The results are as follows: for the lowest state at 3.6Å spacing, the probabilities for the proton in the two wells, with the wave function normalized, are 0.9990 and 0.8954 x 10^{-3}, compared to 1.35 x 10^{-3} and 0.9986 with the field incremented by 10^{-7} a.u. (0.5 x 10^{5} V m^{-1}). For 3.2 Å the shift is less drastic: probabilities 0.8795 and 0.1205, compared to 0.1018 and 0.8982 with the field incremented by 10^{-7} a.u. If the field is decremented by 1.8 x 10^{-6} a.u., the probabilities at 3.2 Å become .9998 and 1.5 x 10^{-4}. If the field is incremented from this value by the relatively huge change of 10^{-5} a.u. (still about half that produced by the membrane potential), the two peaks become 8 x 10^{-6} and 0.9999+. Even if the direction of the membrane field is somewhat different, there is obviously adequate field to produce the required proton transfer.

TABLE VIII and IX give the PES's and FGH results of model MPM32HF and MPM36HF, with two switching fields, respectively; TABLE X and XI give the PES's and FGH results of model MPM32MP2 and MPM36MP2, with two switching fields, respectively. The strength differences for HF calculation are 2 order larger than that of MP2 calculation. This is due to the time-consuming PES scanning prevent us further searching a finer switching pair of fields. Compare with MP2 results, it is very positive for the existence of such a consistent finer switching pair for HF models.

TABLE VIII

PES and FGH Results of MPM32HF at Switching Fields

	Field 1= (-0.00103, 0.0, -0.0010000) Field 1 Strength = 0.738 x 10^{9} Vm^{-1} Field 1 – Field 2 = 0.0000394 a.u.	Field 2= (-0.00103, 0.0,-0.0010394) Field 2 strength = 0.752 x 10^{9} Vm^{-1} Field 2 – Field 1 = -0.0000394 a.u.
Strength	1.4 x 10^{7} Vm^{-1}	1.4 x 10^{7} Vm^{-1}

difference		
PES	-190.22847121 (118914 kcal/mole)	-0.19022857839D+03
	-190.5631787160000	-0.19056328735D+03
	-190.7306672030000	-0.19073077749D+03
	-190.8095538020000	-0.19080966608D+03
(a.u.)	-190.8408655360000	-0.19084098030D+03
	-190.8470253820000	-0.19084714331D+03 (well 1)
	-190.8407141050000	-0.19084083609D+03
	-190.8293519840000	-0.19082947918D+03
	-190.8174885330000	-0.19081762224D+03
	-190.8080297900000	-0.19080817126D+03
	-190.8027919050000	-0.19080294208D+03
	-190.8026846060000	-0.19080284384D+03 (barrier)
	-190.8077337330000	-0.19080790171D+03
	-190.8170748090000	-0.19081725064D+03
	-190.8289225630000	-0.19082910500D+03
	-190.8403905060000	-0.19084057825D+03
	-190.8469512030000	-0.19084714308D+03 (well 2)
	-190.8412319360000	-0.19084142703D+03
	-190.8106588870000	-0.19081085651D+03
	-190.7330309680000	-0.19073323061D+03
	-190.5677693570000	-0.19056797066D+03
	-190.2371818190000	-0.19023738456D+03
Well difference	- 0.0000742 (0.195 kJ/mol)	0.00000023 (0.000604 kJ/mol)
Barrier height	0.0343 (90.1 kJ/mol)	0.0443 (116. kJ/mol)
Well difference	1.2 A	1.2 A
FGH	0.0132354933150 (34.76 kJ/mol)	1.3487752393143E-02
	0.0132821389273	1.3600594155545E-02
energy	0.0198714391416	2.0079900869628E-02
	0.0199272680064	2.0229389502106E-02
	0.0200158780170	2.0261935809940E-02
	0.0200346208647	2.0374258657683E-02
	0.0256869595031	2.6002749756684E-02
	0.0259421715194	2.6147675458957E-02
	0.0265426418515	2.6795042759086E-02
	0.0266028507855	2.6810043593583E-02
	0.0267217993466	2.7007607409837E-02
	0.0267828958402	2.7024306863026E-02
	0.0271339523633	2.7338651441085E-02
	0.0272561852810	2.7475289622091E-02
	0.0316887124441	3.2223038212280E-02
	0.0320246384132	3.2436775894031E-02
	0.0321474494237	3.2450740397715E-02
	0.0323891508900	3.2602184890900E-02
	0.0330964073134	3.3442132204720E-02
	0.0332192483339	3.3447407648068E-02
Splitting	0.0000467 (0.0293 kcal/mole)	0.000113 (0.0709 kcal/mole)

Ground	0.0000045094191	3.1318747536834E-06	
	-0.0000280303997	-2.9926685983217E-06	
state WF	-0.0014524297406	2.8032094123849E-06	
	-0.0335690389629	1.3146078177569E-05	
	-0.1690923665026	6.1520015553955E-05	
	-0.2701815625187	1.1867290819773E-04	(peak 1)
	-0.1750017292268	5.4266620722435E-05	
	-0.0568309797070	3.6112644399748E-05	
	-0.0112215074363	-1.0623045615114E-05	
	-0.0014860954872	1.9889079902769E-05	
	-0.0002083854029	-4.2086783717225E-06	
	0.0000079985883	1.8351738639971E-04	
	-0.0000252823553	1.3599210311380E-03	
	0.0000160569673	1.0407170555128E-02	
	-0.0000423651388	5.4108454806085E-02	
	-0.0000486570997	1.7093020002908E-01	
	-0.0001337768752	2.7089110101462E-01	(peak 2)
	-0.0000537997996	1.7580787257195E-01	
	-0.0000200944869	3.6316131980275E-02	
	0.0000004753816	1.6354474751041E-03	
	0.0000010240250	3.3892948396100E-05	
	-0.0000019502958	-6.1170392017511E-06	
Ratio of peak 1 and peak 2	2702 : 1	1 : 2709	

* Electric Field Strength: 1 a.u. = 5.1423 x 10^{11} Vm^{-1}:

TABLE IX

FGH Results of MPM36HF at Switching Fields

	Field 1= (-0.000540000, 0.00010, -0.000622) Field 1 strength = 0.427 x 10^{9} Vm^{-1} Field 1 – Field 2 = 0.0000811	Field 2= (-0.000621144, 0.00010, -0.000622) Field 2 = strength = 0.455 x 10^{9} Vm^{-1} Field 2 – Field 1 = - 0.0000811
Strength difference	2.8 x 10^{7} Vm^{-1}	2.8 x 10^{7} Vm^{-1}
PES	-190.4214917300000	-190.4215207650000
	-190.6572792790000	-190.6573111770000
	-190.7723060400000	-190.7723410960000
	-190.8225470920000	-190.8225857590000
	-190.8378533990000	-190.8378963120000 (well 1)
	-190.8347136570000	-190.8347616990000
	-190.8224465640000	-190.8225009360000
	-190.8064734420000	-190.8065357290000

	-190.7901029250000	-190.7901750940000
	-190.7754800470000	-190.7755643330000
	-190.7640573080000	-190.7641559290000
	-190.7567962560000	-190.7569110210000
	-190.7542485720000	-190.7543805130000 (Barrier)
	-190.7566031560000	-190.7567523210000
	-190.7637037880000	-190.7638692240000
	-190.7750227720000	-190.7752027210000
	-190.7896081840000	-190.7898004390000
	-190.8060029050000	-190.8062052180000
	-190.8220481050000	-190.8222584790000
	-190.8344179360000	-190.8346347620000
	-190.8376742620000	-190.8378963140000 (well 2)
	-190.8224848100000	-190.8227111890000
	-190.7723536410000	-190.7725836960000
	-190.6574303670000	-190.6576636380000
	-190.4217448690000	-190.4219810550000
Wells difference	- 0.000179 (-0.470 kJ/mol)	0.000000002 (0.000005 kJ/mol)
Barrier height	0.0836 (219 kJ/mol)	0.0835 (219 kJ/mol)
Well distance	1.6 A	1.6 A
FGH	0.0134928411709 (35.4 kJ/mol)	0.0134615186286
	0.0136386992603	0.0134909850462
energy	0.0198944165690	0.0197996687796
	0.0199773007468	0.0198929738655
	0.0200046986001	0.0199328502299
	0.0201104669605	0.0200032834662
	0.0261070979350	0.0259654320136
	0.0261432612396	0.0261057857208
	0.0264063672866	0.0262711073817
	0.0264402554611	0.0263222059144
	0.0264491685044	0.0264053578258
	0.0265001906848	0.0264392059205
	0.0280657899993	0.0280616930313
	0.0282533194266	0.0280784591904
	0.0322341471928	0.0320560773099
	0.0322550491067	0.0322539334750
	0.0324484566206	0.0322891772802
	0.0324671973338	0.0324473492143
	0.0328706125244	0.0326921533289
	0.0328726820482	0.0327022023187
Splitting	0.000146 (0.383 kJ/mol)	0.0000295 (0.0774 kJ/mol)
Ground	0.0000072033204	-0.0000079052677
	-0.0002341121697	0.0000128240220
state WF	-0.0115193979205	-0.0000687989134
	-0.1051754469847	-0.0003997638281
	-0.2581364177243	-0.0010956314365 (peak 1)

	-0.2205255821191	-0.0008916826545	
	-0.0819441457895	-0.0003455325843	
	-0.0156344301800	-0.0000602049837	
	-0.0017525651604	-0.0000084276038	
	-0.0001446708534	-0.0000013865003	
	0.0000019384087	0.0000024599923	
	-0.0000076617173	-0.0000040670258	
	0.0000054186148	0.0000057480050	
	-0.0000037945886	-0.0000080639489	
	0.0000022487048	0.0000029632884	
	-0.0000007264433	-0.0001386085796	
	-0.0000027360608	-0.0016737085696	
	-0.0000080509427	-0.0151003515164	
	-0.0000738749356	-0.0799648461759	
	-0.0001622091103	-0.2174699240230	
	-0.0002444043895	-0.2570827072417	(peak 2)
	-0.0000532898238	-0.1056884863873	
	-0.0000312900763	-0.0116739448899	
	0.0000138410858	-0.0002374261729	
	-0.0000081374448	0.0000067995782	
Ratio of peak 1 and peak 2	2581 : 2	1 : 257	

TABLE X

FGH Results of MPM32MP2 at Switching Fields

	Field 1= (0.0004, 0.00000, -0.0014618) Field1 strength = 0.77934 x 10^9 vm^{-1} Field 1 – Field 2 = - 0.0000001 a.u.	Field 2= (-0.0004, 0.00000, -0.0014619) Field2 strength = 0.77939 x 10^9 Vm^{-1} Field 2 – Field 1 = 0.0000001 a.u.	
Strength difference	0.5 x 10^5 Vm^{-1}	0.5 x 10^5 Vm^{-1}	
PES	-190.8781707960000	-190.8781710798000	
	-191.1736365676700	-191.1736368554500	
	-191.3221958445300	-191.3221961369000	
	-191.3923710949000	-191.3923713927700	
(a.u.)	-191.4204670351800	-191.4204673399000	
	-191.4265225436300	-191.4265228570700	(well 1)
	-191.4219557662200	-191.4219560908700	
	-191.4134656580400	-191.4134659967800	
	-191.4050159999000	-191.4050163555100	
	-191.3988064956800	-191.3988068702400	
	-191.3958544978600	-191.3958548924600	(barrier)
	-191.3964891071100	-191.3964895220400	
	-191.4006601455000	-191.4006605803300	

	-191.4078563357100 -191.4166853765600 -191.4243391715600 -191.4259159881700 -191.4131507574400 -191.3718282092400 -191.2767380919800 -191.0815686393500	-191.4078567890800 -191.4166858460900 -191.4243396543400 -191.4259164813700 (well 2) -191.4131512587200 -191.3718287168900 -191.2767386047900 -191.0815691565200
Well difference	0.000607 (1.59 kJ/mol)	0.000606 (1.59 kJ/mol)
Barrier height	0.0307 (80.6 kJ/mol)	0.0307 (80.6 kJ/mol)
Well distance	1.1 A	1.1 A
FGH energy	0.0127507277595 (8.00 kcal/mole) 0.0127508487491 0.0190623065889 0.0191641559060 0.0191926418990 0.0192624912808 0.0239035048350 0.0239121523077 0.0253451091052 0.0255020449500 0.0255467744755 0.0256564263184 0.0256570910438 0.0257927993024 0.0298958384029 0.0300497983462 0.0300682488956 0.0301768406489 0.0317032772405 0.0317502497254	0.0127506327402 0.0127507630127 0.0190620033478 0.0191641962744 0.0191924753583 0.0192625360857 0.0239034180047 0.0239120222625 0.0253445651675 0.0255019131825 0.0255468919767 0.0256562740787 0.0256570777885 0.0257929322129 0.0298955071373 0.0300494611488 0.0300683047671 0.0301769148623 0.0317026617026 0.0317500134572
Splitting	0.000000121 (0.000318 kJ/mol)	0.000000130 (0.000341 kJ/mol)
Ground state WF	-0.0000038141480 0.0000279975727 0.0016068119581 0.0311257221709 0.1477258272729 0.2428372411710 0.1769039025692 0.0700457658253 0.0180840625331 0.0035218492420 0.0006881885256 0.0005197390375 0.0024436398512 0.0113823418517	0.0000004285916 0.0000060629601 0.0005521979029 0.0105796703964 0.0502603196401 0.082598158614 (peak 1) 0.0601779251614 0.0238297575613 0.0061566154623 0.0012329718348 0.0004005516414 0.0012023808863 0.0066006776483 0.0310848319615

	0.0385386689360 0.0794298105605 0.0827488773046 0.0347182252747 0.0045232450660 0.0001186670851 0.0000041569002	0.1051999791980 0.2168882516108 0.2259105238852 (peak 2) 0.0948140342742 0.0123346274019 0.0003362445760 0.0000013177985
Ratio of peak 1 and peak 2	2428 : 827	826 : 2259

TABLE XI

FGH Results of MPM36MP2 at Switching Fields

	Field 1= (0.00038, 0.00000, -0.0014223) Field 1 strength = 0.75704 x 10^9 Vm^{-1} Field 1 – Field 2 = - 0.0000001	Field 2= (-0.00038, 0.00000, -0.0014224) Field 2 strength = 0.75709 x 10^9 Vm^{-1} Field 2 – Field 1 = 0.0000001
Strength difference	0.5 x 10^5 Vm^{-1}	0.5 x 10^5 Vm^{-1}
PES	-191.1280316960900 -191.2966751428000 -191.3772382694100 -191.4102574061400 -191.4178454131200 -191.4124074742500 -191.4010964850900 -191.3881696581700 -191.3761887012300 -191.3666052383900 -191.3600876313200 -191.3568075672400 -191.3567454501900 -191.3599118977900 -191.3663505628000 -191.3759134454800 -191.3879401972500 -191.4009586087400 -191.4123549632700 -191.4177872577700 -191.4099737427500 -191.3763067956200 -191.2943325192000 -191.1228836531300 -190.7833376361000	-191.1280319785400 -191.2966754291800 -191.3772385601700 -191.4102577019800 -191.4178457151000 (well 1) -191.4124077838800 -191.4010968044400 -191.3881699898200 -191.3761890479700 -191.3666056026800 -191.3600880147200 -191.3568079704000 -191.3567458732900 (barrier) -191.3599123408100 -191.3663510252600 -191.3759139259000 -191.3879406931900 -191.4009591173400 -191.4123554818700 -191.4177877842300 (well 2) -191.4099742754900 -191.3763073335400 -191.2943330615700 -191.1228841994600 -190.7833381860200
Wells difference	0.0000582 (0.153 kJ/mol)	0.0000579 (0.152 kJ/mol)
Barrier	0.0611 (160. kJ/mol)	0.0611 (160. kJ/mol)

height		
FGH	0.0130982346325	0.0130981263544
	0.0130983776601	0.0130982428402
energy	0.0190812608483	0.0190811361677
	0.0191797339828	0.0191797689679
	0.0192121154558	0.0192115488893
	0.0192678325913	0.0192678759114
	0.0248128409866	0.0248126297176
	0.0249066751553	0.0249067595254
	0.0251630845252	0.0251624027200
	0.0252265880747	0.0252259395957
	0.0252616935635	0.0252618038047
	0.0253742888803	0.0253743649353
	0.0264279067757	0.0264279316630
	0.0264856707288	0.0264854486338
	0.0305641233775	0.0305638298293
	0.0306507163912	0.0306508265551
	0.0307891918613	0.0307893512379
	0.0307929056709	0.0307921362533
	0.0312242644877	0.0312232829763
	0.0312440225089	0.0312434841229
Splitting	0.000000143 (0.000375 kJ/mol)	0.000000116 (0.000305 kJ/mol)
Ground	0.0000217220386	0.0000022294364
	0.0011225377292	-0.0000437954728
state WF	0.0278457044768	-0.0010214582739
	0.1505824356451	-0.0055364132487
	0.2593029458266	-0.0095292010142 (peak 1)
	0.1804521225937	-0.0066347879181
	0.0615834793885	-0.0022606208052
	0.0121899838271	-0.0004515976898
	0.0015532667754	-0.0000527432945
	0.0001736448562	-0.0000117315949
	-0.0000025613934	0.0000067875392
	0.0000119866746	-0.0000089189636
	-0.0000086068838	0.0000123277823
	0.0000066284187	-0.0000034507263
	-0.0000103302270	0.0001698270666
	-0.0000411138232	0.0015169717924
	-0.0003631324449	0.0120067840174
	-0.0018242824943	0.0610246871322
	-0.0053743152596	0.1793909713668
	-0.0077040461737	0.2573513810504 (peak 2)
	-0.0044376097155	0.1481002922479
	-0.0008034871601	0.0269238734614
	-0.0000345979530	0.0010532985173
	0.0000027507466	0.0000202455141
	-0.0000033552387	-0.0000030956389
Ratio of peak 1 and peak 2	2593 : 77	95 : 2573

From these tables we find that as the two wells become more and more closely matched in model MPM32HF, the potential barrier between them is still of the same order. while the corresponding energy splitting becomes one or two orders of magnitude smaller. This contradicts the 'common sense' belief that enhancing the 'coherence' of the two wells should increase the transition rate. This apparent contradiction may result from the sensitivity of the splitting to the barrier height. Note that even for the same model with the two different switching fields, the first produces 0.0343 a.u. barrier while the second produces 0.0443 a.u.. But the difference of the consequent splittings of them is huge, for the first field the splitting is 0.0000467 a.u. while for the second field it is 0.000113 a.u. This is another contradiction if we do not take into account the well difference factor. By combining the two factors of well difference and barrier height, one could be impressed by the sensitivity of the splitting to them and feel comfortable with all these apparently paradoxical results. Let us look at the tables again. This time we focus on the models with larger NN distance: 3.2 Å and 3.6 Å. Obviously the well-well distance is an important factor affecting the splittings. At the beginning of this section, we mentioned that the general rule is the longer the distance the smaller the splitting. For TABLE X and XI the results are consistent with the rule. But for TABLE VIII and IX this is not true. The splitting in TABLE VIII is 0.0000467 a.u. but the splitting in TABLE IX is 0.000146 a.u. This 'abnormal' phenomenon cannot be simply resolved by the NN distance, because our model PES's are all three-dimensional. The details of the topology of the PES therefore are dependent on only three parameters. Compare with the peak ratio in these two TABLES, 2700 : 1 is for TABLE VIII and 1300:1 is for TABLE IX. Further examination of the two ground state wave functions one can also find the two peaks in MPM36HF wave function have more soft slopes than the two peaks in

(a) (b)

Fig.16 --- (a) PES of MPM32HF-f1; (b) GSWF of MPM32HF-f1

(d)

(c)

Fig.16 --- (c) PES of MPM32HF-f2; (d) GSWF of MPM32HF-f2

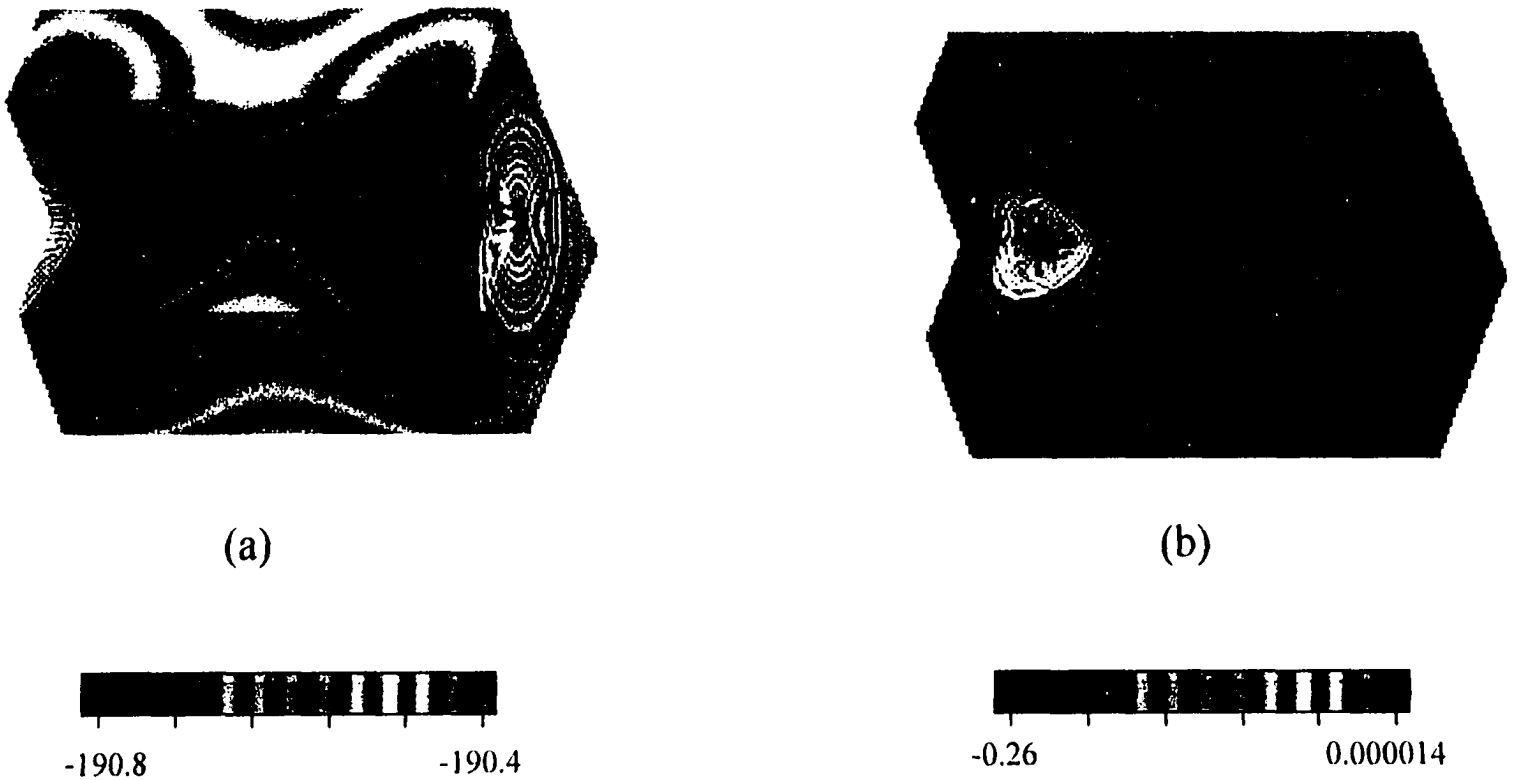

Fig.17 --- (a) PES of MPM36HF-f1; (b) GSWF of MPM36HF-f1

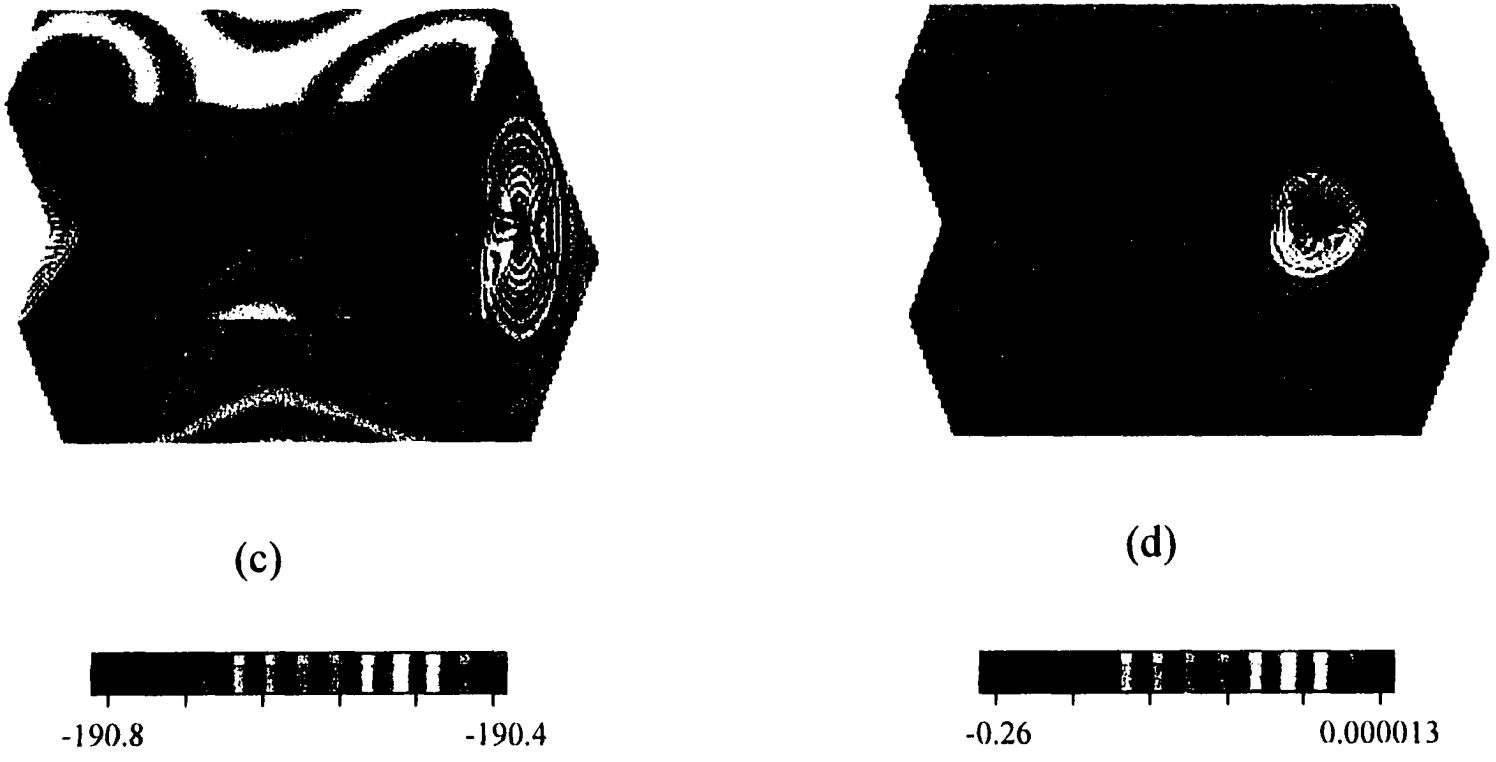

Fig.17 --- (c) PES of MPM36HF-f2; (d) GSWF of MPM36HF-f2

(b)

(a)

Fig.18 --- (a) PES of MPM32MP2-f1; (b) GSWF of MPM32MP2-f1

(d)

(c)

Fig.18 --- (c) PES of MPM32MP2-f2; (d) GSWF of MPM32MP2-f2

MPM32HF wave function. All these means the PES of the model MPM32HF in TABLE VIII is more diffuse from the center of NN axis than the PES of the model MPM36HF in TABLE IX does, i.e. the actual PES centers of the double wells for model MPM36 are nearer than that of model MPM32 relative to the corresponding barrier heights and well differences. That make the splitting in MPM36 larger than the splitting in MPM32.

Since there is no experimental data and theoretical calculation of our models in the literature and our main interest is on the switching pair of fields, we will not go into detail further on these results.

*Fig.*16 shows the PES's and wave functions of model MPM32HF-f1,f2, which correspond to the data given in TABLE VIII. *Fig.*17 shows the PES's and wave functions of model MPM36HF-f1,f2, which correspond to the data given in TABLE IX. *Fig.*18 shows the PES's and wave functions of model MPM32MP2-f1,f2, which correspond to the data given in TABLE X. In *Fig.*16 - 18 we show only 3D PES's and no corresponding 2D slices, like we do in *Fig.*12 - 15. The magnitude of potential energies, however, are shown by color like before.

3. POTENTIAL ENERGY SURFACE (PES) AND FOURIER GRID HAMILTONIAN CALCULATION OF MODEL: WATER + PROTON + METHYLAMIN

The model MPM was selected in order to simulate the basic residues on the channel proteins. Since the pore of the channel is filled with water molecules, proton tunneling between one basic residue and one water molecule is also a possibility. We tested this hypothesis by using the model system: Water + Proton + Methylamine. The procedure is similar to the procedure used in MPM model. Instead of going through a complete run twice with different *ab initio* methods, we use only the HF method. Sample runs showed that there is no qualitative difference between HF level and MP2 level for our purpose. The full optimization, 3.0 Å, 3.3 Å, and 3.6 Å

Fig.19 --- Fully optimized configuration of WPMhf

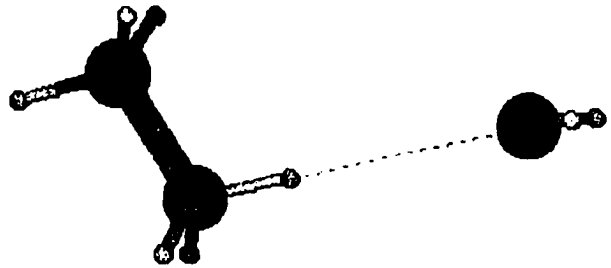

Fig.20. --- Partially optimized configuration of WPM36hf

partial optimizations have been done on HF/6-31G** level. The optimized results are given in TABLE XII below. *Fig.*19 an 20 show the fully and partially optimized configurations of the MPW, respectively. *Fig.*21(a)-(d) show the PES of model WPM36hf-f1, i.e. WPM partially optimized at fixed NO separation (3.6 Å) at level HF/6-31+G* and then the corresponding PES obtained at the same level of *ab initio* calculation, under the field f1=(-0.011240, 0.0000, -0.011). *Fig.*22(a)-(c) show the corresponding ground state wave function (GSWF). *Fig.*23(a)-(d) and *Fig.*24(a)-(c) are the same things but under another field f2=(-0.011245, 0.0000, -0.011). We give the detailed PES results and FGH results with two switching fields in TABLE XIII. One of the major difference between these PES figures and the PES figures of the MPM model is the presence of four wells in the PES of the MPW model. This occurs because the two deepest wells are not on the same 'layer' of the lattice in the scanning grid, one is on the fifth layer and the other is on the eighth layer. Therefore proton transfer in the double-well structure will not be parallel to the O-N orientation. When we applied a background external field in the PES calculation, we found the field for switching the wells relative positions to be in the range of 10^{11} to 10^{12} Vm^{-1} in the case of full optimization. A simple calculation shows that this is near the range of the field inside a chemical bond, which is approximately 10^{12} to 10^{13} Vm^{-1}. Therefore it is not plausible to apply such a field to a chemical system. There is no evidence, experimental or theoretical, showing a field as high as 10^{12} Vm^{-1} can exist inside a biological system. However, for the 3.6 Å separation, the field for switching the wells is slightly below the range 10^{11} to 10^{12} Vm^{-1}. Since a water molecule is polarizable in a field, but in our PES calculation all the methylamines and water are taken as rigid bodies, it is possible to lower the value of the switching field by readjusting the water molecule configuration. Nevertheless, the switching field range is our major concern, not the absolute value of the field. Therefore we tried only the 3.6 Å separation model, MPW36hf. We will not do further analysis of these results, as we did for the MPM model. The only thing we want to emphasize is the switching field range is 10^{6} to 10^{7} Vm^{-1}. If this is true, it seems too high for tunneling of a proton between a water molecule and an

amino acid residue in channel protein under the membrane potential threshold.

TABLE. XII.a)
Optimized HF energies and corresponding dipole moments of MPW

Opt[a] methods (HF/6-31G**)	Energy (a.u.)	Zero-point freq. (cm^{-1})	Dipole moment (Debye)	N-N Direction:
Fopt	-171.6433	44.9896	(0.6899, 1.5420, -0.0031) Tot= 1.6893	(2.6813, 0.8112, -0.0021)
3.0 Popt	-171.6403	58.2746	(-1.4417, 1.6635, 0.3425) Total: 2.2278	(-2.9713, 0.7931, -0.0041)
3.3 Popt	-171.6361	73.2484	(1.9988, 2.0677, 0.0001) Total: 2.9759	(3.2558, 0.7890, -0.0000)
3.6 Popt	-171.6335	79.4104	(2.6415, 1.7991, -0.0026) Total: 3.1959	(3.5169, 0.7740, -0.0021)

[a]Fopt, fully optimized: Popt, partially optimized, N - N distance constrained

TABLE XII.b)
Optimized HF configurations of MPW

Level Opt[a]	N-N Distance (Å)	N-P Distance (Å)	P-O Distance (Å)	N-P-O angle (deg)	C-N-O Angle (deg)	C-N-P-O Dihedral angle (deg)
Fopt	2.801	1.026	1.778	174.3	107.2	-2.781
3.0 Popt	3.000	1.024	2.055	174.5	109.6	-68.58
3.3 Popt	3.350	1.020	2.332	175.8	114.1	-180.0
3.6 Popt	3.601	1.018	2.583	179.6	111.2	79.51

TABLE XIII
FGH Results of MPMW36HF at Switching Fields

	Field 1= (-0.011240, 0.0000, -0.011) Field 1 strength = 0.8087 x 10^{10} Vm^{-1} Field 1 – Field 2 = - 0.0000001	Field 2= (-0.011245, 0.0000, -0.011) Field 1 strength = 0.8089 x 10^{10} Vm^{-1} Field 2 – Field 1 = 0.0000001
Strength difference	2.0 x 10^{6} Vm^{-1}	2.0 x 10^{6} Vm^{-1}
PES	1st minimum : -171.544803396000 Minimum Location: (8, 8,14) -170.745784552000 -171.342543972000 -171.513921911000 -171.541705838000	1st minimum : -171.544781441000 Minimum Location: (8,8,14) -170.745784689000 -171.342543438000 -171.513920514000 -171.541703338000

	-171.522541401000 -171.492812553000 -171.467458590000 -171.452891983000 -171.451047454000 -171.461198941000 -171.481097504000 -171.507021298000 -171.532577212000 -171.544803396000 -171.513370036000 -171.361935714000 -170.884871228000 2nd minimum: -171.543882598000 Minimum Location: (5,8,3) -171.400305609000 -171.514664820000 -171.543882598000 -171.531188588000 -171.502865293000 -171.473090533000 -171.449459501000 -171.435742306000 -171.432962732000 -171.440316179000 -171.455874627000 -171.476644246000 -171.498052631000 -171.512564624000 -171.506616540000 -171.455470211000 -171.318541804000	-171.522537474000 -171.492806751000 -171.467450394000 -171.452881006000 -171.451033653000 -171.461182621000 -171.481079149000 -171.507001390000 -171.532556141000 -171.544781441000 -171.513347387000 -171.361912498000 -170.884847522000 2nd minimum: -171.543881376000 Minimum Location: (5,8,3) -171.400306032000 -171.514664492000 -171.543881376000 -171.531186255000 -171.502861533000 -171.473084904000 -171.449451499000 -171.435731562000 -171.432949200000 -171.440300136000 -171.455856526000 -171.476624556000 -171.498031737000 -171.512542803000 -171.506593981000 -171.455447036000 -171.318518081000
Wells difference	0.000921 (2.42 kJ/mol)	0.000900 (2.36 kJ/mol)
Barrier height	?	?
FGH energy	0.0131108392159 0.0131234160256 0.0145690716845 0.0156630282917 0.0163865015035 0.0177449864895 0.0191583618576 0.0191606774696 0.0196144286010 0.0196792994985 0.0208123011721 0.0212826059327 0.0216371336069	0.0131015000500 0.0131120443210 0.0145491607468 0.0156423693327 0.0163657046254 0.0177243862312 0.0191377062651 0.0191401843803 0.0196143740556 0.0196792390858 0.0207923053343 0.0212617119516 0.0216164461536

	0.022500996681 5 0.0227227041327 0.0238564164440 0.0244570616427 0.0250256731985 0.0254799959113 0.0257808079732	0.0224802681121 0.0227017002082 0.0238357710243 0.0244365315301 0.0250050078430 0.0254595407045 0.0257807375559
Splitting	0.0000126 (0.0331 kJ/mol)	0.0000105 (0.0276 kJ/mol)
Ground state WF	1st peak and 2nd peak: -0.0000919061223 0.0001975718325 0.0047934717195 0.0278854958894 (8, 8, 4) 0.0065884281242 0.0000371560296 0.0001808182536 -0.0002178896007 0.0003162201301 -0.0005175728332 0.0011904853047 0.0111221373554 0.1973483854745 0.5310780187006 (8, 8, 14) 0.0865114645192 -0.0007202361651 0.0002012300204 3rd peak and 4th peak: 0.0002831575689 0.0204089337574 0.0870394987578 at (5, 8, 3) 0.0340300236779 0.0023355904989 0.0001484480940 -0.0000560752105 0.0000323231998 -0.0000179877966 0.0000070615363 0.0000074035275 0.0000697184838 0.0014420995071 0.0042828445609 at (5, 8, 14) 0.0015971474113 -0.0000499833385 0.0000631831926	1st Peak: 0.0000076110765 -0.0000332648868 0.0225840480073 0.1093530200969 0.0270917120616 0.0003123439502 0.0003157644586 -0.0001905424711 0.0001639374664 -0.0001905732977 0.0003515912063 0.0029056561528 0.0519996972932 0.1402087363129 0.0226631152425 -0.0001445943023 0.0000310940938 2nd peak: 0.0013137263259 0.0933617193058 0.3971736004205 0.1543498765161 0.0104803891900 0.0006825888024 -0.0002632072768 0.0001557024844 -0.0000935909733 0.0000509392271 -0.0000106741821 -0.0000174622342 0.0005040265936 0.0007908289569 0.0009192012525 -0.0003994968904 0.0002806234664
Ratio of peak 1 and peak 2	53 : 9	14 : 39

(a)

(b)

Fig.21 --- (a) PES of WPM36HF-f1; (b) 1/4 cut-off cross-section at top-front of (a)

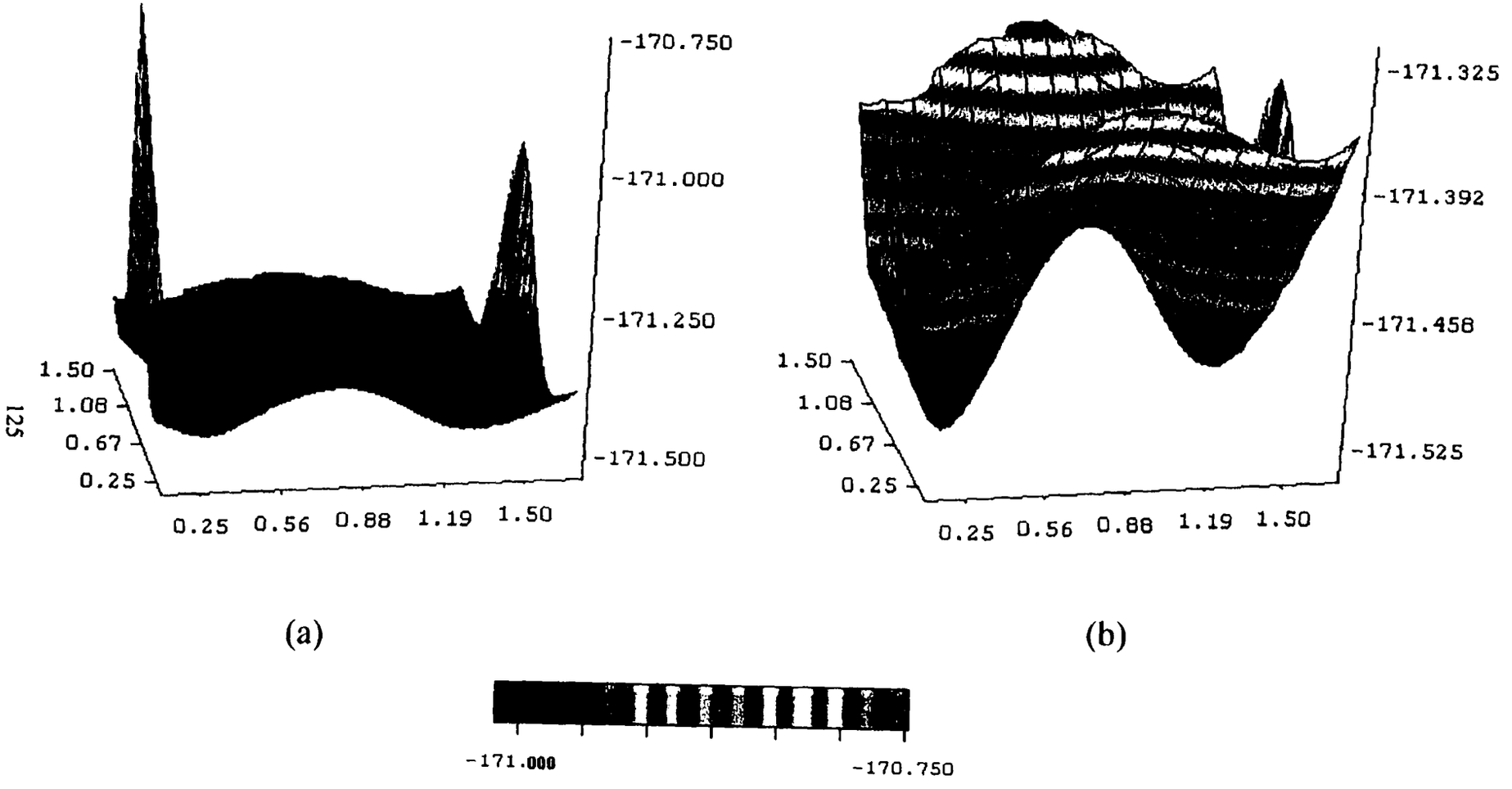

Fig.21 --- (c) Middle cross-section of Fig.21(a); (d) 5th slice cross-section of Fig.21(a)

(a)

Fig.22 --- (a) GSWF of WPM36HF-f1

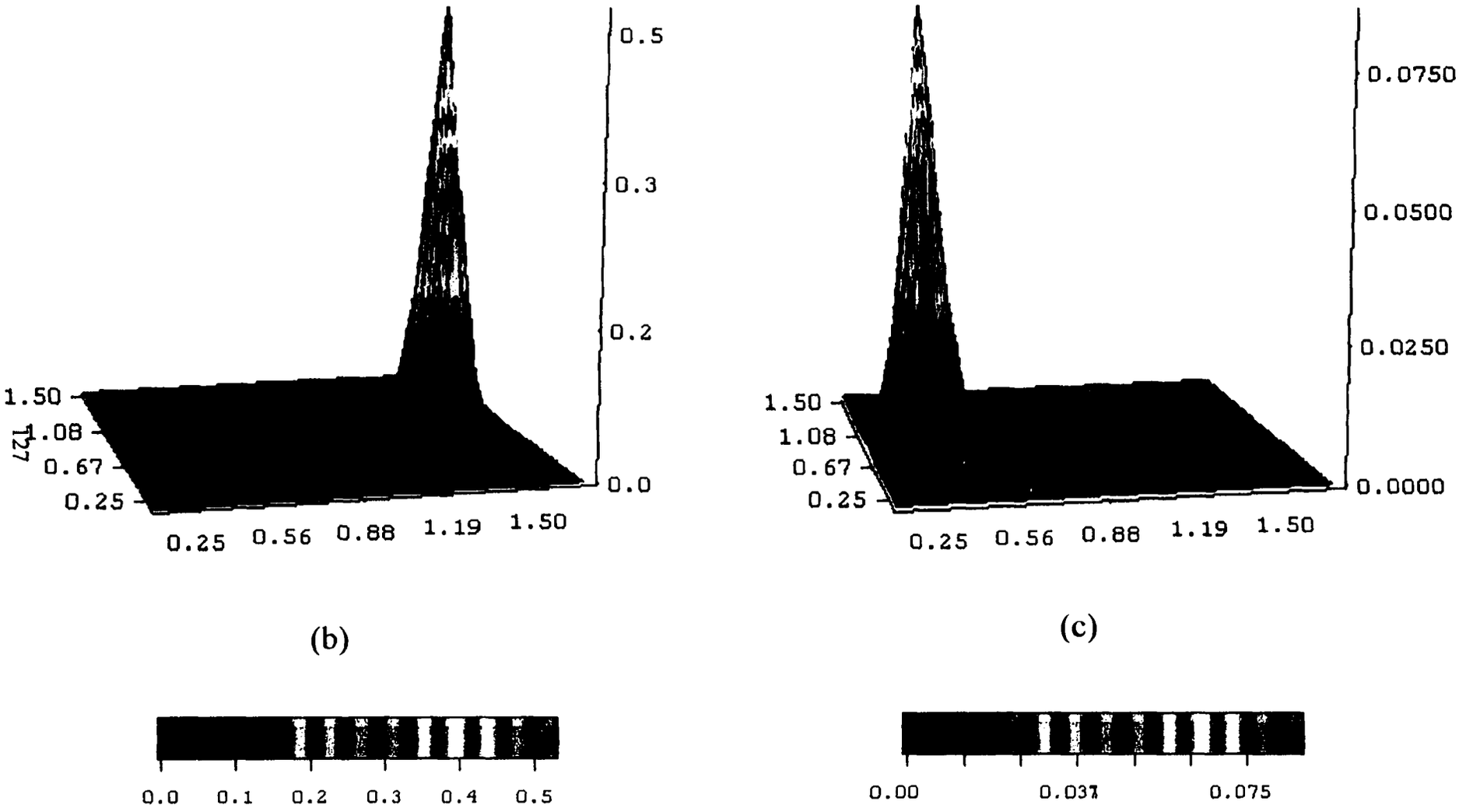

Fig.22 --- (b) Middle cross-section of Fig.22(a); (c) 5th slice cross-section of Fig.22(a)

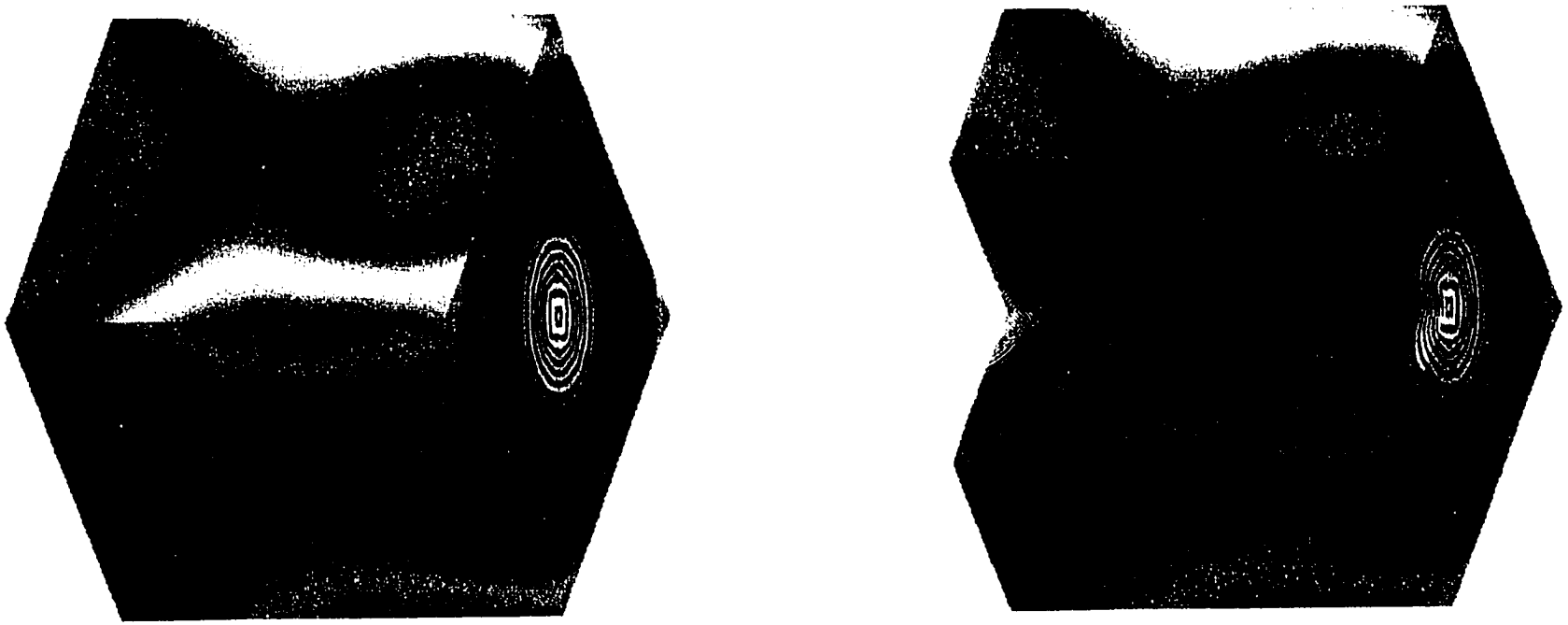

(a) (b)

Fig.23 --- (a) PES of WPM36HF-f2; (b) 1/4 cut-off cross-section at top-front of (a)

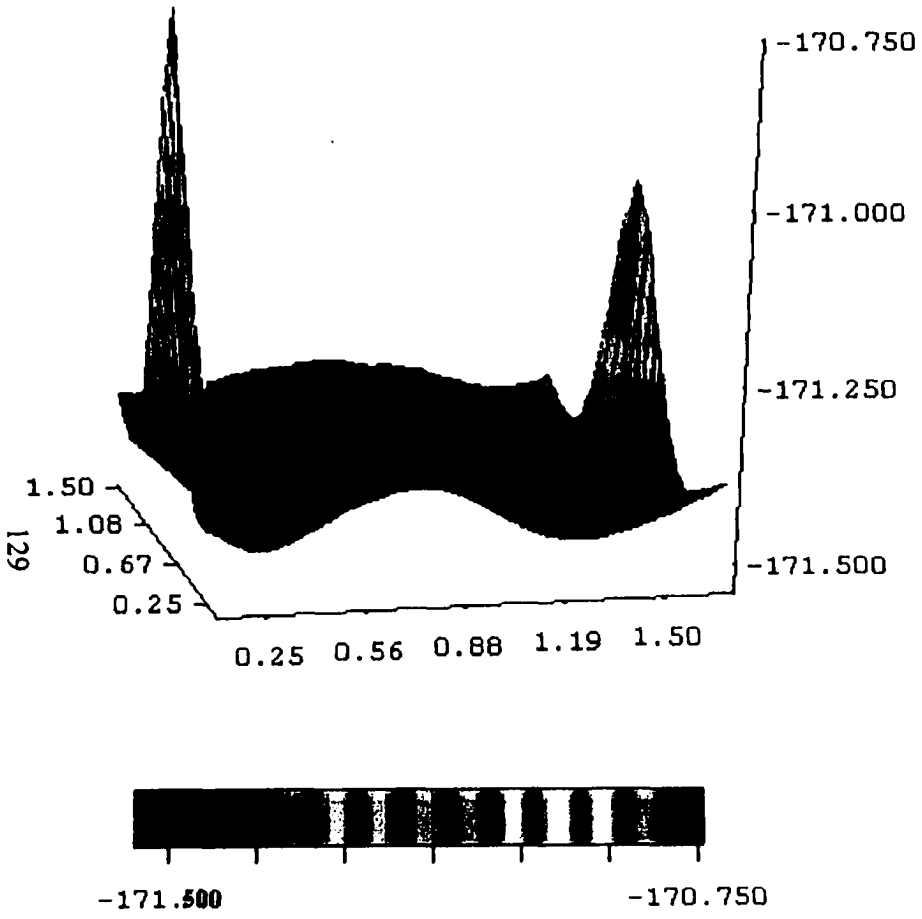

(c)

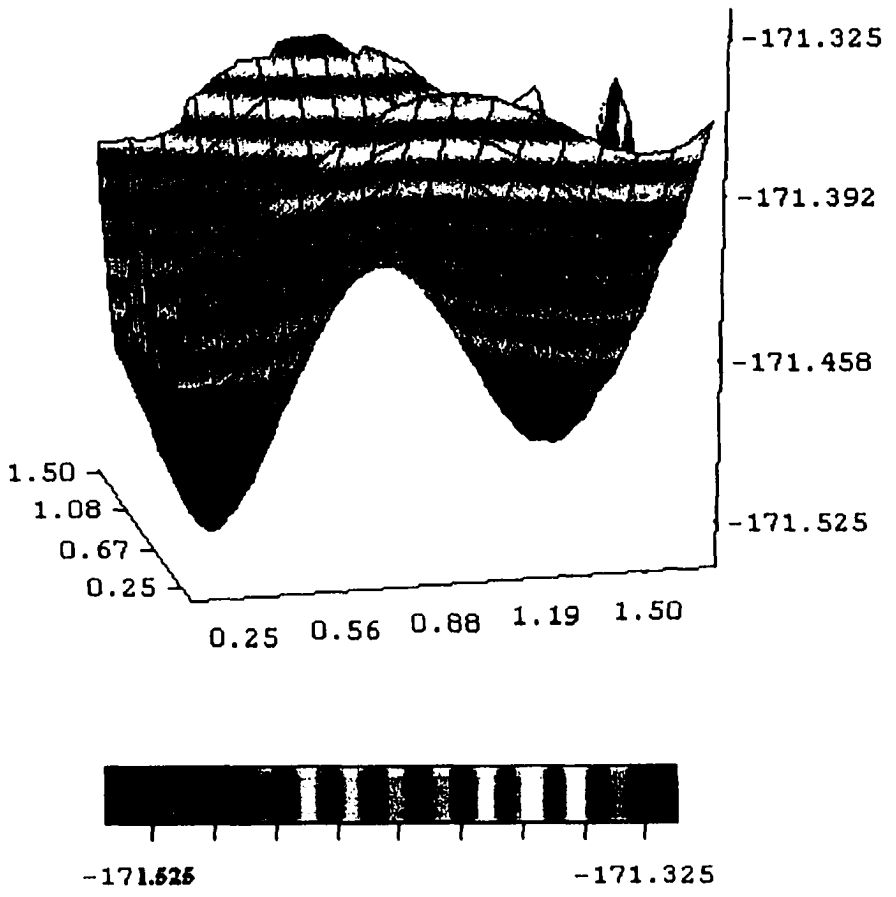

(d)

Fig.23 --- (c) Middle cross-section of Fig.23(a); (d) 5th slice cross-section of Fig.23(a)

(a)

Fig.24 --- (a) GSWF of WP36HF-f2

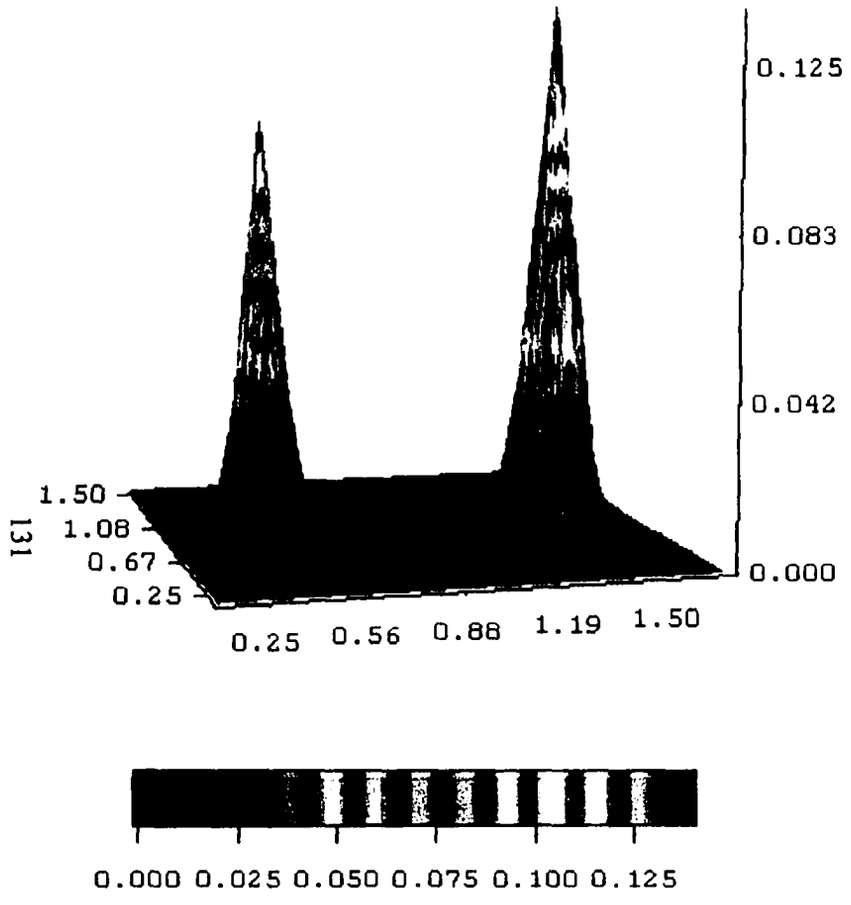

(b)

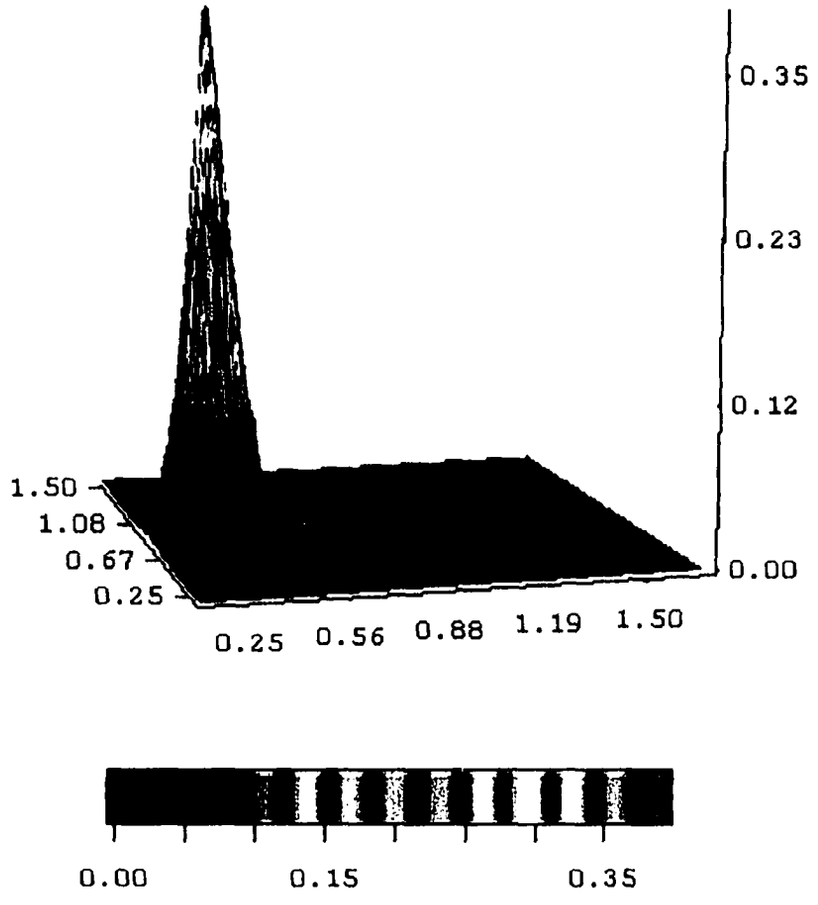

(c)

Fig.24 --- (b) Middle cross-section of Fig.24(a); (c) 5th slice cross-section of Fig.24(a)

4. CONCLUSION

In summary, if the vibrational frequencies are much faster and the medium relaxation rate is much slower than proton transfer rates, calculation on proton transfer in the gas phase will possess significant meaning, even for systems in a condensed phase. Especially when we apply our results to the ion channel gating mechanism, our calculation results seem close to matching the kinetic and energetic scales for the data of gating process. I would like to connect the above results with the gating mechanism in voltage-dependent ion channels.

We have established that a small change in field causes a nearly complete shift of a proton between two wells. This is relevant to the situation in a biological membrane containing ion channels. Calculations have shown that fields of the order of 10^9 V m^{-1} can exist in a protein[1, 3, 28]. There is also experimental evidence which suggests that an acetylcholine receptor channel may have a comparable field[125]. A Stark Effect experiment[3] has given a field of approximately 0.4 x 10^9 V m^{-1} at the end of an uncharged peptide. The existence of a field of this magnitude in an ion channel, for example, or some other types of proteins, is quite plausible.

The question of the *change* in field is actually more critical for the application of this calculation to an ion channel. The electrical potential present, for example, across the membrane of a neuron, is typically approximately 70 mV. The potential drops across a membrane of slightly less than 70 A, so that there is a field of, on average, approximately 10^7 V m^{-1} across the membrane. This is greater than the change in field required at 3.6 Å for effectively complete proton shift by a factor of approximately 200, so that a shift by this amount is clearly possible in the membrane protein, on depolarization of the membrane. The actual initial activation potential in voltage-gated channels is about 5 mV or less, which corresponds to a field change less than 10^6 Vm^{-1}. This is exactly in the range of the field switching of our calculation for MPM at higher *ab initio* level.

It is at least plausible that the shift of a proton under the influence of change of the membrane field could occur, if the basic amino acids present in the protein channel (in the S4

segment of sodium and potassium channels, especially[2]) are constrained in position by other groups in the protein. If the groups come too close, they would transfer the proton without control by the field. If the groups are too far apart, they could not transfer the proton at all. This would be equivalent to having the splitting of the energy levels caused by interaction of the molecules so small that the transfer time would be much too long. Since at least two of the groups in the S4 segment are known to be salt bridged to other groups[126], the necessary rigidity could exist.

The system studied here differs from a protein in several respects. Not only is a methylamine not an amino acid, but the calculation is done *in vacuo*. In a real protein the potentials produced by surrounding protein and water would change the local field; in fact, we must assume, for the applicability of the model, that the local fields *are* the background fields needed to match the wells. The order of magnitude of the field required is correct. Unless the change in the field required to transfer the proton is larger by over one order of magnitude, the conclusion that the proton could be transferred by the depolarization of the membrane stands.

For this calculation to apply to an ion channel it would be necessary to have the distances in the protein rather firmly fixed, and to allow little fluctuation in the fields. However, unless the fields are much less than the expected value in all critical parts of the protein of the channel, the same requirement would exist in any model of channel gating, for each model requires *some* transition with the same potential. If fluctuations as large as the field produced by the membrane potential existed, the channel would open at random, not under control of the membrane potential. Fluctuations of the structure larger than those permitted here would seem to lead to fluctuations of the local field of at least comparable magnitude. This consideration appears to lead to a model with the structure more rigid than that has heretofore been expected. Recent study on the structure of Shaker K+ channels by Mackinnon and coworkers.[127] (see Fig 3), suggests a very rigid selectivity filter and possibly other parts of the channel.

Since the 1970's, workers in the field expected the voltage-gated channel to work through a physical blocker, such as the well-known Armstrong and Bezanilla ball-and-chain gating model[128] (*Fig.*25a). Although it turned out to be correct for inactivation later[2], there seems to be tremendous difficulty in looking for a blocker which may be controlled by a external field as small as 10^6 Vm^{-1}. Recently Yang and Horn[55], and Isacoff et.al.[59], proposed gating models of a different kind, which may be simply demonstrated by *Fig.*25b)), trying a way of gating in which a block was replaced by the S4 segment which pops up into the extracellular region to release the block in the channel, and pops down back into the channel protein to block it. We would argue against this S4 movement on the energetic and kinetic grounds. All of the gating models of voltage-gated channels but ours involve first a move of some part of a tertiary or a quaternary sub-unit of the channel protein. Consider that the gating is initiated by a field less than 10^6 Vm^{-1}. How can it be possible? Professor Green raised a completely different mechanism by way of proton tunneling to try to avoid the above obstacles. The working mechanism of this model is shown in *Fig.*26). Since water will fill up the pore, the water molecules are immobilized by the local field in the pore, and then block the channel. Since the two transmembrane segment gates with protons, it is possible that the S1-S4 transmembrane segments function as a membrane potential to proton current transducer. It is already known that there is a proton current accompaning gating if 2 hystidines are substituted for arginines, and that the shape of the two transmembrane segment K+ channel agrees with the pore of the six transmembrane K+ channels, therefore the transducer function is consistent with known data. When the protons, hydrogen bonded on the positively charged residues on the S4 segments, sense a change in their local field, we would like call it the 'gating field change', they then tunnel away from the residue to which they had been bound, two more protons per segment follow, the blocking field in the channel is lifted, and water molecules become free to move. This is the basic idea of the tunneling-gating mechanism of voltage-gated ion channel. Our present results in this thesis give theoretical support for this hypothesis.

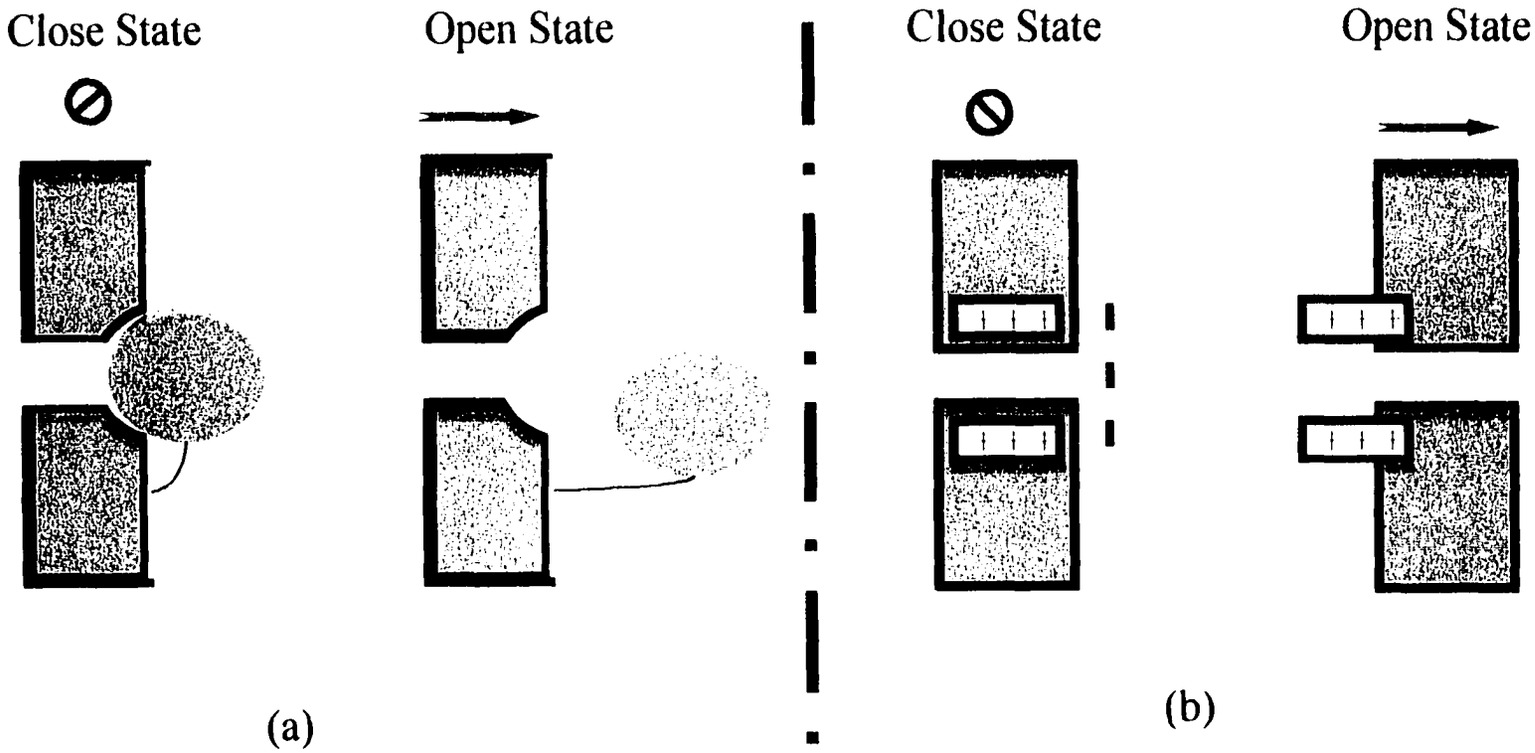

Orientation of figures: extracellular to the left and intracellular to the right

Fig.25 --- Two gating models for voltage-dependent ion channels. (a) Ball-and-chain model; (b) Toaster model

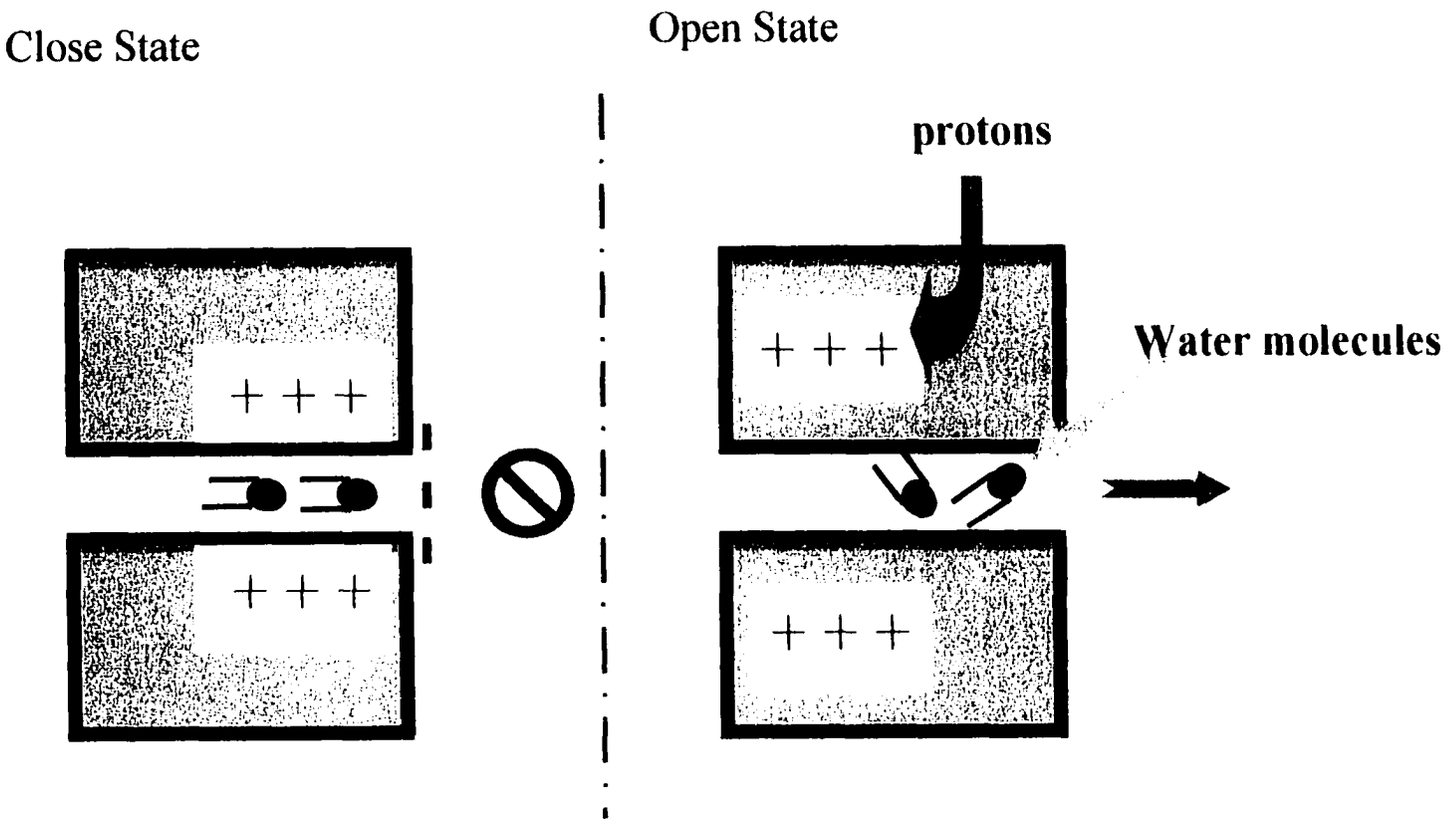

Orientation of figures: extracellular to the left and intracellular to the right

Fig.26 --- Our gating model for voltage-dependent ion channels: proton tunneling

Finally, a brief summary of our conclusions is stated as follows:

1. We have improved a method, Fourier Grid Hamiltonian method, for determining the three dimensional wave function of a predetermined potential energy surface.

2. We have extended the method to allow the inclusion of an electric field, and found a way to calculate the effect of a small change in field on the intermolecular transfer of a proton.

3. There is a range of a few tenths of an angstrom in intermolecular spacing within which nearly complete proton transfer between molecules which are plausible models for basic amino acids can occur under control of a change in field less than that found in biological membranes. This result is consistent with one of the requirements of a model we have proposed for ion channel gating. It is plausible that proton transfer with fields of the magnitudes considered here occur in certain important proteins.

Additional work will be needed to test the applicability of the idea in an actual protein. In fact, in recent work by Stefani, Bezanilla, and coworkers, two types of evidence have been found to confirm the coupling between gating and proton transport across membrane[129]. Usually valuable insights into the mechanism of gating can be obtained with site-directed labeling of substituted cysteines. However, the resolution of the confined space is limited by the large size of the thiol probe and the movement and charge of the original residue may be significantly disturbed by cysteine substitution and probe attachment. Stefani, Bezanilla and coworkers examined the environment of charged residues by replacing the voltage-sensing residue R365 or R368 with histidine, instead of cysteine. They performed individual histidine substitutions on a non-conducting (W434F)[130], noninactivating[131] version of the *Shake* H4 K+ channel[132]. The consistency between the voltage of maximum proton current and the midpoint of the Q-V curve for gating and the similarity of the steepness of the voltage-dependence for these two processes, gave the first and strong support of the coupling, also the closeness of the temperature dependence of proton current and of the kinetics of the gating current gave further evidence. Although their results confirmed the coupling of the movement of protons with the gating state of

an ion channel, their gating model is still based on the movement of the tertiary structure S4 transmembrane segment. This means that the gating proton transport must not be directly under the influence of the membrane potential change but is driven by the S4 segment. In a case, we are still interested in their result, since the proton movement experiment is consistent with our tunneling model.

5. PROSPECT

The MPM model has been used to simulate the positively charged amino acid residues (Arginine and Lysine) on the side-chain of channel protein. The same calculations may be carried out for carboxylic acid, for example ethanoic acid CH_3CO_2H, instead, to simulate the c-terminus of the side-chain. There are extensive studies on the carboxylic dimer[30,31] in the literature, and from them, we can safely predict that a similar result will be obtained if the same kind of calculation is carried out for system: carboxylic acid + proton + carboxylic acid (CPC), instead of MPM.

To improve our results, the following factors should be taken into account. a) fluctuation of the whole skeleton of the methylamine molecules, which include rotation of the hydrogens on the two methyl-carbons and two nitrogens, as well as vibration of the heavy atom skeleton. b) the reaction field of the system should also be added into the calculation, for the amino acid residues are not an isolated system but a part of the channel protein and therefore stabilized by their environment. c) the time factor should also be introduced into the calculation for a molecular dynamic analysis.

Factors a) and c) are closely connected and may be achieved partially by quantum mechanical vs. molecular mechanical (QM/MM) molecular dynamical calculation. That is, use Newtonian dynamics but with the interaction potential set up by quantum mechanics (Car-

Parrinello[39]). Up till now explicitly including the time coordinate in a three-dimensional quantum mechanical calculation is beyond the ability of computation. As to factor b), the well-known methods, such as the Born model and the Onsager model seem not suitable for our target, since the charged residues on the S4 segment are buried in the channel protein. The hybrid MM/QC[35] calculations are more flexible to suit this kind of problem. In MM/QC, the chemical system is divided into three regions (unlike in Born and Onsager models, which divide the system into two regions). The methodology allows QC-treatment of bond-breaking combined with Monte-Carlo or Molecular-dynamic simulation of solvent dynamics. However, the drawback of the complexity of three-dimensional calculation remains.

As a last comment, we would like to emphasis that control of tunneling process by external fields will has a significant impact on our future high technology. For instance, a recent study of a tunneling approach to intramolecular hydrogen transfer reactions controlled by ultra-short laser pulse, by Došlic et. al.[142], shows that the required laser field intensities are fifty times smaller than the pump-dump approach which drives the reactant wave packet over the potential barrier towards the product state without tunneling. From both kinetic and energetic aspects the tunneling mechanism is, in some circumstances, superior to the classical mechanisms. Quantum mechanical industrial technique is nevertheless great potential in the next century.

APPENDIX

3D FOURIER GRID HAMILTONIAN FORTRAN PROGRAM

SEPTEMBER 1998

------ THE FOLLOWING IS A FORTRAN PROGRAM IMPLEMENTED TO CARRY OUT OUR 3D FGH CALCULATION

```
C>>>>>>>>>>>>>>>>>>>>>>>>>>>  MAIN BLOCK BEGINS  <<<<<<<<<<<<<<<<<<<<<<<<<<<<<C
      REAL*8,DIMENSION(:),ALLOCATABLE :: T,V,U,W
      REAL*8,DIMENSION(:,:,:),ALLOCATABLE :: VA
      REAL*8,DIMENSION(:),ALLOCATABLE :: AR,AI
      REAL*8,DIMENSION(:),ALLOCATABLE :: ZR
      REAL*8,DIMENSION(:,:),ALLOCATABLE :: ZRV,ZIR,ZI
      COMPLEX*16,DIMENSION(:),ALLOCATABLE :: IM_V
      REAL*8 TT,TJ,TK,TI,V_MIN,PI,M_P,DELTA_X,SELECT_M
      INTEGER*4 NW,NWR,MJ,MK,MI,N1,N2,N3,MATZ,COUNTER,EISN,IERR
      INTEGER*4 J_MIN,CT,M1,M2,M3,NSQ,MSQ,N1H,N2H,N3H
      INTEGER*4 I,J,K,N1HD,N2HD,N3HD,RN1,RN2,RN3
      INTEGER*4 P(15)
      INTEGER*4, DIMENSION(:),ALLOCATABLE :: JUMP
      CHARACTER*18 TITLE
C
      COMMON/BLK1/COUNTER
      COMMON/BLK2/P
C ---- ASSIGN DATA -----
      PI=3.14159265358979D0
      M_P=1822.8880D0
      PRINT*,'M =',M_P
      DELTA_X=0.1D0/0.529177249D0
      PRINT*,'DELTA_X =',DELTA_X
```

```
C ---- STEP.1 ---- CONSTRUCTION OF H (NOTE: THE ORDER OF N1,N2, AND N3
C              CANNOT BE CHANGED AS FREE)
      N1=5
      N2=7
      N3=6
      M1=N2*N3
      M2=N3*N1
      M3=N1*N2
      NW=M3*N3
      NWR=NW
      MSQ=MOD(NW+1,2)
      NSQ=(NW+1-MSQ)/2
      MSQ=MOD(NW,2)
      NSQ=NSQ*(NW+1-MSQ)
      MSQ=NW*NW
C  SHIFT STRIDE SIZE IN EACH DIRECTION
      N1H=(N1-1)/2 + 1
      N2H=(N2-1)/2 + 1
      N3H=(N3-1)/2 + 1
      N1HD=N1/2
      N2HD=N2/2
      N3HD=N3/2
      RN1=MOD(N1+1,2)
      RN2=MOD(N2+1,2)
      RN3=MOD(N3+1,2)
      MATZ=1
      EISN=30
      EISN=MIN(EISN,60)
C
      OPEN(13,FILE='PES_M',ACCESS='SEQUENTIAL',STATUS='UNKNOWN',
     +          FORM='FORMATTED',ACTION='READ',POSITION='REWIND')
      ALLOCATE(VA(N1,N2,N3))
      READ(13,'(F23.13)')(((VA(I,J,K),K=1,N3),J=1,N2),I=1,N1)
      CLOSE(13)
      PRINT*,"PRECISION OF VARIABLES:",PRECISION(VA)
      PRINT*,"MINIMUM : ", MINVAL(VA)
      V_MIN=MINVAL(VA)
      FORALL (I=1:N1,J=1:N2,K=1:N3) VA(I,J,K)=VA(I,J,K)-V_MIN
C
      ALLOCATE(JUMP(NW))
      JUMP(1)=0
      DO J=1, NW-1
        JUMP(J+1)=JUMP(J)+J
      ENDDO
      VA = CSHIFT(VA,SHIFT=-N3HD, DIM=3)
      VA = CSHIFT(VA,SHIFT=-N2HD, DIM=2)
      VA = CSHIFT(VA,SHIFT=-N1HD, DIM=1)
C
      ALLOCATE(T(NW))
      TT=PI/DELTA_X
```

```
      DO KB=1, N1
        TK = SELECT_M(KB,N1H,RN1,N1,TK)
        DO JB=1, N2
              TJ = SELECT_M(JB,N2H,RN2,N2,TJ)
              DO IB=1, N3
                    TI = SELECT_M(IB,N3H,RN3,N3,TI)
                    MK=(KB-1)*M1
                    MJ=(JB-1)*N3
                    I=MJ+MK
         T(IB+MI)=(TI+TJ+TK)*TT*TT*2.D0/M_P
              ENDDO
        ENDDO
      ENDDO
C
      CT=0
      ALLOCATE(V(NW))
      FORALL (I=1:N1,J=1:N2,K=1:N3) V(K+(J-1)*N3+(I-1)*M1)=VA(I,J,K)
      DEALLOCATE(VA)
      ALLOCATE(AR(NSQ),AI(NSQ),IM_V(NW))
      DO 222 KB=1,NW
        DO JB=1,NW
            IM_V(JB)=(0.0D0,0.0D0)
        ENDDO
    IM_V(KB)=(1.0D0,0.0D0)
C  CONSTRUCT KINETIC OPERATOR MATRIX BY 1) FORWARD FFT
        CALL FFT3(1,NW,N1,N2,N3,M1,M2,M3,IM_V)
        NW=NWR
    DO JB=1,NW
            IM_V(JB)=IM_V(JB)*DCMPLX(T(JB))
        ENDDO
C  2) BACKWARD FFT
        CALL FFT3(-1,NW,N1,N2,N3,M1,M2,M3,IM_V)
        DO JB=1,NW
            IF(JB.LT.KB)GOTO 111
      AR(JB+(KB-1)*NW-JUMP(KB))=REAL(IM_V(JB))
      AI(JB+(KB-1)*NW-JUMP(KB))=IMAG(IM_V(JB))
            CT=CT+1
 111  ENDDO
C  ADD KINETIC OPERATOR MATRIX AND POTENTIAL OPERATOR MATRIX TOGETHER
      IM_V(KB)=IM_V(KB)+DCMPLX(V(KB))
      AR(KB+(KB-1)*NW-JUMP(KB))=REAL(IM_V(KB))
      AI(KB+(KB-1)*NW-JUMP(KB))=IMAG(IM_V(KB))
 222  CONTINUE
      DEALLOCATE(T,V)
C  FINISH OF CONSTRUCTING HAMILTONIAN H
      CT=(NW+MOD(NW,2))/2
      CT=CT*(NW+1-MOD(NW,2))
C ---- STEP.2 ---- SOLVE THE HOMOGENEOUS HAMILTONIAN EQUATIONS
      ALLOCATE(ZR(MSQ),W(NW),ZI(NW,60))
      CALL CH(NW,NW,AR,AI,W,ZR,ZI,MATZ,EISN,IERR,NSQ,MSQ,JUMP)
```

```
C FINISH SOLVING EIGENSYSTEM.  EIGENVALUES AND EIGENFUNCTIONS ARE FOUND
      NW=NWR
C
      IF(IERR.NE.0)THEN
        PRINT*,'SOMEWHERE WRONG !!'
        GOTO 444
      ENDIF
C
      ALLOCATE(VA(N1,N2,N3))
      ALLOCATE(ZRV(NW,60),ZIR(NW,60))
      DO K1=1,EISN
        DO J=1,NW
              ZRV(J,K1)=ZR(J+(K1-1)*NW)
        ENDDO
C SHIFT BACK TO ORIGINAL PHASE OF EIGENVECTORS
        FORALL (I=1:N1,J=1:N2,K=1:N3) VA(I,J,K)=ZRV(K+(J-1)*N3+
     +       (I-1)*M1,K1)
      VA = CSHIFT(VA,SHIFT=N3HD, DIM=3)
      VA = CSHIFT(VA,SHIFT=N2HD, DIM=2)
      VA = CSHIFT(VA,SHIFT=N1HD, DIM=1)
      FORALL (I=1:N1,J=1:N2,K=1:N3) ZRV(K+(J-1)*N3+(I-1)*M1,K1)=
     +       - VA(I,J,K)
      FORALL (I=1:N1,J=1:N2,K=1:N3) VA(I,J,K)=ZI(K+(J-1)*N3+
     +      (I-1)*M1,K1)
      VA = CSHIFT(VA,SHIFT=N3HD, DIM=3)
      VA = CSHIFT(VA,SHIFT=N2HD, DIM=2)
      VA = CSHIFT(VA,SHIFT=N1HD, DIM=1)
      FORALL (I=1:N1,J=1:N2,K=1:N3) ZIR(K+(J-1)*N3+(I-1)*M1,K1)=
     +       VA(I,J,K)
C FINISH ONE EIGENVECTOR, THEN GOING INTO THE NEXT ONE OR DONE
      ENDDO
C
      OPEN(10,FILE='ZR_M',ACCESS='SEQUENTIAL',STATUS='UNKNOWN',
     +  FORM='FORMATTED',ACTION='WRITE',POSITION='REWIND')
      WRITE(10,'(F20.13)')((ZRV(J,K),J=1,NW),K=1,EISN)
      CLOSE(10)
      OPEN(11,FILE='ZI_M',ACCESS='SEQUENTIAL',STATUS='UNKNOWN',
     +  FORM='FORMATTED',ACTION='WRITE',POSITION='REWIND')
      WRITE(11,'(F20.13)')((ZIR(J,K),J=1,NW),K=1,EISN)
      CLOSE(11)
C
 444  PRINT*,'FINISH',TITLE,'CALCULATION'
      STOP
      END
C>>>>>>>>>>>>>>>>>>>>     MAIN BLOCK FINISHED     <<<<<<<<<<<<<<<<<<<<C
C                                                                       C
C>>>>>>>>>>>>>>>>     SUBROUTINES & FUNCTIONS BEGIN     <<<<<<<<<<<<<<<<C
      REAL*8 FUNCTION SELECT_M(B,NH,RN,N,T)
      INTEGER*4 B,NH,RN,N
      REAL*8 T
```

```
      SELECT CASE (B-NH)
      CASE (:0)
       T=DBLE(B-1+RN)/DBLE(N)
      CASE (1:)
       T=DBLE(N-B+1)/DBLE(N)
      END SELECT
      SELECT_M = T*T
      RETURN
      END FUNCTION SELECT_M
C-----------------------------------------------------------------------
      SUBROUTINE FFT1(SIGMA,N,IMME_VEC)
      DIMENSION P(15),PM(15)
      COMPLEX*16 IMME_VEC(N)
      REAL*8 CART_VEC,NORM
      INTEGER*4 N,M,P,Q,NM,QM,PM,COUNTER,SIGMA

      COMMON/BLK1/COUNTER
      COMMON/BLK2/P
      M=N
      CALL FACT_N(N)
C
      NORM=DSQRT(DBLE(M))
      DO J=1,M
        IMME_VEC(J)=IMME_VEC(J)/DBLE(NORM)
                        !SCALING
      ENDDO
C
      IF(COUNTER.EQ.1)THEN
      CALL ITF_M(SIGMA,M,N,N,1,IMME_VEC)
      GOTO 444
      ENDIF
      DO J=1,COUNTER
        IF(P(J).GT.89)GOTO 444
      ENDDO
      NM=M
      QM=1
      PM(1)=1
      DO J=1,COUNTER
          PM(J+1)=P(J)
      ENDDO
      DO I=1,COUNTER-1
            NM=NM/PM(I)
            QM=QM*PM(I)
            Q=NM/PM(I+1)
         DO L=1,QM
       CALL P_M(M,NM,Q,L,IMME_VEC)
                CALL ITF_M(SIGMA,M,NM,PM(I+1),L,IMME_VEC)
            CALL T_M(SIGMA,M,NM,PM(I+1),L,IMME_VEC)
            CALL P_M(M,NM,PM(I+1),L,IMME_VEC)
         ENDDO
```

```
200     ENDDO
        DO L=1,QM
        CALL ITF_M(SIGMA,M,NM,Q,L,IMME_VEC)
        CALL P_M(M,NM,Q,L,IMME_VEC)
        ENDDO
        IF(COUNTER.GT.2)THEN
        DO I=COUNTER-2,1,-1
          NM=NM*PM(I+1)
          QM=QM/PM(I+1)
        Q=Q*PM(I+2)
        DO L=1,QM
       CALL P_M(M,NM,Q,L,IMME_VEC)
          ENDDO
        ENDDO
        ENDIF
C  OUT OF BACKWARD LOOP
 444    RETURN
        END
C-------------------------------------------------
        SUBROUTINE FFT3(SIGMA,NF3,N1,N2,N3,M1,M2,M3,IMM_VF3)
        COMPLEX*16 IMM_VF3(NF3),IMME_VEC(NF3)
        INTEGER*4 NF3,NREC,N1,N2,N3,M1,M2,M3,SIGMA
        INTEGER*4 N1REC,N2REC,N3REC
C
        NREC=NF3
        N1REC=N1
        N2REC=N2
        N3REC=N3
C
        DO JF3=1,M3
        DO KF3=1,N3
         IMME_VEC(KF3)=IMM_VF3(KF3+(JF3-1)*N3)
        ENDDO
          CALL FFT1(SIGMA,N3,IMME_VEC)
          N3=N3REC
          DO KF3=1,N3
               IMM_VF3(KF3+(JF3-1)*N3)=IMME_VEC(KF3)
          ENDDO
        ENDDO
        CALL P_M(NREC,NREC,N3,1,IMM_VF3)
        DO JF3=1,M2
        DO KF3=1,N2
       IMME_VEC(KF3)=IMM_VF3(KF3+(JF3-1)*N2)
        ENDDO
          CALL FFT1(SIGMA,N2,IMME_VEC)
          N2=N2REC
          DO KF3=1,N2
               IMM_VF3(KF3+(JF3-1)*N2)=IMME_VEC(KF3)
          ENDDO
        ENDDO
```

```
      CALL P_M(NREC,NREC,M3,1,IMM_VF3)
      CALL P_M(NREC,NREC,M1,1,IMM_VF3)
      DO JF3=1,M1
      DO KF3=1,N1
     IMME_VEC(KF3)=IMM_VF3(KF3+(JF3-1)*N1)
      ENDDO
      CALL FFT1(SIGMA,N1,IMME_VEC)
        N1=N1REC
     DO KF3=1,N1
        IMM_VF3(KF3+(JF3-1)*N1)=IMME_VEC(KF3)
     ENDDO
      ENDDO
      CALL P_M(NREC,NREC,N1,1,IMM_VF3)
C
      RETURN
      END
C-----------------------------------------------------
      SUBROUTINE FACT_N(N)
      DIMENSION P(15)
      INTEGER*4 COUNTER,SGNAL,I,J,P,Q,N,M
      REAL*8 QT,ROOT
      COMMON/BLK1/COUNTER
      COMMON/BLK2/P
      COMMON/BLK3/QT,ROOT

      I=1
      J=0
      SGNAL=1
      CALL FAC2(N,I,1,SGNAL,J)
      I=1
100   DO WHILE (SGNAL.EQ.1)
         CALL FAC2(N,I,2,SGNAL,J)
      ENDDO
400   COUNTER=J+1
      P(COUNTER)=N
      RETURN
      END
C-----------------------------------------------------
      SUBROUTINE FAC2(N,I,K,SIGNL,J)
      DIMENSION P(15)
      INTEGER*4 SIGNL,I,K,J,P,Q,N,M
      REAL*8 QT,ROOT
      COMMON/BLK2/P
      OMMON/BLK3/QT,ROOT

      I=I+K
      DO WHILE (SIGNL.EQ.1)
         ROOT=DSQRT(DBLE(N))
         IF(DBLE(I).LE.ROOT)THEN
            QT=DMOD(DBLE(N),DBLE(I))
```

```
            IF(QT.LT..1D0)THEN
               J=J+1
               P(J)=I
               N=NINT(DBLE(N)/DBLE(I))
            ELSE
               GO TO 400
            ENDIF
         ELSE
            SIGNL=0
         ENDIF
300   ENDDO
400   RETURN
      END
C-----------------------------------------------------------
      SUBROUTINE ITF_M(SIGMA,NIFW,NM,RD,L,IMME_VEC)
      COMPLEX*16 IMM(NM),IMME_VEC(NIFW),F(90,90)
      INTEGER*4 NM,NIFW,L,RD,PD,SIGMA
      CALL F_M(RD,F,SIGMA)
      PD=NM/RD
      DO K=1,PD
         DO J=1,RD
            IMM(J)=(0.D0,0.D0)
            DO I=1,RD
         IMM(J)=IMM(J)+F(J,I)*IMME_VEC(I+
     +                  (K-1)*RD+(L-1)*NM)
            ENDDO
         ENDDO
         DO J=1,RD
         IMME_VEC(J+(K-1)*RD+(L-1)*NM)=IMM(J)
         ENDDO
      ENDDO
      RETURN
      END
C-----------------------------------------------------------
      SUBROUTINE F_M(RD,F,SIGMA)
      COMPLEX*16 PI,UB,F(90,90)
      INTEGER*4 RD,SIGMA
      PI=(3.14159265358979323D0,0.D0)
      UB=(0.D0,1.D0)
      UB=UB*(2.D0,0.D0)*PI
      UB=UB/DCMPLX(RD)
      UB=CDEXP(DCMPLX(SIGMA)*UB)
      DO K=1,RD
         DO J=1,RD
            F(J,K)=UB**((J-1)*(K-1))
         ENDDO
      ENDDO
      RETURN
      END
C-----------------------------------------------------------
```

```
      SUBROUTINE P_M(NW,NM,QD,L,IMM)
      DIMENSION IMM(NW),IMMP(NM)
      INTEGER*4 J,J1,K,NM,QD,L
      COMPLEX*16 IMM,IMMP
      FORALL (J=1:NM) IMMP(J)=IMM(1+(J-1)*QD/NM+MOD((J-1)*QD.
     +          NM)+(L-1)*NM)
      FORALL (I=1:NM) IMM(I+(L-1)*NM)=IMMP(I)
  200 RETURN
      END
C-----------------------------------------------------------
      SUBROUTINE T_M(SIGMA,NTW,ND,FD,LD,IMMV)
      DIMENSION IMMV(NTW)
      COMPLEX*16 IMMV,V
      REAL*8 PI
      INTEGER*4 NTW,ND,FD,RESJ,RATJ,SIGMA
      PI=3.14159265358979323D0
      V=(0.D0,1.D0)
      V=2.D0*SIGMA*PI*V/DBLE(ND)
      DO J=1,ND
         RESJ=MOD(J-1,INT(FD))
         RATJ=(J-1)/FD
         IMMV(J+(LD-1)*ND)=IMMV(J+(LD-
     +                1)*ND)*CDEXP(DBLE(RESJ*RATJ)*V)
      ENDDO

  400 RETURN
      END
C-----------------------------------------------------------
      SUBROUTINE CH(NM,N,AR,AI,W,ZR,ZI,MATZ,EISN,IERR,NSQ,MSQ,JUMP)
      INTEGER*4 I,J,N,NM,IERR,MATZ,EISN,NSQ,MSQ,JUMP(N)
      DOUBLE PRECISION AR(NSQ),AI(NSQ),W(N),ZR(MSQ),ZI(N,60)
      DOUBLE PRECISION FV1(N),FV2(N),FM1(2,N)
C
      IF (N .LE. NM) GO TO 10
      IERR = 10 * N
      GO TO 50
C
   10 CALL  HTRIDI(NM,N,AR,AI,W,FV1,FV2,FM1,NSQ,JUMP)
      PRINT*,'MATZ=',MATZ
      IF (MATZ .NE. 0) GO TO 20
C    ..... FIND EIGENVALUES ONLY .....
      CALL  TQLRAT(N,W,FV2,IERR)
      GO TO 50
C    ..... FIND BOTH EIGENVALUES AND EIGENVECTORS .....
   20 DO 40 I = 1, N
      DO 30 J = 1, N
      ZR(J+(I-1)*N) = 0.0D0
   30 CONTINUE
C
      ZR(I+(I-1)*N) = 1.0D0
```

```
 40     CONTINUE
C
        CALL  TQL2(NM,N,W,FV1,ZR,IERR,MSQ)
        PRINT*,'GOING INTO HRTIBK  - - - - - - -'
        IF (IERR .NE. 0) GO TO 50
        CALL  HTRIBK(NM,N,AR,AI,FM1,EISN,ZR,ZI,NSQ,MSQ,JUMP)
C
 50     OPEN(12,FILE='W_M',ACCESS='SEQUENTIAL',STATUS='UNKNOWN',
   +    FORM='FORMATTED',ACTION='WRITE',POSITION='REWIND')
        WRITE(12,'(F20.13)')(W(J),J=1,EISN)
        CLOSE(12)
C
        RETURN
        END
C-------------------------------------------------------
        DOUBLE PRECISION FUNCTION EPSLON (X)
        DOUBLE PRECISION X
        DOUBLE PRECISION A,B,C,EPS
C
        A = 4.0D0/3.0D0
  10    B = A - 1.0D0
        C = B + B + B
        EPS = DABS(C-1.0D0)
        IF (EPS .EQ. 0.0D0) GO TO 10
        EPSLON = EPS*DABS(X)
        RETURN
        END
C-------------------------------------------------------
        SUBROUTINE HTRIBK(NM,N,AR,AI,TAU,M,ZR,ZI,NSQ,MSQ,JUMP)
C
        INTEGER*4 I,J,K,L,M,N,NM,NSQ,MSQ,JUMP(N)
        DOUBLE PRECISION AR(NSQ),AI(NSQ),TAU(2,N),
   X    ZR(MSQ),ZI(N,60)
        DOUBLE PRECISION H,S,SI
C
        PRINT*,'IN HTRIBK - - - - - -'
        IF (M .EQ. 0) GO TO 200
C     ..... TRANSFORM THE EIGENVECTORS OF THE REAL SYMMETRIC
C           TRIDIAGONAL MATRIX TO THOSE OF THE HERMITIAN
C           TRIDIAGONAL MATRIX. .....
        DO 50 K = 1, N
C
        DO 50 J = 1, M
        ZI(K,J) = -ZR(K+(J-1)*N) * TAU(2,K)
        ZR(K+(J-1)*N) = ZR(K+(J-1)*N) * TAU(1,K)
  50    CONTINUE
C
        IF (N .EQ. 1) GO TO 200
C     ..... RECOVER AND APPLY THE HOUSEHOLDER MATRICES .....
        DO 140 I = 2, N
```

```
      L = I - 1
      H = AI(I+(I-1)*N-JUMP(I))
      IF (H .EQ. 0.0D0) GO TO 140
C
      DO 130 J = 1, M
      S = 0.0D0
      SI = 0.0D0
C
      DO 110 K = 1, L
        S = S + AR(I+(K-1)*N-JUMP(K)) * ZR(K+(J-1)*N) -
     X      AI(I+(K-1)*N-JUMP(K)) * ZI(K,J)
        SI = SI + AR(I+(K-1)*N-JUMP(K)) * ZI(K,J) +
     X      AI(I+(K-1)*N-JUMP(K)) * ZR(K+(J-1)*N)
  110   CONTINUE
C     ..... DOUBLE DIVISIONS AVOID POSSIBLE UNDERFLOW .....
      S = (S / H) / H
      SI = (SI / H) / H
C
      DO 120 K = 1, L
        ZR(K+(J-1)*N) = ZR(K+(J-1)*N) - S * AR(I+(K-1)*N-
     X      JUMP(K)) - SI * AI(I+(K-1)*N-JUMP(K))
        ZI(K,J) = ZI(K,J) - SI * AR(I+(K-1)*N-JUMP(K)) +
     X      S * AI(I+(K-1)*N-JUMP(K))
  120   CONTINUE
C
  130 CONTINUE
C
  140 CONTINUE
C
  200 RETURN
      END
C-------------------------------------------------------
      SUBROUTINE HTRIDI(NM,N,AR,AI,D,E,E2,TAU,NSQ,JUMP)
C
      INTEGER*4 I,J,K,L,N,II,NM,JP1,NSQ,JUMP(N)
      DOUBLE PRECISION AR(NSQ),AI(NSQ),D(N),E(N),
     X      E2(N),TAU(2,N)
      DOUBLE PRECISION F,G,H,FI,GI,HH,SI,SCALE,PYTHAG
C
            TAU(1,N) = 1.0D0
      TAU(2,N) = 0.0D0
C
      DO 100 I = 1, N
  100 D(I) = AR(I+(I-1)*N-JUMP(I))
C     ..... FOR I=N STEP -1 UNTIL 1 DO -- .....
      DO 300 II = 1, N
      I = N + 1 - II
            L = I - 1
      H = 0.0D0
      SCALE = 0.0D0
```

```
      IF (L .LT. 1) GO TO 130
C     ..... SCALE ROW (ALGOL TOL THEN NOT NEEDED) .....
      DO 120 K = 1, L
  120    SCALE = SCALE + DABS(AR(I+(K-1)*N-JUMP(K))) + DABS(AI(I+(K-
     X       1)*N-JUMP(K)))
         IF (SCALE .NE. 0.0D0) GO TO 140
         TAU(1,L) = 1.0D0
         TAU(2,L) = 0.0D0
  130    E(I) = 0.0D0
         E2(I) = 0.0D0
         GO TO 290
  140    DO 150 K = 1, L
         AR(I+(K-1)*N-JUMP(K)) = AR(I+(K-1)*N-JUMP(K)) / SCALE
         AI(I+(K-1)*N-JUMP(K)) = AI(I+(K-1)*N-JUMP(K)) / SCALE
         H = H + AR(I+(K-1)*N-JUMP(K)) * AR(I+(K-1)*N-JUMP(K)) +
     X       AI(I+(K-1)*N-JUMP(K)) * AI(I+(K-1)*N-JUMP(K))
  150 CONTINUE
C
      E2(I) = SCALE * SCALE * H
      G = DSQRT(H)
      E(I) = SCALE * G
      F = PYTHAG(AR(I+(L-1)*N-JUMP(L)),AI(I+(L-1)*N-JUMP(L)))
C     ..... FORM NEXT DIAGONAL ELEMENT OF MATRIX T .....
      IF (F .EQ. 0.0D0) GO TO 160
      TAU(1,L) = (AI(I+(L-1)*N-JUMP(L)) * TAU(2,I) - AR(I+(L-
     X       1)*N-JUMP(L)) * TAU(1,I)) / F
      SI = (AR(I+(L-1)*N-JUMP(L)) * TAU(2,I) + AI(I+(L-
     X    1)*N-JUMP(L)) * TAU(1,I)) / F
      H = H + F * G
      G = 1.0D0 + G / F
      AR(I+(L-1)*N-JUMP(L)) = G * AR(I+(L-1)*N-JUMP(L))
      AI(I+(L-1)*N-JUMP(L)) = G * AI(I+(L-1)*N-JUMP(L))
      IF (L .EQ. 1) GO TO 270
      GO TO 170
  160 TAU(1,L) = -TAU(1,I)
      SI = TAU(2,I)
      AR(I+(L-1)*N-JUMP(L)) = G
  170 F = 0.0D0
C
      DO 240 J = 1, L
      G = 0.0D0
      GI = 0.0D0
C     ..... FORM ELEMENT OF A*U .....
      DO 180 K = 1, J
         G = G + AR(J+(K-1)*N-JUMP(K)) * AR(I+(K-1)*N-JUMP(K)) +
     X     AI(J+(K-1)*N-JUMP(K)) * AI(I+(K-1)*N-JUMP(K))
         GI = GI - AR(J+(K-1)*N-JUMP(K)) * AI(I+(K-1)*N-JUMP(K)) +
     X     AI(J+(K-1)*N-JUMP(K)) * AR(I+(K-1)*N-JUMP(K))
  180    CONTINUE
C
```

```
      JP1 = J + 1
      IF (L .LT. JP1) GO TO 220
C
      DO 200 K = JP1, L
         G = G + AR(K+(J-1)*N-JUMP(J)) * AR(I+(K-1)*N-JUMP(K)) -
     X     AI(K+(J-1)*N-JUMP(J)) * AI(I+(K-1)*N-JUMP(K))
         GI = GI - AR(K+(J-1)*N-JUMP(J)) * AI(I+(K-1)*N-JUMP(K)) -
     X     AI(K+(J-1)*N-JUMP(J)) * AR(I+(K-1)*N-JUMP(K))
  200 CONTINUE
C     ..... FORM ELEMENT OF P .....
  220 E(J) = G / H
      TAU(2,J) = GI / H
      F = F + E(J) * AR(I+(J-1)*N-JUMP(J)) - TAU(2,J) * AI(I+(J-
     X    1)*N-JUMP(J))
  240 CONTINUE
C
      HH = F / (H + H)
C     ..... FORM REDUCED A .....
      DO 260 J = 1, L
      F = AR(I+(J-1)*N-JUMP(J))
      G = E(J) - HH * F
      E(J) = G
      FI = -AI(I+(J-1)*N-JUMP(J))
      GI = TAU(2,J) - HH * FI
      TAU(2,J) = -GI
C
      DO 260 K = 1, J
        AR(J+(K-1)*N-JUMP(K)) = AR(J+(K-1)*N-JUMP(K)) - F * E(K)
     X        - G * AR(I+(K-1)*N-JUMP(K)) + FI * TAU(2,K) +
     X        GI * AI(I+(K-1)*N-JUMP(K))
        AI(J+(K-1)*N-JUMP(K)) = AI(J+(K-1)*N-JUMP(K)) - F *
     X        TAU(2,K) - G * AI(I+(K-1)*N-JUMP(K)) - FI *
     X        E(K) - GI * AR(I+(K-1)*N-JUMP(K))
  260 CONTINUE
C
  270 DO 280 K = 1, L
      AR(I+(K-1)*N-JUMP(K)) = SCALE * AR(I+(K-1)*N-JUMP(K))
      AI(I+(K-1)*N-JUMP(K)) = SCALE * AI(I+(K-1)*N-JUMP(K))
  280 CONTINUE
C
      TAU(2,L) = -SI
  290 HH = D(I)
      D(I) = AR(I+(I-1)*N-JUMP(I))
      AR(I+(I-1)*N-JUMP(I)) = HH
      AI(I+(I-1)*N-JUMP(I)) = SCALE * DSQRT(H)
  300 CONTINUE
C
      RETURN
      END
```

```
C-----------------------------------------------------------
      SUBROUTINE TQLRAT(N,D,E2,IERR)
C
      INTEGER*4 I,J,L,M,N,II,L1,MML,IERR
      DOUBLE PRECISION D(N),E2(N)
      DOUBLE PRECISION B,C,F,G,H,P,R,S,T,EPSLON,PYTHAG
C
            IERR = 0
      IF (N .EQ. 1) GO TO 1001
C
      DO 100 I = 2, N
  100 E2(I-1) = E2(I)
C
      F = 0.0D0
      T = 0.0D0
      E2(N) = 0.0D0
C
      DO 290 L = 1, N
      J = 0
      H = DABS(D(L)) + DSQRT(E2(L))
      IF (T .GT. H) GO TO 105
      T = H
      B = EPSLON(T)
      C = B * B
C     ..... LOOK FOR SMALL SQUARED SUB-DIAGONAL ELEMENT .....
  105 DO 110 M = L, N
      IF (E2(M) .LE. C) GO TO 120
C     ..... E2(N) IS ALWAYS ZERO, SO THERE IS NO EXIT
C           THROUGH THE BOTTOM OF THE LOOP .....
  110 CONTINUE
C
  120 IF (M .EQ. L) GO TO 210
  130 IF (J .EQ. 30) GO TO 1000
      J = J + 1
C     ..... FORM SHIFT .....
      L1 = L + 1
      S = DSQRT(E2(L))
      G = D(L)
      P = (D(L1) - G) / (2.0D0 * S)
      R = PYTHAG(P,1.0D0)
      D(L) = S / (P + DSIGN(R,P))
      H = G - D(L)
C
      DO 140 I = L1, N
  140 D(I) = D(I) - H
C
      F = F + H
C     ..... RATIONAL QL TRANSFORMATION .....
      G = D(M)
      IF (G .EQ. 0.0D0) G = B
```

```
      H = G
      S = 0.0D0
      MML = M - L
C     ..... FOR I=M-1 STEP -1 UNTIL L DO -- .....
      DO 200 II = 1, MML
      I = M - II
      P = G * H
      R = P + E2(I)
      E2(I+1) = S * R
      S = E2(I) / R
      D(I+1) = H + S * (H + D(I))
      G = D(I) - E2(I) / G
      IF (G .EQ. 0.0D0) G = B
      H = G * P / R
  200 CONTINUE
C
      E2(L) = S * G
      D(L) = H
C     ..... GUARD AGAINST UNDERFLOW IN CONVERGENCE TEST .....
      IF (H .EQ. 0.0D0) GO TO 210
      IF (DABS(E2(L)) .LE. DABS(C/H)) GO TO 210
      E2(L) = H * E2(L)
      IF (E2(L) .NE. 0.0D0) GO TO 130
  210 P = D(L) + F
C     ..... ORDER EIGENVALUES .....
      IF (L .EQ. 1) GO TO 250
C     ..... FOR I=L STEP -1 UNTIL 2 DO -- .....
      DO 230 II = 2, L
      I = L + 2 - II
      IF (P .GE. D(I-1)) GO TO 270
      D(I) = D(I-1)
  230 CONTINUE
C
  250 I = 1
  270 D(I) = P
  290 CONTINUE
C
      GO TO 1001
C     ..... SET ERROR -- NO CONVERGENCE TO AN
C           EIGENVALUE AFTER 30 ITERATIONS .....
 1000 IERR = L
 1001 RETURN
      END
C-----------------------------------------------------------
      DOUBLE PRECISION FUNCTION PYTHAG(A,B)
      DOUBLE PRECISION A,B
C
C     FINDS DSQRT(A**2+B**2) WITHOUT OVERFLOW OR DESTRUCTIVE UNDERFLOW
C
      DOUBLE PRECISION P,R,S,T,U
```

```
      P = DMAX1(DABS(A),DABS(B))
      IF (P .EQ. 0.0D0) GO TO 20
      R = (DMIN1(DABS(A),DABS(B))/P)**2
 10   CONTINUE
      T = 4.0D0 + R
      IF (T .EQ. 4.0D0) GO TO 20
       S = R/T
      U = 1.0D0 + 2.0D0*S
      P = U*P
      R = (S/U)**2 * R
      GO TO 10
 20   PYTHAG = P
      RETURN
      END
C-----------------------------------------------------------------
      SUBROUTINE TQL2(NM,N,D,E,Z,IERR,MSQ)
C
      INTEGER*4 I,J,K,L,M,N,II,L1,L2,NM,MML,IERR,MSQ
      DOUBLE PRECISION D(N),E(N),Z(MSQ)
      DOUBLE PRECISION C,C2,C3,DL1,EL1,F,G,H,P,R,S,S2,TST1,TST2,PYTHAG
C
      IERR = 0
      IF (N .EQ. 1) GO TO 1001
C
      DO 100 I = 2, N
 100  E(I-1) = E(I)
C
      F = 0.0D0
      TST1 = 0.0D0
      E(N) = 0.0D0
C
      DO 240 L = 1, N
      PRINT*,L
      J = 0
      H = DABS(D(L)) + DABS(E(L))
      IF (TST1 .LT. H) TST1 = H
C     ..... LOOK FOR SMALL SUB-DIAGONAL ELEMENT .....
      DO 110 M = L, N
      TST2 = TST1 + DABS(E(M))
      IF (TST2 .EQ. TST1) GO TO 120
C     ..... E(N) IS ALWAYS ZERO, SO THERE IS NO EXIT
C           THROUGH THE BOTTOM OF THE LOOP .....
 110  CONTINUE
C
 120  IF (M .EQ. L) GO TO 220
 130  IF (J .EQ. 30) GO TO 1000
      J = J + 1
C     ..... FORM SHIFT .....
      L1 = L + 1
      L2 = L1 + 1
```

```
      G = D(L)
      P = (D(L1) - G) / (2.0D0 * E(L))
      R = PYTHAG(P,1.0D0)
      D(L) = E(L) / (P + DSIGN(R,P))
      D(L1) = E(L) * (P + DSIGN(R,P))
      DL1 = D(L1)
      H = G - D(L)
      IF (L2 .GT. N) GO TO 145
C
      DO 140 I = L2, N
  140 D(I) = D(I) - H
C
  145 F = F + H
C     ..... QL TRANSFORMATION .....
      P = D(M)
      C = 1.0D0
      C2 = C
      EL1 = E(L1)
      S = 0.0D0
      MML = M - L
C     ..... FOR I=M-1 STEP -1 UNTIL L DO -- .....
      DO 200 II = 1, MML
      C3 = C2
      C2 = C
      S2 = S
      I = M - II
      G = C * E(I)
      H = C * P
      R = PYTHAG(P,E(I))
      E(I+1) = S * R
      S = E(I) / R
      C = P / R
      P = C * D(I) - S * G
      D(I+1) = H + S * (C * G + S * D(I))
C     ..... FORM VECTOR .....
      DO 180 K = 1, N
         H = Z(K+(I+1-1)*N)
         Z(K+(I+1-1)*N) = S * Z(K+(I-1)*N) + C * H
         Z(K+(I-1)*N) = C * Z(K+(I-1)*N) - S * H
  180 CONTINUE
C
  200 CONTINUE
C
      P = -S * S2 * C3 * EL1 * E(L) / DL1
      E(L) = S * P
      D(L) = C * P
      TST2 = TST1 + DABS(E(L))
      IF (TST2 .GT. TST1) GO TO 130
  220 D(L) = D(L) + F
  240 CONTINUE
```

```
C     ..... ORDER EIGENVALUES AND EIGENVECTORS .....
      DO 300 II = 2, N
      I = II - 1
      K = I
      P = D(I)
C
      DO 260 J = II, N
      IF (D(J) .GE. P) GO TO 260
      K = J
      P = D(J)
 260  CONTINUE
C
      IF (K .EQ. I) GO TO 300
      D(K) = D(I)
      D(I) = P
C
      DO 280 J = 1, N
      P = Z(J+(I-1)*N)
      Z(J+(I-1)*N) = Z(J+(K-1)*N)
      Z(J+(K-1)*N) = P
 280  CONTINUE
C
 300  CONTINUE
C
      GO TO 1001
C     ..... SET ERROR -- NO CONVERGENCE TO AN
C           EIGENVALUE AFTER 30 ITERATIONS .....
 1000 IERR = L
 1001 RETURN
      END

C>>>>>>>>>>>>>>>>>  SUBROUTINES & FUNCTIONS FINISHED  <<<<<<<<<<<<<<<<<C
```

REFERENCES

1. a) J. Lu and M. E. Green, *Progr. Colloid Polym. Sci.* **103**, 121 (1997); b) M. E. Green and J. Lu, *J. Colloid Interface Sci.* **171**, 117 (1995); c) M. E. Green and J. Lu, *J. Phys. Chem.* **101**, 6512 (1997)

2. B. Hille, *Ionic Channels of Excitable Membranes*, 2nd ed. (Sinauer, Sunderland, MA, 1992)

3. D. J. Lockhart and P. S. Kim, *Science* **257**, 947 (1992)

4. a) E.F. Caldin and V. Gold, *Proton Transfer Reactions* (Halsted, New York, 1975); b) R. Stewart, *The Proton: Applications to Organic Chemistry* (Academic, Orlando, 1985)

5. M. Meot-Ner and S.C. Smith, *J.Amer. Chem. Soc.* **113**, 862 (1991)

6. a) A. Piekara, *Bull. Ampere* (Leipzig) **10**, 15 (1961); b) A. Piekara, *J. Chem. Phys.* **36**, 2145 (1962); c) I. Danielewicz-Ferchmin, *Z. Phys. Chemie* (Leipzig) **259**, 1(1978); d) G. Zundel, *J. Molec. Struct.* **177**, 43 (1988); e) J. Brickmann *in "The Hydrogen Bond—Recent developments in theory and experiments"* (Ed. P. Schuster) (North Holland, Amsterdam, 1976) p219 ff; f) E. G. Weidemann *ibid*, p. 246 ff; g) G. L. Hofacker, Y. Marechal, and M. A. Ratner *ibid*, p. 295 ff; h) D. Borgis, *Chemical Physics* **170**, 315 (1993); i) F. Fillaux and J. Tomkinson, *Chemical Physics* **158**, 113 (1991)

7. M. E. Tuckerman, D. Mark, M. L. Klein, and M. Parrinello, *Science* **275**, 817 (1997)

8. G. Gamow, a) *Z. Physik* **51**, 204, (1928); b) *Z. Physik* **52**, 510, (1928)

9. R.W. Gurnney and E.U. Condon, *Phys. Rev.* **33**, 127 (1929)

10. D.M. Dennison and G.E. Uhlenbeck, *Phys. Rev.* **41**, 313 (1932)

11. a) R.J. Saykally, *Science* **239**, 157 (1988); b) A. Blake, *ibid.* **259**, 1570 (1993)

12. R. Pomes and B. Roux, *J. Chem. Phys.* **100**, 2519 (1996)

13. P. M. Kiefer, V. B. P. Leite and R. M. Whitnell, *Chemical Physics* **194**,33 (1995)

14. Y. Guo, T. D. Sewall, and D. L. Thompson, *Chem. Phys. Letters* **224**,470 (1994)

15. A. Sanchez and M. Galan, *J. Phys. Chem.*, **100**, 18415 (1996)

16. Y. Dakhnovsky, *J. Chem. Phys.* **100**, 6492 (1994)

17. Y. Dakhnovsky and T. Coalson *J. Chem. Phys.* **103**, 2908 (1995)

18. M. Morillo, C. Denk, and R. I. Cukier, *Chem. Phys.* **212**, 157 (1996)

19. R. I. Cukier and M. Morillo, *Chem. Phys.* **183**, 375 (1994)

20. M. Morillo and R. I. Cukier, *J. Chem. Phys.* **92**, 4833 (1990)

21. a) R. I. Cukier and M. Morillo, *J. Chem. Phys.* **91**, 857 (1989); b) *Phys. Rev.* **B 54**, 13962 (1996)

22. M. Morillo and R.I. Cukier, *J. Chem. Phys.* **98**, 4548 (1993)

23. a) C. L. Schauf and J. O. Bullock, *Biophys. J.*, **30**, 295 (1980); b) Schauf, C. L. and J. O. Bullock, *Biophys. J.* **27**, 193 (1979)

24. D. A. Alicata, M. D. Rayner, and J. G. Starkus, *Biophys. J.* **57**, 745 (1990)

25. E. Stefani and F. Bezanilla, *Biophys. J.* **72**, A131 (1997)

26. F. Noceti, D. Sigg, F. Bezanilla, and E. Stefani, *Biophys. J.* **74**, A214 (1998)

27. M. Sprik , J.Hutter, and M. Parrinello, *J.Chem.Phys.* **105**, 1142, (1996)

28. a) C. R. D. Lancaster, H. Michel, B. Honig, M. Gunner, *Biophys. J.* **70**, 2469 (1996); b) M. R. Gunner, A. Nicholls, and B. Honig, *J. Phys. Chem.* **100**, 4277 (1997)

29. 22. G. J. Kearley, F. Fillaux, M.-H. Baron, S. Bennington and J. Tomkinson, *Science*, **264**, 1285 (1994)

30. a) R. Meyer and R. R. Ernst, *J. Chem. Phys.* **86**, 784 (1987). b) B. H. Meier, F. Graf, and R. R. Ernst, *J. Chem. Phys.* **76**, 767 (1982)

31. F. Graf, R. Meyer, T-K. Ha, and R. R. Ernst, *J. Chem. Phys.* **75**, 2914 (1981)

32. P. Ehrenfest, *Z. Phys.* **45**, 455 (1927)

33. P.A.M. Dirac, *Proc. Cambridge Philos. Soc.* **26**, 376 (1930)

34. N.F. Mott, *Proc. Cambridge Philos. Soc.***27**, 533 (1931)

35. Bala, P; Lesyng, B; Truong, T.N.; McCammon, J.A. In *The Role of Computational Models and Theories in Biotechnology*; Bertran, J., Ed; NATO ASI Series; Kluwer Academic Publishers; Dordrecht, pp299-326 (1992)

36. Bala, P; Lesyng, B.; McCommon, J.A. *Chem.Phys.Lett.* **219**, 259 (1994)

37. a) B. J. Berne and D. Thirumalai, *Annu. Rev. Phys. Chem.* **37**, 401 (1986); b) D. M. Ceperley, *Rev. Mod. Phys.* **67**, 279 (1995).

38. a) R. O. Jones and O. Gunnarsson, *Rev. Mod. Phys.* **61**, 689 (1989); b) M. C. Payne, ... , J. D. Joannopoulos, *Rev. Mod. Phys.* **64**, 1045 (1992)

39. a) R. Car and M. Parrinello, *Phys. Rev. Lett.* **55**, 2471 (1985); b) D. Marx and M. Parrinello, *Z. Phys.* **B**(rapid note) **95**, 143 (1996); c) D. Marx and M. Parrinello, *J. Chem. Phys.* **104**, 4077 (1996)

40. a) J. Theilhaber, *Phys. Fluids* **B** (*Plasma Phys.*) 4.(part2), 2044 (1992); b)Theilhaber, J. *Int. J. Quantum Chem., Quantum Chem. Symp.*, **28**, 611 (1994)

41. R. Alimi, R.B. Gerber, A.D. Hammerich, R. Kosloff, *J.Chem. Phys.* **93**, 6484 (1990)

42. Berendsen, H.J.C.; Marvi, J. *J.Phys.Chem.* **97**, 13464 (1993)

43. Sigworth, F.J., *Quart. Rev. Biophys.* **27**, pp1 - 40 (1993)

44. L. Salkoff, K. Baker, A. Butler, M. Covarrubias, M. Pak, and A. Wei, *TINS* **15:5**, 161 (1992)

45. A. L. Hodgkin and A. F. Huxley , *J. Physiol.* **117**, 500 (1952)

46. Lauger, *Biochim. Biophys. Acta* **311**, 423 - 441(1973)

47. Hille and Schwarz, *J. Gen. Physiol* **72**, 409 - 442 (1978)

48. a) Levitt (1986), *Annu. Rev. Biophys. Biophys. Chem* **15**, 29 - 57; b) McGill and Schumaker, *Biophys.* **71**, 1723 - 1742 (1996)

49. C. Miller, *Science* **252**, 1092 (1991)

50. Dian M. Papazian et. al, *Neuron* **14**, 1293 (1995)

51. C.M.Armstrong, *Q.Rev.Biophys* 7, 179 (1975)

52. M. Noda, S. Shimizu, T. Tanabe, T. Takai, T. Kayano, T. Ikeda, H. Takahashi, H. Nakayama, Y. Kanaoka, N. Minamino, et al., *Nature* **312**, 121 (1984)

53. H. R. Guy and P. Seetharamulu, *Proc. Natl. Acad. Sci. USA* **83**, 508 (1986)

54. S. Seoh. D. Sigg, D. M. Papazian, and F. Bezanilla, *Neuron* **16**, 1159 (1996)

55. N. Yang, A. L. George, and R. Horn, *Neuron* **16**, 113 (1996)

56. S. K. Aggarwal and R. MacKinnon, *Neuron* **16**, 1169 (1996)

57. Conti, and Stuhmer, *Eur. Biophys. J.* **17**, 53 (1989)

58. S. R. Durell and H. R. Guy, *Biophys. J.* **62**, 243 (1992)

59. H. Peter Larsson, Oiiver S. Baker, Dalvinder S. Dhilon, and Ehud Y. Isacoff. *Neuron* **16**, 387 (1996)

60. D.R. Hartree, *Proc.Camb.Phil.Soc.*, **24**, a) 89; b)111; c) 426 (1928)

61. V. Fock, *Z. Phys.* **61**, 126 (1930)

62. a) C.C.J. Roothaan, *Rev.Mod.Phys.* **23**, 69 (1951); b)G.G. Hall, *Proc.R.Soc. A.***205**, 541: **208**, 328 (1951)

63. C.C.J. Roothaan, *Rev.Mod.Phys.* **32**, 179 (1960)

64. J.A. Pople, and R.K. Nesbet, *J.Chem.Phys.* **22**, 571 (1954)

65. Dunning, T. H. and Hay, P. J., Basis Sets for Molecular Calculations, in *Modern Theoretical Chemistry* **1977**, v. 3, (H. Schaefer, ed) (Plenum, NY) chap.1

66. Kollman, P. **1977** Basis Sets for Molecular Calculations, in *Modern Theoretical Chemistry* v. 3, (H. Schaefer, ed) (Plenum, NY) chap. 3

67. Hehre, W. J., Radom, L., Schleyer, P.v.R. and Pople, J. A. **1986**, *Ab initio Molecular Orbital Theory* (Wiley, New York)

68. M.J. Frisch, J.E. Del Bene, K. Raghavachari and J.A. Pople, *Chem.Phys.Lett.* **83**, 240 (1981)

69. B.O. Roos, *Ab initio Methods in Quantum Chemistry* — II, edited by K.P. Lawley, John Wiley & Sons Ltd, pp403 - 446 (1987);

70. G. Chalasiñski and M. M. Szczesniak, *Chem. Rev.* **94**, 1723 (1994);

71. S.M. Cybulski, G. Chalasiñski, and R. Moszyñski, *J. Chem. Phys.* **92**, 4357(1990)

72. C. Møller and M.S.Plesset, *Phys.Rev.* **46**, 618 (1934)

73. R.A. Friesner, *Ann. Rev. Phys. Chem.* **42**, 341 (1991)

74. a) B. Jeziorski and W. Kolos, in *Molecular Interactions*, H. Ratajczak, W.J. Orville-Thomas, Eds., Wiley, New York, 1982 Vol.3, p1; b) K. Szalewicz and B. Jeziorski, *Mol. Phys.* **38**, 191(1979)

75. R. McWeeny, '*Methods of Molecular Quantum Mechanics*', Academic Press, edit by D.P. Craig in *Theoretical Chemistry* (1989)

76. a) F. Coester, *Nucl. Phys.* 7, 421 (1958); b) F. Coester and H. Kümmel, *Nucl. Phys.* **17**, 477 (1960)

77. J. Cizek, a) *J. Chem. Phys.* **45**, 4256 (1966); b) *Adv. Chem. Phys.* **14**, 35 (1969)

78. B.O. Roos, *Adv. Chem. Phys.* **69**, 402 (1987)

79. P. Hohenberg and W. Kohn *Phys. Rev.* **B 136**, 864 (1964)

80. W. Kohn and L.J. Sham, *Phys. Rev.* **A 140**, 1133 (1965)

81. a) S.Baroni and E.Tuncel, *J.Chem.Phys.* **79**, 6140 (1983); b) A. Gorling and M.Levy, *Phys. Rev.* **B 47**, 13105 (1993); c) K.Kim and K.D.Jordan, *J.Phys.Chem.* **98**, 10089(1994); d) E.Ruiz, D.R.Salahub, and A.Vela, *J.Am.Chem.Soc.* **117**, 1141 (1995)

82. A. Gorling and M. Levy, *J.Chem.Phys.* **106**, 2675 (1996)

83. A.D. Becke, *J.Chem.Phys.* **98**, 5648 (1993)

84. J. C. Slater, *Quantum Theory of Molecular and Solids.* **Vol.4**: *The Self-Consistent Field for Molecular and Solids*, McGraw-Hill: New York(1974)

85. A.D. Becke, *Phys. Rev.* **A 38**, 3098 (1988)

86. S.H. Vosko, L.Wilk and M. Nusair, *Canadian J. Phys.* **58**, 1200-1211 (1980)

87. C. Lee, W. Yang and R.G. Parr, *Phys. Rev.* **B 37**, 785-789(1988)

88. J.A. Pople, M. Head-Gordon, D.J. Fox, K. Raghavachari, and L.A. Curtiss, *J. Chem. Phys.* **90**, 5622 (1989)

89. C. C. Marston and G. G. Balint-Kurti *J. Chem. Phys.* **91**, 3571 (1989)

90. D.O.Harris, G. G. Engerholm, and W.D.Gwinn, *J. Chem. Phys.* **43**, 1515 (1965)

91. A. S. Dickinson and P. R. Certain, *J. Chem. Phys.* **49**, 4209 (1968)

92. J. V. Lill, G. A. Parker, and J. C.Light, *Chem. Phys. Lett.* **89**, 483 (1982)

93. J. C. Light, I. P. Hamilton, and J. V. Lill, *J. Chem. Phys.* **82**, 1400 (1985)

94. a) R. Kosloff, *J. Phys. Chem.* **92**, 2087 (1988); b) D. Kosloff and R. Kosloff, J. Comput. Phys. **52**, 35(1983)

95. P.Dutta, S. Adhikari and S.P. Bhattacharyya. *Chem Phys. Lett.* **212**, 677 (1993)

96. a) R. Guardiola and J. Ros, *J. Comput. Phys.* **45**, 373 (1982); b) A. Sharafeddin, *J. Chem. Phys.* **103**, 642 (1995); c) *J.Chem. Phys.* **105**, 1084(1996); d) *Chem. Phys. Lett.* **247**,470 (1995)

97. a) A. Askar, *J. Chem. Phys.* **74**, 6133 (1981); b) J.R. Flores, E. Clementi, and V. Sonnad, *J. Chem. Phys.* **91**, 7030 (1989); c) H.Yu, A.D. Bandrauk and V.Sonnad, *J. Math. Chem.* **115**, 1(1994); d) ibid, **119**, 1(1994); e)H.Yu and A.D. Bandrauk, *J. Chem. Phys.* **102**, 1257 (1995)

98. a) M.D. Feit, J.A. Fleck, JR, and A. Steiger , *J. Comput. Phys.* **47**, 412 (1982); b) M.D. Feit and J.A. Fleck, JR, *J. Chem. Phys.* **78**, 301 (1983)

99. a) E. Balslev and J. Combes, *Commun. Phys.* **22**, 280 (1971); b) B. Simon, *Math. Phys.* **27**, 1(1972); c) ibid, *Ann. Math.* **97**, 247 (1973); d) Per-O. Lowdin, *Adv. Quan. Chem.* **19**, 87 (1988); e) N. Moiseyev and J.O. Hirschfelder, *J. Chem. Phys.* **88**, 1063 (1988); f) S. Chu, *Chem. Phys. Lett.* **167**,155 (1989); g) V. A. Mandelshtam and N. Moiseyev, *J. Chem.*

Phys. **104**, 6192 (1996)

100. a) B. Szabó and I. Babuška, *Finite Element Analysis* (Wiley, New York, 1992); b) B.A. Finlayson, *Method of Weighted Residues* (Academic, New York, 1974)

101. J.A. Fleck, JR., J.R. Morris, and M.D. Feit, *Appl. Phys.* **10**, 129 (1976)

102. S. Kanfer and M. Shapiro, *J. Phys. Chem.* **88**, 3964(1984))

103. a) G.C. Corey and D. Lemoine, *J. Chem. Phys.* **97**, 4115 (1992); b) G.C.Corey, J.W.Tromp, and D. Lemoine, in *NATO ARW Proceedings on Grid Methods in Atomic and Molecular Quantum Calculation*, edited by C. Cerjan (Kluwer Academic, Dordrecht, The Netherlands, 1993); c) U. Manthe, *J. Chem. Phys.* **105**, 6989 (1996); d) G. C. Corey and J. W. Tromp, *J. Chem. Phys.* **103**, 1812 (1995)

104. J. W. Cooley and J. W. Tukey, *Math. Comp.* **19**, 297 (1965)

105. R. Tolimieri, M. An, and C. Lu, *Algorithms for Discrete Fourier Transform and Convolution* (Springer Verlag, New York, 1989), pp72-118

106. C.E. Shannon, *Proc.IRE.* **37**, 10 (1949)

107. G.L. Hofacker, Y. Marechal and M.A. Ratner, *The hydrogen bond – recent developments in theory and experiments*, chapt. 6, Eds. P. Schuster *et al.* North-Holland Publ. Co., Amsterdam, 1976)

108. M. J. Davis and E. J. Heller, *J.Chem.Phys.* **75**, 246 (1981)

109. E.G. Weidemann and G. Zundel, *Z. Naturforsch* **A28**, 236 (1970)

110. C.F. Bernasconi and P.J. Wenzel, *J. Am. Chem. Soc.* **116**, 5405 (1994), and references there in

111. R. Meyer, *J. Mol. Spectrosc.* **76**, 767(1979)

112. K. Loth, F. Graf, and Hs. H. Gunthard, *Chem. Phys.* **13**, 95 (1976)

113. a) D. McMorrow and M. Kasha, *J. Phys. Chem.* **88**, 2235 (1984); b) G.A. Brucker and D.F. Kelley, *J. Phys. Chem.* **91**, 2856 (1987); c) **92**, 3805 (1988)

114. A. J. G. Strandjoid and P. F. Barbara, *J. Phys. Chem.* **89**, 2362 (1985)

115. H. Ushiyama and K. Takatsuka, *J. Chem Phys.* **106**, 7023 (1997)

116. Hehre, W. J., Radom, L., Schleyer, P.v.R. and Pople, J. A., *Ab initio Molecular Orbital Theory* (Wiley, NY, 1986)

117. S. Baroni and E. Tuncel, *J.Chem.Phys.* **79**, 6140 (1983)

118. A. Seidl, A. Gorling, A. Majewski, and P. Vogl, *Phys. Rev.* **B 53**, 3764 (1996)

119. K. Kim and K.D. Jordan, *J.Chem.Phys.* **98**, 10089 (1994)

120. V. Barone and C. Adamo, *J. Chem. Phys.***105**, 11007 (1996)

121. S. Xantheas, *J. Am. Chem. Soc.* **117**, 10373 (1995)

122. Y. Xie, R. B. Remington, and H. F. Schaefer III, *J. Chem. Phys.* **101**, 4878(1994)

123. Adams, J. C. *spline3u.f subroutine series*, Nat'l Center Atm. Res. (1994)

124. Sathyamurthy, N. and Raff, L. M., *J. Chem. Phys.* **63**, 464 (1975)

125. M. S. P. Sansom, G. R. Smith, C. Adcock, and P. C. Biggin, *Biophys. J.* **73**, 2404 (1997)

126. D. M. Papazian, X. M. Shao, S-A Seoh, A. F. Mock, Y. Huang, and D. H. Wainstock, *Neuron* **14**, 1293 (1995)

127. D. A. Doyle, J. M. Cabral, R. A. Pfuetzner, A. Kuo, J. M. Gulbis, S. L. Cohen, B. T. Chait, R. Mackinnon, *Science* **280**, 69 (1998)

128. C.M. Amstrong and F. Bezanilla, *J. Gen. Physiol.* **70**, 567 (1977)

129. D. M. Starace, E. Stefani, and F. Bezanilla, *Neuron* **19**, 1316 (1997)

130. E. Perozo, R. Mackinnon, F. Bezanilla, and E. Stefani, *Neuron* **11**, 353 (1993)

131. T Hoshi, W.N. Zagotta, and R.W. Aldrich, *Science* **250**, 533 (1990)

132. T.L. Schwarz, B.L. Tempel, D.M. Papazine, Y.N. Yan, and L.Y. Yan, *Nature* **331**, 137 (1988)

133. R. Hoffmann, *J. Chem. Phys.* **39**, 1397 (1963)

134. a) J.A. Pople, D.P. Sandry, and G.A. Segal, *J. Chem. Phys.* **43**, S129 (1965); b) J.A. Pople

and G.A. Segal, *J. Chem. Phys.* **44**, 3289 (1966)

135. R.C. Bingham, M.J.S. Dewar, and D.H. Lo, *J. Am. Chem. Soc.* **97**, 1285 (1975)

136. M.J.S. Dewar, E.G. Zoebisch, E.F. Healy, and J.J.P. Stewart, *J. Am. Chem. Soc.* **107**, 3902 (1985)

137. J. J. P. Stewart, *J. Comput. Chem.* **10**, 209 (1989)

138. N.L. Allinger, *J. Am. Chem. Soc.* **99**, 8127 (1977)

139. U. Berkert and N.L. Allinger, *Molecular Mechanics*; American Chemical Society: Washington, DC, 1982

140. N.L. Allinger, Y.H. Yuh, and J.-H. Lii, *J. Am. Chem. Soc.* **111**, 8551 (1989)

141. Gaussian 94, Revision D.1, M. J. Frisch,. G. W. Trucks, H. B. Schlegel, P. M. W. Gill, B. G. Johnson, M. A. Robb, J. R. Cheeseman, T. Keith, G. A. Petersson, J. A. Montgomery, K. Raghavachari, M. A. Al-Laham, V. G. Zakrzewski, J. V. Ortiz, J. B. Foresman, J. Cioslowski, . B. B. Stefanov, A. Nanayakkara, . M. Challacombe, C. Y. Peng, P. Y. Ayala, W.Chen, M. W. Wong, J. L. Andres, E. S. Replogle, R. Gomperts, R. L. Martin, D. J. Fox, J. S., Binkley, D. J. Defrees, J. Baker, J. P. Stewart, M. Head-Gordon, C. Gonzalez, and J. A.Pople, **1995** Gaussian, Inc., Pittsburgh PA

142. N. Doslic, O. Kuhn, J. Manz, and K.Sundermann, *J. Phys. Chem.* (1998, in press)